University of Alberta

Initial Coking of a NiMo/γ-Al_2O_3 Bitumen Hydroprocessing Catalyst

by

Susan Mary Richardson ©

A thesis submitted to the Faculty of Graduate Studies and Research in partial fulfillment
of the requirements for the degree of Doctor of Philosophy

Department of Chemical and Materials Engineering

Edmonton, Alberta

Fall, 1996

National Library
of Canada

Acquisitions and
Bibliographic Services Branch

395 Wellington Street
Ottawa, Ontario
K1A 0N4

Bibliothèque nationale
du Canada

Direction des acquisitions et
des services bibliographiques

395, rue Wellington
Ottawa (Ontario)
K1A 0N4

Your file Votre référence

Our file Notre référence

The author has granted an irrevocable non-exclusive licence allowing the National Library of Canada to reproduce, loan, distribute or sell copies of his/her thesis by any means and in any form or format, making this thesis available to interested persons.

L'auteur a accordé une licence irrévocable et non exclusive permettant à la Bibliothèque nationale du Canada de reproduire, prêter, distribuer ou vendre des copies de sa thèse de quelque manière et sous quelque forme que ce soit pour mettre des exemplaires de cette thèse à la disposition des personnes intéressées.

The author retains ownership of the copyright in his/her thesis. Neither the thesis nor substantial extracts from it may be printed or otherwise reproduced without his/her permission.

L'auteur conserve la propriété du droit d'auteur qui protège sa thèse. Ni la thèse ni des extraits substantiels de celle-ci ne doivent être imprimés ou autrement reproduits sans son autorisation.

ISBN 0-612-18098-0

Canada

University of Alberta

Library Release Form

Name of Author: Susan Mary Richardson

Title of Thesis: Initial Coking of on a $NiMo/\gamma\text{-}Al_2O_3$ Bitumen Hydroprocessing Catalyst.

Degree: Doctor of Philosophy

Year This Degree Granted: 1996

Permission is hereby granted to the University of Alberta Library to reproduce single copies of this thesis and to lend or sell such copies for private, scholarly, or scientific research purposes only.

The author reserves all other publication and other rights in association with the copyright in the thesis, and except as hereinbefore provided, neither the thesis or any substantial portion thereof may be printed or otherwise reproduced in any material form without the author's prior written permission.

Susan Richardson

Susan Mary Richardson
#301 - 10025 85 Ave
Edmonton. Alberta
T6E 2J9
Canada

September 9, 1996

University of Alberta

Faculty of Graduate Studies and Research

The undersigned certify that they have read, and recommend to the Faculty of Graduate Studies and Research for acceptance, a thesis entitled Initial Coking of a NiMo/γ-Al_2O_3 Bitumen Hydroprocessing Catalyst in partial fulfillment of the requirements for the degree of Doctor of Philosophy.

Murray Gray

Sieghard Wanke

Karl Chuang

Karl Chuang

Karlis Muehlenbach

Kevin Smith

September 5, 1996

ABSTRACT

Primary upgrading of heavy hydrocarbons by catalytic hydroprocessing has become widespread, using alumina-supported transition metal sulfide catalysts. In the presence of non-distillable fractions, the catalysts suffer from rapid deactivation under hydroprocessing conditions. The initial deactivation is attributed to deposition of coke on the catalyst surface. This project was carried out in order to understand the coke deposition observed on one commercially-produced catalyst, and to modify this behaviour through doping of the catalyst with alkali metals.

A commercial NiMo/γ-Al_2O_3 catalyst was used in the hydroprocessing of Athabasca bitumen in 15 mL micro batch and 1L CSTR reactors at 430°C and hydrogen pressures ranging from 6.9 to 15.2 MPa. Coke deposition on the surface of the catalyst was studied with respect to reaction time, hydrogen pressure, feed composition, and cumulative oil to catalyst ratio. The concentration of carbon in the spent catalyst was used to monitor the deposition of coke. Carbon concentration in the spent catalyst decreased from 17.5% at 6.9 MPa to 11.3% at 15.2 MPa. This decrease was used as the foundation for a mechanistic model of coke deposition which explained the dependence of coke deposition on residue concentration and time on stream. The mass transfer implications of the proposed model were examined through the use of hindered diffusion theory and the random pore model of Wakao and Smith.

The inherent acidity of the alumina support is considered a major contributing factor to catalyst coking during hydrocracking. The commercial catalyst was doped with KNO_3, KOH, NaOH, and LiOH at concentrations ranging from 0.26 to 9.8 meq/g catalyst. The latter three dopants were shown to cause decreased catalyst coking and increased activity for hydrodesulfurization (HDS) in the batch reactor. NaOH and LiOH doped catalysts

contained 17% (relative) less carbon, and had 20% increased HDS activity. The NaOH doped catalyst also improved HDS activity in the CSTR with an 11% increase in sulfur conversion relative to the commercial catalyst. Asphaltene conversion increased marginally for the doped catalyst compared to the commercial catalyst. Hydrodenitrogenation, pitch conversion and metals removal did not change for the alkali-doped catalyst.

ACKNOWLEDGEMENTS

I would like to acknowledge the financial support provided by the Alberta Oilsands Research and Technology Authority, the Natural Sciences and Engineering Research Council, Syncrude Canada Ltd., Petro Canada, the Province of New Brunswick and the University of Alberta.

The technical advice and support provided by the support staff of the Department of Chemical Engineering, University of Alberta, and Syncrude Canada Ltd Research were instrumental in the completion of the experimental work described in the thesis.

I would like to thank Murray Gray for his supervision, support and advice.

To Suzanne Kresta, Andree Koenig and all my fellow graduate students, especially Alan Ayasse, Carolyn Blanchard and Patricia Stelmack: thank you for keeping me sane.

Table of Contents

				Page
1	Introduction			1
	1.1	Literature Cited		4
2	The Relationship Between Coke Deposition and Reaction Parameters			5
	2.1	Introduction		5
	2.2	Experimental		7
		2.2.1	Materials	7
		2.2.2	Analysis Techniques	8
		2.2.3	Reactors and Reaction Procedures	9
		2.2.4	Reaction Protocols	11
	2.3	Results and Discussion		15
		2.3.1	Deposition of Coke with Time and Feed/Catalyst Ratio	15
		2.3.2	Dependence of Coking on Residue Concentration	17
		2.3.3	Dependence of Coke Deposition on Hydrogen Pressure	19
	2.4	Conclusions		23
	2.5	Literature Cited		24
3	Model for Initial Coke Deposition			26
	3.1	Introduction		26
	3.2	Experimental		28
	3.3	Model Development		28
		3.3.1	The Monolayer Concept	28
		3.3.2	The Steady State Model	31
		3.3.3	Transient Deposition of Coke	40
		3.3.4	The Model Predictions for Other Reaction Parameters	41
	3.4	Comparison of Model to Literature Data		43
	3.5	Conclusions		43
	3.6	Literature Cited		45
4	Validation of the Model			47
	4.1	Introduction		47
		4.1.1	The Chemistry of the Carbonaceous Deposit	47
		4.1.2	Nature of the Carbon-Surface Interaction	48
		4.1.3	Distribution of Carbon on Catalyst Surface	48
		4.1.4	Proposed Validation Experiments	50
	4.2	Experimental		50
		4.2.1	Materials	50
		4.2.2	Model Feed Preparation	51
		4.2.3	Analysis Techniques	52

Page

- 4.2.4 Reaction Procedures 54
- 4.3 Results and Discussion 54
  - 4.3.1 The Chemistry of the Carbonaceous Deposit 54
  - 4.3.2 Nature of the Carbon- Surface Interaction 55
  - 4.3.3 Validation of the Annulus Model 57
  - 4.3.4 Summary of Model Validations 59
- 4.4 Conclusions 60
- 4.5 Literature Cited 61

5 Mass Transfer Effects in Coked Catalyst 62
- 5.1 Introduction 62
- 5.2 Experimental 62
- 5.3 Results and Discussion 64
  - 5.3.1 Hindered Diffusion Theory 64
  - 5.3.2 Wakao and Smith's Random Pore Model 65
  - 5.3.3 Uniform Deposition of Coke Versus Pore-Mouth Plugging 68
- 5.4 Conclusions 70
- 5.4 Literature Cited 71

6 Base Doping of Hydroprocessing Catalysts 72
- 6.1 Introduction 72
  - 6.1.1 Surface Acidity 72
  - 6.1.2 Other Effects of Alkali Treatment 78
- 6.2 Experimental 80
  - 6.2.1 Materials 80
  - 6.2.2 Catalyst Properties and Base Doping 80
  - 6.2.3 Analytical Techniques 82
  - 6.2.4 Reactors and Reaction Procedures 82
- 6.3 Results and Discussion 84
  - 6.3.1 Catalyst Deactivation and the Effect of Presulfidation 84
  - 6.3.2 Addition of KNO_3 86
  - 6.3.3 Addition of Alkali Metal Hydroxides - Catalyst Screening Experiments 89
  - 6.3.4 Catalyst Stability and Multi-Function Activity 97
- 6.4 Conclusions 101
- 6.5 Literature Cited 103

7 Conclusions 106

Appendix 2.1 Carbon Concentrations On Catalysts from Batch Reactor Experiments 109

Page

Appendix 2.2 Catalyst Carbon Content Related to Product Residue Content and MCR Content 109

Appendix 3.1: Determination of Surface Carbon Concentration Resulting From a Monolayer of Various Substances 110

Appendix 3.2 Sensitivity Analysis of Monolayer Carbon Content 113

Appendix 3.3 Comparison of Model Parameter b to Literature Values 114

Appendix 4.1 Distribution of the Strength of Acid Sites of Selected Catalysts 115

Appendix 5.1 Calculations for the Random Pore Model of Wakao and Smith 116

Appendix 6.1 Sulfur Removal Activity of Various Catalysts 122

Appendix 6.2 Distribution of the Strengths of Acid Sites of Selected Catalysts 124

Appendix 6.3 Statistical Analysis of HDS Conversions for Alkali Doped Catalyst 125

Appendix 6.4 Metals Analysis of Product Residue Fractions 127

List of Tables

Page

2.1 Characterization of the Feed and Selected Products 7

2.2 Summary of Reaction Conditions and Carbon Content for CSTR Experiments 14

2.3 Product Composition and Hydrogen to Carbon Ratios of Selected CSTR Catalysts 19

3.1 Estimated Parameters for Alternative Models for Coke Deposition 36

4.1 Model Compound Feed Experiments in Batch Reaction with 1 h Reaction Time per Step at 430°C and 13.8 MPa. 52

6.1 Prior Studies on Doping of γ- Alumina Catalysts with Alkali and Alkaline Earth Metals 73

6.2 Alkali Metal Content for Base Doped Catalysts 81

6.3 Carbon Content of Base Doped Catalyst 89

6.4 Characterization of the Feed and CSTR Products from Experiments Using the Commercial Catalyst and a Sodium Doped Catalyst 98

6.5 Sulfur and Nitrogen Content of Product Fractions 98

6.6 Comparison of the Apparent First Order Rate Constants for Sulfur Removal for the Na-Doped and Commercial Catalysts 99

Appendices:

A2.1 Carbon Concentrations on Catalysts from Batch Reactor Experiments 109

A2.2 Catalyst Carbon Content Related to Residue Content and MCR Content 109

A3.2 Effect of Density, Carbon Content and Molecular Weight on the Prediction of Carbon Content Arising from Monolayer Carbon Coverage 113

A4.1 Distributions of the Strength of Acid Sites of Fresh Catalyst and Spent Catalysts 115

Page

A6.1 Sulfur Removal Activity of Various Catalysts 122

A6.2 Distribution of the Strengths of Acid Sites of Selected Catalysts 124

A6.4 Metals Analysis of Product Residue Fractions 127

List of Figures

		Page
2.1	Schematic Diagram of the Batch Reactor	10
2.2a	Batch Reactor with Cut Away Section Showing Relative Amounts of Hydrogen, Bitumen and Catalyst after Loading	13
2.2b	Batch Reactor Showing Expected Condition of Reactor Contents During Agitation at Operating Conditions.	13
2.3	Carbon Content of Spent Catalyst as a Function of Cumulative Feed Oil to Catalyst Ratio	16
2.4	Carbon Content of Spent Catalyst as a Function of Residue Concentration in the CSTR	18
2.5	Carbon Content of Spent Catalyst as a Function of Hydrogen Pressure for CSTR Experiments	20
3.1	Schematic Representation of Catalyst Surface, Showing a Cross Section through Metal Crystallite	32
3.2	Surface Concentration of Carbon as a Function of Hydrogen Pressure (Models 1 and 2)	37
3.3	Surface Concentration of Carbon as a Function of Hydrogen Pressure (Models 3,4, and 5)	39
3.4	Carbon Concentration in Spent Catalyst as a Function of Cumulative Feed Oil to Catalyst Ratio in the Batch Reactor	42
4.1	Distribution of Strengths of Acid Sites by Stepwise Thermal Desorption.	58
5.1	Pore Size Distribution (PSD) Based on Surface Area and the Reduction in Effective Diffusivity Caused by Coke Deposition.	63
6.1	Hydrodesulfurization Activity for Commercial Catalyst and Presulfided Commercial Catalyst.	85
6.2	Distribution of the Strengths of Acid Sites for Commercial Catalyst as Delivered, Crushed and Calcined Commercial Catalyst, and Low Concentration (0.26 meq / g catalyst) KNO_3 Doped Catalyst.	87

Page

6.3 Hydrodesulfurization Activity for Commercial Catalyst and Catalyst Doped with 9.8 meq KNO_3/ g catalyst. 88

6.4 Hydrodesulfurization Activity for Commercial Catalyst and Catalysts Doped with 0.28 meq KOH / g catalyst, 0.59 meq KOH / g catalyst and 5.22 meq KOH / g catalyst. 90

6.5 Hydrodesulfurization Activity for Commercial Catalyst and Catalysts Doped with 0.28 meq KOH / g catalyst, 0.26 meq NaOH / g catalyst and 0.26 meq LiOH / g catalyst. 92

6.6 Average Hydrodesulfurization Activity for Commercial Catalyst and Catalysts Doped with 0.28 meq KOH / g catalyst, 0.26 meq NaOH / g catalyst and 0.26 meq LiOH / g catalyst. 93

6.7 Distribution of Strengths of Acid Sites for Commercial Catalyst, KOH Doped Catalyst (0.28 meq/g catalyst), NaOH Doped Catalyst (0.26 meq/g catalyst), and LiOH Doped Catalyst (0.26 meq/g catalyst). 94

LIST OF SYMBOLS

a = empirical parameter (MPa)

B = an empirical coefficient

b = empirical parameter (m^2 metal / m^2 surface)

C = the actual concentration of carbon in the catalyst (wt % C, on a spent catalyst basis)

c = empirical parameter (MPa)

C_{max} =the maximum carbon concentration in the catalyst (wt % C, on a spent catalyst basis)

C_p = the surface concentration of coke precursor (mol / m^2).

D_b = the bulk diffusivity (m/s^2)

D_e = effective (hindered) diffusivity in the catalyst pellet (m/s^2)

$D_{p,i}$ = the effective diffusivity in pore i (m^2/s).

F_{crit} = the critical surface flux of hydrogen (mol/ms)

k = the rate constant for production of surface hydrogen (mol/ MPa s)

k = an adsorption rate constant (g cat / g feed)

k_d = the deposition rate coefficient for hydrocarbon (m^{-1})

M = the actual surface carbon concentration (g carbon / m^2)

M_{max} = the maximum surface carbon concentration (g carbon / m^2 of surface)

MW = the molecular weight (Da)

N = the number of metal crystallites (crystallites / m^2)

NA = Avagadro's number (6.02×10^{26} molecules / kgmol)

P_{H_2} = the pressure of hydrogen (MPa)

R = the cumulative feed to catalyst ratio, a pseudo time coordinate (g feed / g catalyst)

r = the radius of the cleared zone (m)

r_c = the radius of the metal crystallite (m)

r_{dep} = the rate of carbon deposition on the catalyst (g residue / g catalyst)

r_i = the radius of pore i (m)

r_m = the macro pore radius (m)

r_p = the pore radius (m)

r_r = the radius of a residue molecule (m)

r_μ = the micropore radius (m).

T_d = the pyridine desorption temperature (K)

T_d^* = the theoretical maximum temperature for pyridine desorption (K)

x_c = the mass fraction carbon in the residue.

Greek Symbols

ε_c = the porosity of the coked catalyst

ε_f = the porosity of the fresh catalyst

ε_p = the pellet porosity

λ = the ratio of molecule size to pore size: $\lambda = r_r / r_p$,

θ_v = the fraction of possible adsorption sites currently vacant

ρ = the density of oil (kg/m^3).

σ = the stoichiometric coefficient for reaction of surface hydrocarbon with hydrogen

τ = the catalyst tortuosity

1 INTRODUCTION

Canada's energy future includes non-conventional petroleum sources, such as the Athabasca Oilsands. Current production of sythetic crude oil from oilsand at Syncrude Canada Ltd. alone is 74 million barrels per year (Syncrude Annual Report, 1994). Bitumen is produced from the oilsand ore through a hot water extraction process. The bitumen requires two upgrading steps to become a product suitable for use as feed to conventional refineries. The first step, or primary upgrading, breaks the high molecular weight components into lower molecular weight, lower viscosity, higher volatility components. The secondary upgrading step removes remaining heteroatoms (sulfur and nitrogen) and hydrogenates the products from the primary stage. Primary upgrading is accomplished through two main technologies, thermal processing (coking) and catalytic processing with addition of hydrogen (hydroprocessing / hydrocracking).

Hydroprocessing is becoming the technology of choice for primary upgrading because of higher liquid yields compared with coking (Beaton and Bertolacini, 1991). Catalyst deactivation is a major concern, with catalyst lifetimes on the order of weeks (Oballa et al., 1994). Catalyst deactivation occurs through two major modes: deposition of coke and deposition of heavy metals. Coke deposition occurs rapidly early in the catalyst lifetime, and it is believed responsible for the rapid deactivation that occurs during the same time frame (Carruthers, et al., 1994). Deposition of heavy metals such as vandium and nickel occurs slowly over the lifetime of the catalyst, and is considered responsible for the final catastrophic deactivation which occurs at the end of the catalyst's lifetime (Tamm, et al., 1981). Although anecdotal information exists regarding coke deposition, limited systematic information exists on the effect of various reaction parameters, such as feed composition or hydrogen pressure. The goal of this project is to provide systematic information regarding the effect of reaction time, hydrogen pressure, feed composition and feed to catalyst ratio.

Hydrogen pressure was chosen as the primary reaction parameter for study. This choice was based on the importance of hydrogen pressure in the design of hydroprocessing technology. Increased hydrogen pressure was expected to reduce catalyst deactivation by suppressing coke deposition (Thakur and Thomas, 1985), reduce fouling of process equipment due to formation of coke in the liquid products (Gray, 1994) and increase the rates of reaction for such desirable reactions as hydrodesulfurization (HDS), hydrodenitrogenation (HDN) and hydrogenation (HYD) (Gray, 1994). Unfortunately, these advantages cannot be achieved without a price. Increased process pressure causes much higher capital costs (Ulrich, 1984). This trade off between capital and operating costs and conversion goals is the impetus for a better understanding of the role of hydrogen. The main focus of this thesis is the role of hydrogen in coking of the catalyst. In these studies the coke content of the spent catalyst was determined by measuring the concentration of carbon.

Given an improved understanding of the coking phenomenon, the composition of the catalyst was modified in an attempt to reduce the coke deposition, and therefore reduce the initial deactivation. These catalysts were doped with alkali metal nitrates and hydroxides to reduce the surface acidity of the alumina support. Since the inherent acidity of the alumina surface contributes to coking (Gray et al., 1992), reduction of the acidity was expected to reduce the coking propensity of the catalyst.

This thesis consists of five main sections. The data which relate coke content of catalysts, based on carbon concentration, to the reaction time; hydrogen pressure; feed composition; and feed to catalyst ratio are presented in Chapter 2. These data were collected from two reactors, a 15 mL microbatch reactor and a 1 L continuous stirred reactor (CSTR). In Chapter 3 the data were synthesized into a mechanistic model for the deposition of coke on the catalyst surface to account for the observed carbon concentrations. Several issues arose from this model, including the nature of the coke-surface interaction and the chemical and physical structure of the deposited coke. These issues and the ensuing validation experiments are discussed in Chapter 4. The mass transfer implications of the proposed model are discussed in Chapter 5. Chapter 6 describes the experimental findings from catalysts which were doped with alkali metal salts in an attempt to reduce surface coking and thereby reduce mass transfer limitations within the pore network of the catalyst.

1.1 LITERATURE CITED

Anonymous. Syncrude Canada Ltd. Annual Report. **1994.**

Beaton, W.I.; Bertolacini, R.J. Resid Hydroprocessing at Amoco. *Catal. Rev. Sci. Eng.* **1991**, 33, 281-317.

Carruthers, J.D; Brinen, J.S; Komar, D.A; Greenhouse, S. "Catalyst Poisoning During Tar Sands Bitumen Upgrading" in Catalytic Hydroprocessing of Petroleum and Distillates, eds. Oballa, M.C. and Shih, S. S., Marcel Dekker, Inc., New York, **1994**, 175-202.

Gray, M. R. Upgrading Petroleum Residues and Heavy Oils, Marcel Dekker, Inc., New York, **1994**.

Gray, M. R.; Khorasheh, F.; Wanke, S. E.; Achia, U.; Krzywicki, A.; Sanford, E. C.; Sy, O. K. Y.; Ternan, M. Role of Catalyst in Hydrocracking of Residues from Alberta Bitumens. *Energy and Fuels.* **1992,** 6, 478-485.

Oballa, M.C.; Wong, C.; Krzywicki, A. "Catalyst Deactivation in Residue Hydrocracking", in Catalytic Hydroprocessing of Petroleum and Distillates, eds. Oballa, M.C. and Shih, S. S., Marcel Dekker, Inc., New York, **1994**, 33-54.

Tamm, P.W; Harnsburger, H.F; Bridge, A.G. Effects of Feed Metals on Catalyst Aging in Hydroprocessing Residuum. *Ind. Eng. Chem. Proc. Des. Dev.* **1981**, 20, 262-273.

Thakur, D.S.; Thomas, M.G.; Catalyst Deactivation in Heavy Petroleum and Synthetic Crude Processing: A Review. *App. Catal.* **1985**, 15, 197-225.

Ulrich, G.D. A Guide to Chemical Engineering Process Design and Economics, J Wiley and Sons, New York, **1984**.

CHAPTER 2: THE RELATIONSHIP BETWEEN COKE DEPOSITION AND REACTION PARAMETERS.

2.1 INTRODUCTION

As conventional fuel supplies dwindle, and production costs increase, industry can no longer ignore heavy oil supplies, and must process heavier feedstocks. This processing begins with a primary upgrading step, whose first goal is to break down the high molecular weight components into distillable compounds. Simultaneous removal of heteroatoms from the feedstock may be achieved; however, a secondary upgrading step is usually required to meet specifications for heteroatom content. Primary upgrading of bitumen and heavy oil has historically been accomplished through two types of technology: thermal coking and hydroprocessing. In recent years, hydroprocessing has become the technology of choice due to higher yields and greater heteroatom removal (Beaton and Bertolacini, 1991).

The use of this technology has been hindered by high catalyst costs, incurred due to rapid deactivation of the catalyst. Two major deactivation pathways are recognized: initial deposition of carbonaceous substances (coking) and deposition of heavy metals (Thakur and Thomas, 1985). Hydroprocessing and hydrotreating catalysts typically accumulate carbonaceous deposits over the first hours or days of service. The carbon concentration in the spent catalyst, therefore, goes through a rapid initial increase which then asymptotically approaches a stable value (Oballa et al., 1994). This initial coke deposition is often credited with the deactivation that occurs during the same period (Oballa et al., 1994; Hannerup and Jacobsen, 1983). Given this possible link, understanding the phenomenon of coke deposition on hydrocracking catalysts is important. Despite the routine use of catalytic hydroprocessing in industry, the phenomenon of coke deposition is not well understood. In general, an increase in hydrogen pressure reduces coke deposition on catalyst (Thakur and Thomas, 1985).

Aitken et al. (1964) developed an empirical relation between deactivation rate and hydrogen pressure in hydrocracking of bitumen. The deactivation rate increased with decreasing hydrogen pressure. The deactivation rate was inversely proportional to the cube of the hydrogen pressure. The authors did not measure carbon content of the catalyst, therefore, the link between hydrogen pressure and coke content was unknown. Inoguchi et al. (1972) considered the effect of hydrogen flow rate on carbon deposition in a packed bed reactor. They found that coke deposition decreased with increasing hydrogen flow rate. Although they did not measure coke deposition as an explicit function of hydrogen pressure, it was suggested that the data for dependence of coking on flow rate could best be explained by the increase in hydrogen partial pressure with increasing gas flow rates, although concomitant changes in liquid hold up within the reactor were not considered. Similarly, Zeuthen et al. (1995) attributed higher end-of-run carbon concentrations in the catalyst from the third stage of a three-stage pilot plant to lower hydrogen partial pressure in that stage. Douwes et al. (1979) suggested that lower hydrogen partial pressure would result in an increase in deposited coke in the catalyst.

The effect of feed composition has been explored, and the literature shows a correlation between the concentration of high molecular weight compounds and coke deposition on the catalyst (Furimsky, 1978; Stohl and Stephens, 1986). Because these studies were performed on diverse feedstocks, it is difficult to distinguish between the individual contributions of the various feedstock characteristics. For example, correlation of the amount of coke deposited on a catalyst with the residue content of different oils may ignore variations in aromatic carbon content of the residue fractions. Variations in the basic nitrogen content, microcarbon residue content, asphaltene content, or metals content may confound the interpretation of the results, and should be taken into account.

The initial deposition of coke on a commercial Ni-Mo/γ-Al_2O_3 catalyst is described in this chapter. It examines the effect of reaction time, total feed to catalyst ratio, hydrogen pressure and feed compositions. The results will be discussed in detail, while in Chapter 3 a model is developed based on the results of this chapter.

2.2 EXPERIMENTAL

2.2.1 Materials

Athabasca bitumen was provided by Syncrude Canada Ltd., with the properties listed in Table 2.1.

Table 2.1: Characterization of the Feed and Selected Products

	Bitumen	Product 1	Product 2	Product 3	Product 4
C (%)	82.7	83.6	86.0	86.8	86.8
H (%)	10.2	10.9	11.4	11.8	12.5
S (%)	4.9	2.6	1.6	0.59	0.12
N (%)	0.45	0.44	0.38	0.29	0.10
Density (g / mL)	1.008	0.959	0.927	0.888	0.847
MCR (%)	13.7	9.9	7.6	2.3	0.1
Naphtha (IBP-177 °C)	0	9.9	11.8	20.2	28.3
Mid Distill (177-343 °C)	7.0	20.0	30.2	42.4	58.8
Gas Oil (343-524 °C)	38.0	37.9	36.8	28.9	12.2
Residue (524 °C+)	55.0	32.2	21.3	8.5	0.7

The catalyst was a commercial NiMo /γ-Al_2O_3 catalyst with 12.5 wt % MoO_3 and 3.5 wt % NiO. The catalyst had a surface area of 317 m^2/g (by nitrogen BET measurement) and a pore volume of 0.57 mL/g. In one experiment the catalyst was presulfided using CS_2. In other cases, the catalyst was not presulfided prior to use. For the batch experiments the catalyst was crushed and sieved to +350μm -500μm size. In the CSTR experiments, the catalyst was used in the 1 mm cylindrical extrudate form in which it was delivered.

2.2.2 Analysis Techniques

Feed and liquid product characteristics were measured at Syncrude Research, Edmonton, AB. The distillation analysis used an atmospheric spinning band distillation to obtain the naphtha (initial boiling point - 177°C) and middle distillate (177 - 343°C) fractions. The remaining oil was then separated into gas oil (343 - 525° C) and residue (525 °C+) fractions using the ASTM D1160 procedure (Anonymous, 1996). The overall sulfur content was determined by combustion followed by fluorescence detection of the evolved SO_2. Carbon and hydrogen analysis of the petroleum liquids used a Leco 600 analyzer. Nitrogen was determined by combustion of the sample followed by chemiluminescence detection. Micro carbon residue (MCR) content was determined using an Alcor MCR analyzer.

Spent catalyst samples were Soxhlet extracted for 6 h (or until the extract was clear, whichever was longer) in dichloromethane, then vacuum dried at 65°C and 0.01 MPa for 2 h. This extraction removed the oil which wetted the catalyst surface following reaction, and provided a consistent basis for interpretation of the carbon content of the catalyst. In order to ensure representative sampling, a 50 mg portion of the catalyst was crushed to a powder, and a 2 mg sample used for analysis of carbon content. The concentration of carbon in the catalyst was measured at the Micro Analytical Laboratory, University of Alberta. This analysis, performed on a Carlo Erba Stumentazione Elemental Analyzer 1108, used combustion of the sample, followed by gas chromatographic separation of the combustion products and analysis by thermal conductivity detection. All coke content data are reported as weight percent carbon on a spent catalyst basis. The total weight of carbonaceous deposits will be larger than the reported values, since hydrogen and heteroatoms are not reported in the carbon content.

Surface area and pore volume measurements were performed in the Department of Chemical Engineering, University of Alberta on an Omnisorb 360 (Coulter Scientific Instruments, Hialeah, Florida). Nitrogen adsorption measurements were used to calculate surface areas, using the BET equation (Gregg and Sing, 1967). Pore volume was determined using nitrogen desorption data and the Kelvin equation (Gregg and Sing, 1967).

2.2.3 Reactors and Reaction Procedures

Two types of reactors were used for this study. 15 mL micro-batch reactors were constructed from stainless steel tubing and tube fittings, and replaced as required. The design consisted of a 1.9 cm (0.75 inch) tubing body, equipped with a Swagelok cap at the bottom, and a custom fabricated 1.9 cm to 0.32 cm (0.125 inch) reducing union at the top. Attached to the reducing union was a 25 cm length of 0.32 cm stainless steel tubing, topped with a high pressure valve. The reactor is shown in Figure 2.1. This design allowed loading of the catalyst and liquids through the 1.9 cm opening below the reducing union. The valve assembly was temporarily connected to the supply gas cylinder to allow filling of the reactor with the desired gas. The valve assembly was then disconnected from the gas supply, isolating the reactor during reaction.

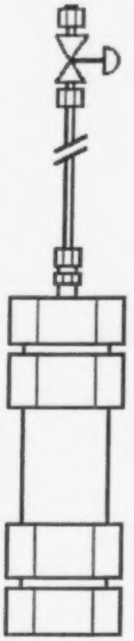

Figure 2.1: Schematic Diagram of the Batch Reactor

A fluidized sand bath was used to heat the microbatch reactor to the required temperature. The reactor was clamped to an external agitator used to shake the reactor at a frequency of approximately 1 Hz. The 25 cm extension between the reactor body and the valve assembly held the valve above the surface of the sand at all times. This allowed the use of low temperature valves, and prevented damage from contamination with sand.

CSTR experiments were performed in a one-litre stirred reactor with continuous gas and oil feed which has been described in detail previously (Gray et al., 1995). In brief, the apparatus consisted of a modified Autoclave Engineering 2 L reactor body, blocked to give a working volume of 1 L to provide a favorable aspect ratio for mixing. Continuous stirring was provided by a magnetic stirrer at 1200 rpm. Hydrogen was supplied at high pressure, with the flow metered at the inlet. Bitumen feed was accomplished through a two-stage pumping arrangement. Bitumen was loaded into one side of a piston-type feed cylinder, and then displaced into the reactor by the metered pumping of kerosene into the other side of the cylinder. The products were separated in a two-stage gas-liquid separator. Liquid products were accumulated for analysis. Gas products were sampled as required by gas chromatography, with the remainder scrubbed and vented to atmosphere.

2.2.4 Reaction Protocols

Micro-batch experiments with bitumen as reactant were carried out in multistep sequences. The sequences were begun with fresh catalyst and bitumen. After reaction, the catalyst was reclaimed by Soxhlet extraction with dichloromethane, and was used with fresh bitumen for the next step. The sequences consisted of two to six repeated steps of extraction and reaction. For each reaction, approximately 0.75 g of catalyst and 3 g of bitumen were loaded into the reactor. The reactor was sealed, purged with nitrogen, then pressurized with hydrogen. The hydrogen pressure at room temperature (25 °C) was 5.7

MPa allowing the pressure to reach 13.8 MPa at the reaction temperature of 430°C. Relative amounts of bitumen, catalyst and hydrogen are indicated in Figure 2.2a, which shows the reactor contents before heating and agitation. The reactor was immersed in a fluidized sand bath heater, and allowed to remain at temperature for the desired time, typically 1 h. Figure 2.2b shows the expected condition of the reactor contents during reaction and agitation. After the reaction was completed, the reactor was cooled quickly in water, and the off gases were vented. A liquid product sample was decanted if necessary, and the remaining oil and catalyst were washed out of the reactor with dichloromethane. The catalyst was Soxhlet extracted in dichloromethane for 6 h, or until the extract ran clear, whichever was longer. The catalyst was vacuum dried for 2 h at 0.01 MPa and 65 °C. The catalyst was then recycled for another reaction step, or sampled for analysis.

Two groups of CSTR experiments were performed. Runs C1 through C7 (see Table 2.2) were single stage experiments at 430°C. In these experiments, 78 g of fresh catalyst was loaded into the reactor, the reactor was heated, then hydrogen and oil feed was begun. The hydrogen flow rate was 4.75 standard liters per minute, and the bitumen flow rate was 400 g/ h. The reactor was brought to steady state, then run at the desired conditions for the desired time. Reaction times listed in Table 2.2 represent total reaction time, including the unsteady-state period. Runs C8 through C12 were experiments with different feed oils and feed rates, listed in Table 2.2, but the other operating procedures remained as described above. Run C8 was one experiment chosen from a group of identical experiments using bitumen feed. In each of the experiments in this group, the steady state liquid products were collected, and the products blended. This blended product was then used as feed in a second series of experiments, represented by Run C9. These products were in turn collected and blended to be used as feed to a third stage,

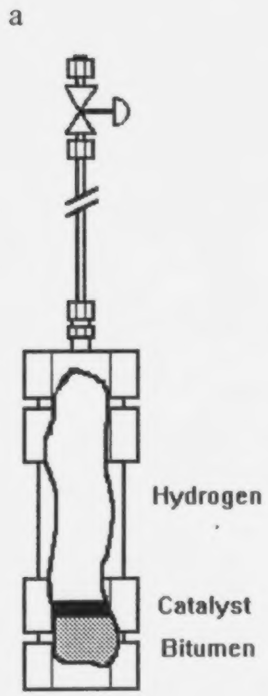
a
Hydrogen
Catalyst
Bitumen

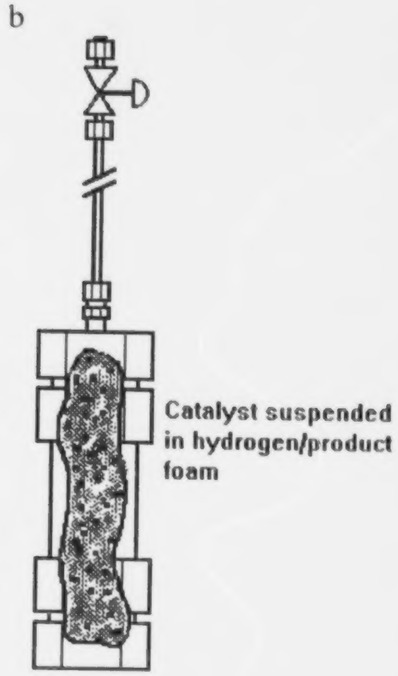
b
Catalyst suspended in hydrogen/product foam

Figure 2.2a: Batch Reactor with Cut Away Section Showing Relative Amounts of Hydrogen, Bitumen and Catalyst after Loading.

Figure 2.2b: Batch Reactor Showing Expected Condition of Reactor Contents During Agitation at Operating Temperature.

Table 2.2: Summary of Reaction Conditions and Carbon Content for CSTR Experiments. All experiments at 430°C.

Run #	Feed	Feed Rate (g/h)	Pressure (MPa)	Feed Ratio (g oil/g cat)	Carbon %	Time on Stream (h)
C1	Bitumen	400	13.8	8.1	9.4	1.5
C2	Bitumen	250	13.8	49.7	12.8	15.5
C3	Bitumen	400	6.9	17.9	17.5	3.5
C4	Bitumen	400	10.3	30.7	16.7	6
C5	Bitumen	400	8.3	30.8	16.4	6
C6	Bitumen	400	11.7	30.8	14.8	6
C7	Bitumen	400	15.2	30.8	11.3	6
C8	Bitumen	1210	13.8	117.5	12.9	7.4
C9	Product oil 1	960	13.8	107.4	14.8	9.1
C10	Product oil 2	370	13.8	41.5	11.2	8.1
C11	Product oil 2	370	13.8	39.6	14.1	7.7
C12	Product oil 3	176	13.8	30.2	6.9	11.9
C13	Bitumen	400	13.8	35.9	14.6	7.0
C14	Bitumen	435	13.8	66.6	15.2	13.0
C15	Bitumen	410	13.8	31.5	17.0	6

represented by Runs C10 and C11. The products from the third stage were blended and used as the feed for a single fourth stage experiment, Run C12. This mode of operation simulated sequential reactors with hydrogen gas makeup between reactors.

2.3 RESULTS AND DISCUSSION

2.3.1 Deposition of Coke with Time and Feed/Catalyst Ratio

A two-step reaction protocol was used to measure the dependence of coke deposition on reaction time. Bitumen was reacted over fresh catalyst. The catalyst was then extracted, reacted with fresh bitumen and extracted again. Total times varied from 1.5 h to 5 h, but carbon concentration was constant at 11.7 ± 0.95 weight % for constant oil to catalyst ratio (see samples B1 to B5 in Appendix 2.1).

The above results appear to contradict the trend towards lower catalyst activity with increased time on stream typically observed in industrial reactors. In the batch reactor, however, the reactant was not renewed with time so that catalyst poisons or compounds that would cause fouling or coking were not replenished by continuous flow.

The effect of feed oil to catalyst ratio on the deposition of coke was studied. Data from the batch reactor and the CSTR was used. In the batch reactions the catalyst was exposed to a varying number of reaction/extraction cycles, from one to six. In all batch reaction series, the first reaction was of 0.5 h duration, while the remaining steps in all series were 1 h in duration. In batch experiments, the operating temperature was 430 °C and the initial hydrogen pressure was 13.8 MPa. The CSTR data represent reactions of varying total time. All CSTR experiments were performed at 430°C and 13.8 MPa hydrogen pressure. The data for the carbon concentration in the catalyst displayed in Figure 2.3 and tabulated in Table 2.2 and Appendix 2.1 show carbon concentration as a function of feed oil to catalyst ratio. The batch and CSTR data show a quick buildup of material to a constant value. The differing values between the batch experiments and CSTR experiments were likely due to the differences in the hydrogen partial pressures.

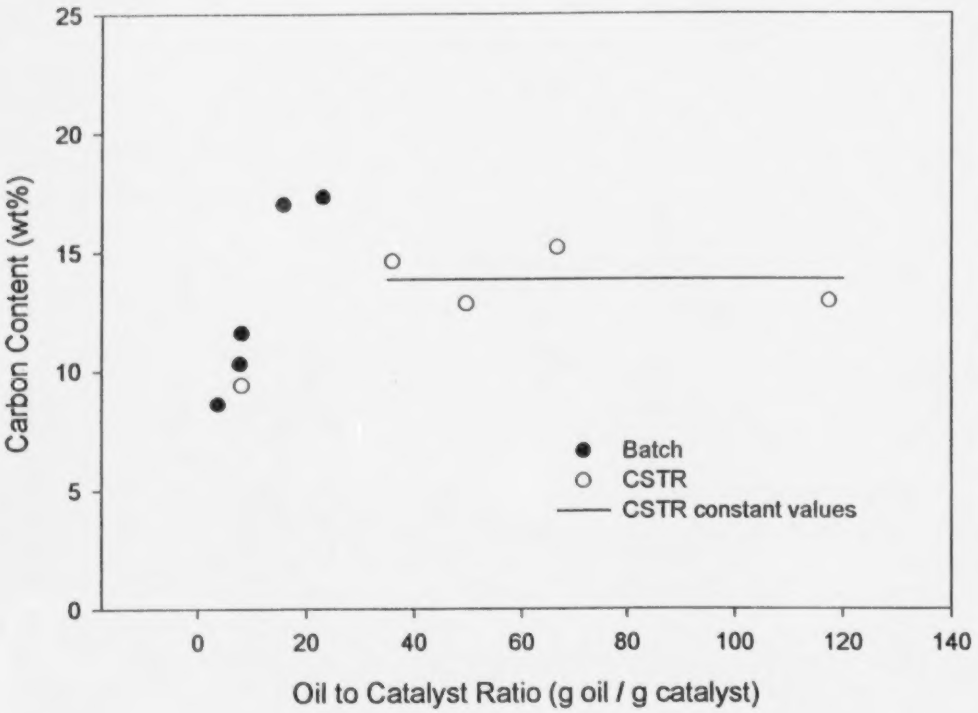

Figure 2.3: Carbon Content of Spent Catalyst as a Function of Cumulative Feed Oil to Catalyst Ratio. All experiments at 13.8 MPa, 430°C. Data for batch reactor are for repeated contacts of catalyst with fresh feed (see samples B1, B2, and B6 to B8 in Appendix 2.1), data for CSTR are from experiments C1,C2,C8,C13,C14 (Table 2.2).

The batch reactor gave catalyst with a constant carbon content between 15 and 20 g oil /g catalyst, while the carbon content of the catalyst in the CSTR reached a constant value at a feed ratio between 30 and 120 g oil /g catalyst.

2.3.2 Dependence of Coking on Residue Concentration

The CSTR reactor was operated to simulate multiple reactors in series with hydrogen makeup, producing products of varying residue contents, in the range 0.7 - 32% (Table 2.1). This repeated hydroprocessing gave two changes in liquid-phase composition; the concentration of residue was reduced and the residue composition was altered by prior reactions. The data for carbon content of the catalysts showed insensitivity to residue concentration at concentrations above 8% (Figure 2.4 and Appendix 2.2)). The concentration of carbon on the catalyst was plotted against product composition since the reactor was well stirred. Despite the number of compositional variables that were varied by successive cracking of the residue, carbon content of the catalyst was constant at 13 ± 1 % over the range of residue concentrations from 8 to 32 %. Carbon content was similarly insensitive to MCR concentration, with a constant carbon content over the range of 2 to 10 weight % MCR in the liquid product.

The effect of liquid composition on the composition of the carbonaceous substance (coke) deposited on the catalyst was investigated. The hydrogen to carbon atomic ratio was found to range between 1.0 and 1.2, with one outlying value at 1.78 (see Table 2.3). No systematic trend was observed between the residue content and the hydrogen to carbon ratio of the carbonaceous deposit on the catalyst. The analytical accuracy of the hydrogen analysis was ±0.2% absolute. Analysis was based on total catalyst weight and hydrogen contents were less than 2% in all cases, which gave an uncertainty in the hydrogen to

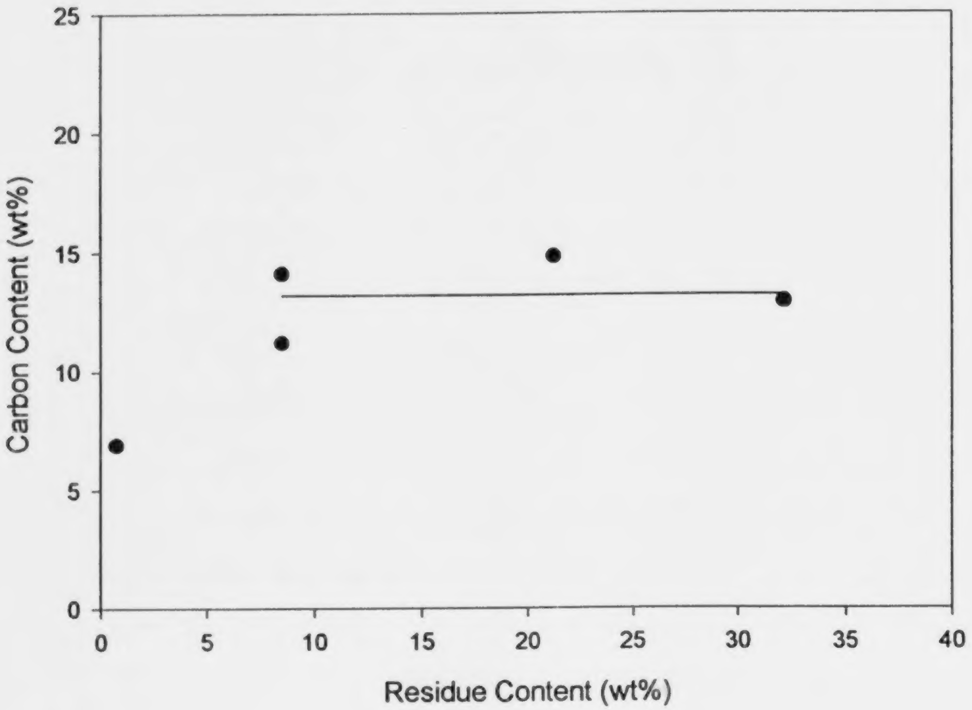

Figure 2.4: Carbon Content of Spent Catalyst as a Function of Residue Concentration in the CSTR. All experiments at 13.8 MPa, 430°C. The line represents the average carbon concentration observed at intermediate residue concentrations. (Data are from Runs C8 - C12, Table 2.2).

Table 2.3: Product Composition and Hydrogen to Carbon Ratios of Selected CSTR Catalysts. Sample numbers Refer to Table 2.2, which includes operating conditions.

Sample	Pressure (MPa)	Product Residue (wt%)	Product Residue H/C ratio	Product Sulfur (wt%)	Catalyst H/C Ratio
C3	6.9	n/a	n/a	n/a	0.83
C5	8.3	18.3	n/a	1.31	1.0
C4	10.3	n/a	n/a	n/a	0.99
C6	11.7	13.6	n/a	1.56	0.86
C7	15.2	20.1	n/a	1.31	1.23
C8	13.8	32.2	1.33	2.59	1.21
C9	13.8	21.3	1.22	1.57	1.01
C10	13.8	8.5	1.06	0.59	1.1
C12	13.8	0.7	1.18	0.12	1.78
C15	13.8	20.4	n/a	1.63	n/a

carbon atomic ratio of approximately 0.2. The variation in the C/H ratio was, therefore, within the range of analytical error. The outlying datum may have been due to unusually high levels of water adsorption, since the catalysts were not dried immediately before analysis, since at the time of analysis, hydrogen content was not being considered.

2.3.3 Dependence of Coke Deposition on Hydrogen Pressure

The hydrogen pressure in the CSTR was varied by changing the total pressure, keeping the gas flow rate (measured in standard liters) constant. The data for carbon content of the catalyst showed a small but analytically significant increase with decreasing hydrogen pressure, from 17.5 % carbon at 6.9 MPa to 11.3% carbon at 15.2 MPa (see Figure 2.5 and Table 2.2). Two points are included in this data set which have oil to catalyst ratios different from the standard. The experiment performed at 13.8 MPa (Run C2) had a greater oil to catalyst ratio than the standard conditions, but given the asymptote observed in Figure 2.3, the inclusion of this datum was justified. The 6.9 MPa experiment (Run

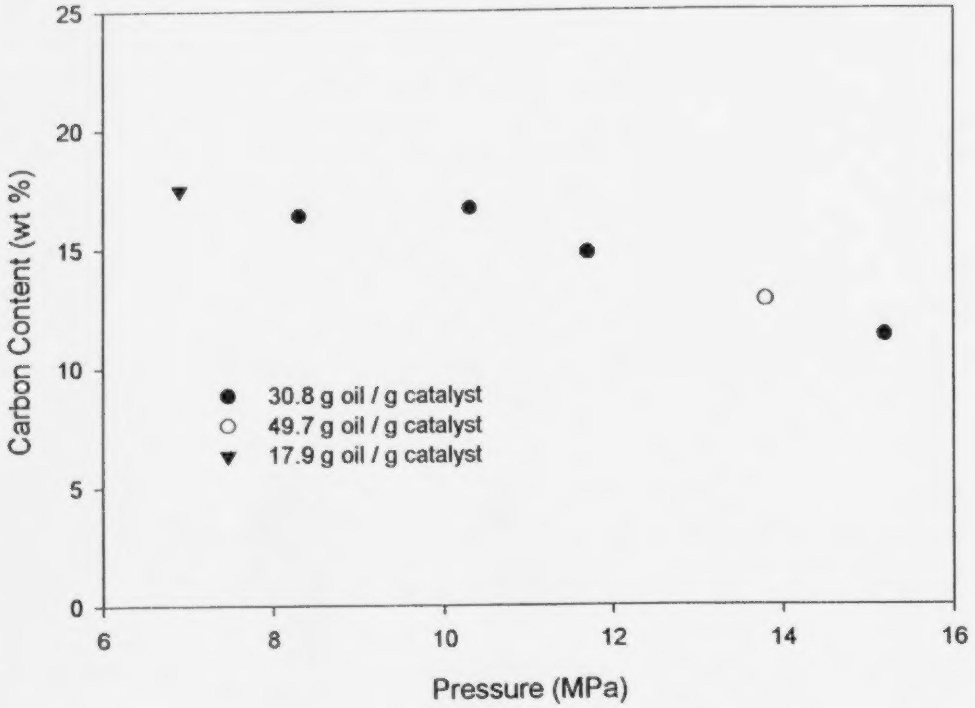

Figure 2.5: Carbon Content of Spent Catalyst as a Function of Hydrogen Pressure for CSTR Experiments. All experiments at 430°C. Data are available in Table 2.2 (Samples C3 to C7).

C3) had a lower oil to catalyst ratio than the standard. Although it is possible that this catalyst had not reached the final carbon content, the data of Figure 2.3 suggest that an oil / catalyst ratio of 17.9 g/g was sufficient to approach constant concentration, so the point was included in the figure and subsequent calculations.

The effect of hydrogen pressure on the hydrogen to carbon atomic ratio of the carbonaceous deposits formed on the catalyst was examined. No systematic change was observed for pressures ranging from 6.9 MPa to 15.2 MPa (see Table 2.3).

The data in Table 2.3 show a slight minimum in the hydrodesulfurization activity as a function of hydrogen pressure. This minimum may be real, or may reflect experimental variability, since the analysis alone has a varability of ±0.15% (absolute). In any case, the data do not reflect the expected increase in HDS activity with increasing hydrogen pressure. As the pressure increased from 8.3 MPa to 13.8 MPa, the sulfur concentration in the product increased from 1.31% to a maximum value of 1.63%. Three phenomena may have contributed to this result. The measured liquid hold-up in the reactor was constant over a wide range of operating conditions, including variations in pressure and product composition (Gray et al., 1995; Nagaishi et al, 1996). As the total pressure increased from 8.3 to 13.8 MPa, the partial pressure of the hydrocarbon species would remain constant while the hydrogen partial pressure increased. This would lead to a gas phase leaner in hydrocarbons. Since the molar flow rate of hydrogen is fixed, less hydrocarbon would be flushed from the reactor. This would cause higher liquid flow rate at reactor conditions at the same nominal feed rate. More liquid flow with constant hold-up would decrease the liquid residence time, giving decreased HDS with increasing hydrogen pressure. In opposition to this trend, higher hydrogen pressures produced catalysts with less coke deposits, which would increase the effective diffusivity of the residue in the catalyst. Higher diffusivities of residue components would give higher sulfur conversions as hydrogen pressure increased. The hydrogenation and hydrodesulfurization rates would increase with hydrogen pressure, with all other parameters held constant. The complex interaction of these opposing factors prevent a meaningful interpretation of the effect of hydrogen pressure on the HDS activity of the catalyst given the data available.

If one considers the data in Figure 2.3, the discrepancy between the batch data and CSTR data is easily explained. The batch reactors was charged with sufficient hydrogen to achieve an initial hydrogen pressure of 13.8 MPa. Since this reactor was operated in batch mode, hydrogen was consumed, causing a decrease in hydrogen partial pressure in the reactor. If one superimposes the data of Figures 2.3 and 2.5, an effective hydrogen pressure of approximately 10.3 MPa can be estimated for the batch experiments. This value is in agreement with literature values for hydrogen consumption in similar reactions (Beret and Reynolds, 1985; Gray, et al., 1991). The data for carbon content in the two reactors were consistent if the changes in hydrogen partial pressure in the batch reactor are taken into account.

An interesting coking phenomenon was observed during CSTR operation. During the CSTR experiment at 6.9 MPa hydrogen pressure, particulate coke was formed in the liquid phase, plugging the outlet lines from the reactor, causing premature shutdown. When the reactor was opened, no agglomerated coke deposits were observed and the carbon content on the catalyst was consistent with results at higher hydrogen pressures (Figure 2.5). As well, during the experiment at 11.7 MPa, a significant amount of coke was formed in the bottom of the reactor. The catalyst for this run was removed from the severely coked catalyst basket, but had a carbon content consistent with experiments at 13.9 and 10.3 MPa. These observations suggest that the coking mechanism in the liquid phase, probably linked to thermal cracking reactions, was quite distinct from the coking mechanism on the catalyst surface. If precipitation of asphaltenes was responsible for the coking of catalyst, as suggested by Absi-Halabi et al. (1991), then we would expect a linkage between deposition of carbon on the catalyst surface and coke formation in the liquid phase.

2.4 CONCLUSIONS

1. Total carbon concentration in the catalyst was independent of reaction time at times greater than one hour, when all other reaction parameters were held constant.
2. Total carbon concentration in the catalyst showed a rapid increase followed by a constant value when plotted versus the feed oil to catalyst ratio. Differences between CSTR experiments and batch experiments were attributable to the differences in the hydrogen partial pressure.
3. Total carbon concentration in the catalyst was independent of the residue content of the liquid phase above a threshhold level of approximately 8 % residue.
4. Carbon concentration in the catalyst decreased from 17.5% at 6.9 MPa hydrogen to 11.3% at 15.2 MPa.
5. Coke deposition on catalyst was not coupled to liquid phase coking reactions.

2.5 LITERATURE CITED

Absi-Halabi, M.; Stanislaus, A.; Trimm, D.L. Coke Formation on Catalysts During the Hydroprocessing of Heavy Oils. *Appl. Catal.* **1991**, 72, 193-215.

Aitken, A.R.; Merrill, W.H.; Pleet, M.P. Hydrogenation of a Coker Distillate Derived from Athabasca Bitumen. *Can. J. Chem. Eng.* **1964**, 234-238.

Anonymous. Standard Test Method for Distillation of Petroleum Products at Reduced Pressure. *1996 Annual Book of ASTM Standards: Section 5, Petroleum Products, Lubricants and Fossil Fuels.* **1996**, 05.01, 389-406.

Beaton, W.I.; Bertolacini, R.J. Resid Hydroprocessing at Amoco. *Catal. Rev. Sci. Eng.* **1991**, 33, 281-317.

Beret, S.; Reynolds, J.G. Hydrogen Incorporation in Residuum Conversion. *ACS Div. Pet. Chem. Preprints.* **1985**, 30, 664-671.

Douwes, C.T.; van Klinken, J.; Wiffles, J.B.; van Zijll Langhout, W.C.; "Developments in Hydroconversion Processes for Residues." *Proceedings of the 10th World Petroleum Congress, Bucharest,* **1979**, 4,175-183.

Furimsky, E. Chemical Origin of Coke Deposited on Catalyst Surface. *Ind. Eng. Chem. Prod. Des.* **1978**, 17, 329-331.

Gray, M.R.; Ayasse, A.R.; Chan, E.W.; Veljkovic, M. Kinetics of Hydrodesulfurization of Thiophenic and Sulfide Sulfur in Athabasca Bitumen. *Energy and Fuels.* **1995**, 9, 500-506.

Gray, M.R.; Jokuty, P.; Yeniova. H.; Nazarewycz, L.; Wanke, S.E.; Achia, U.; Krzywicki, A.; Sanford, E.C.; Sy, O.K.Y. The Relationship Between Chemical Structure and Reactivity of Alberta Bitumens and Heavy Oils. *Can. J. Chem. Eng.* **1991**, 69, 833-843.

Gregg, S.J.; Sing, K.S. Adsorption, Surface Area and Porosity, Academic Press, London, **1967**.

Hannerup, P.N.; Jacobsen, A.C. A Model for the Deactivation of Residual Hydrodesulfurization Catalysts. *ACS Div. Petrol. Chem.* **1983**, 28, 576-599.

Inoguchi, M.; Kaneko, Y.; Satomi, Y.; Inaba, K.; Kagaya, H.; Tate, K.; Mizutori, T.; Nishiyama, R.; Ota, T.; Niume, K. Studies of the Hydrodesulfurization Catalyst of Residual Fuels (Part 6). *Bull. Japan. Petrol. Inst.* **1972**, 14, 7-17.

Nagaishi, H.; Chan, E.W.; Sanford, E.C.; Gray, M.R. Kinetics of High Conversion Hydrocracking of Bitumen. Submitted to *Energy and Fuels*. **1996**.

Oballa, M.C.; Wong, C.; Krzywicki, A. "Catalyst Deactivation in Residue Hydrocracking", in Catalytic Hydroprocessing of Petroleum and Distillates, eds Oballa, M.C. and Shih, S. S., Marcel Dekker, Inc., New York, **1994**, 33-54.

Stohl, F.V.; Stephens, H.P. The Impact of the Chemical Constituents of Hydrotreater Feed on Catalytic Activity. *ACS Div. Pet Chem. Preprints*. **1986**, 31, 251-256.

Thakur, D.S.; Thomas, M.G.; Catalyst Deactivation in Heavy Petroleum and Synthetic Crude Processing: A Review. *App. Catal.* **1985**, 15, 197-225.

Zeuthen, P.; Cooper, B.H.; Clark, F.T.; Arters, D. Characterization and Deactivation Studies of Spent Resid Catalysts from Ebullating Bed Service. *Ind. Eng. Chem. Res.* **1995**, 34, 755-762.

CHAPTER 3 - MODEL FOR INITIAL COKE DEPOSITION

3.1 INTRODUCTION

The data presented in Chapter 2 describe the concentration of carbon in a hydroprocessing catalyst during the first few hours of operation. A mechanistic model to describe this phenomenon was developed. The model is a steady-state model; however, simple extension of the model satisfactorily decribes transient behaviour, especially the deposition of coke in response to total oil to catalyst ratio.

A decrease in coke accumulation with increasing hydrogen partial pressure has been observed previously; however, no mechanistic or empirical relation has been proposed for this phenomenon. Literature available on catalyst deactivation and coke deposition in other petroleum refining processes, such as fluid catalytic cracking, cannot be transferred to hydroprocessing of residue because of the high hydrogen pressure, the presence of a liquid phase and different catalyst chemistry. One of the barriers in accounting for the role of hydrogen is a lack of consensus on the chemical nature of carbonaceous deposits (coke) and their physical distribution within the catalyst. Many authors assume that coke on hydroprocessing catalyst closely resembles fluid coke, while others have demonstrated that the material is more complex (Diez, et al., 1990; Egiebor et al., 1989). In this study, experimental measurements of elemental carbon content are used as a surrogate for the total coke concentration. The nature of the observed carbonaceous deposits will be discussed in Chapter 4.

Two modes of coke deposition have been suggested within catalyst pellets: pore mouth plugging and uniform surface deposition. Muegge and Massoth (1991) studied effective diffusivity in catalysts which had been artificially coked with anthracene/n-heptadecane feeds. At extremely low coke deposition, on the order of 2-3 weight % carbon, effective diffusivity was significantly reduced. While their observations were consistent with plugging of pore mouths, their experiments may not have given the coke deposition one might expect from residue feeds.

Absi-Halabi et al. (1991) found that the initial coke deposition was most significant in the micropores. Coal liquefaction with a catalyst under comparable conditions gave almost complete loss of pore volume in pore of 2-5 nm radius with no loss of pore volume in pores in the 5-50 nm radius range (Thakur and Thomas, 1984). Because the ratio of surface area to pore volume is highest in the smallest pores, uniform deposition would give the largest deposition of coke in these pores. Ternan et al. (1979) studied coke deposition on molybdenum catalysts promoted with various cations. They measured constant values of carbon concentration per unit surface area for three aluminas of different surface area, indicating uniform surface coverage. No significant effect of promoter cation was observed. Using characteristics of fluid coke, they determined that the observed carbon content corresponded to 0.5 monolayers for gas oil hydroprocessing and 1.1 monolayers for Athabasca bitumen hydroprocessing. They observed 96% sulfur conversion after the deposition of 1.1 monolayers of coke and concluded this level of conversion was not consistent with complete loss of hydrogenation activity of the catalyst. The conclusion is supported by results from thermal experiments (Ayasse, 1994). Ternan et al. suggested that the coke deposited on the surface may be continuously exchanged with the bulk, in order to account for the observed activity of the catalyst in the apparent presence of a monolayer.

Diez at al. (1990) proposed that coke forms in a uniform layer on the γ-alumina support, but is thinner near the Ni-Mo metal crystallites due to their hydrogenation activity. As the amount of coke increases, however, the coke layer may occlude the active side surfaces of the metal crystallite, ultimately leading to a catastrophic loss of activity. Melo Faus et al. (1984) reacted model compounds over artificially coked Co / γ-alumina, CoMo / γ-alumina and Mo / γ-alumina catalysts, and found that isomerization decreased more rapidly than hydrogenation with increasing coke deposition. In coal liquefaction studies by Nishijima et al. (1987), hydrocracking activity was reduced more significantly than hydrogenation by increases in coke deposition. If coke was deposited primarily at the pore mouth, deactivation rates of catalyst functions are expected to be equal. Conflicting reports on the probable location of coke deposits in γ- Al_2O_3 hydroprocessing catalysts suggest, therefore, that the deposition process may depend on the compositions of feed and catalyst and the nature of the porous network.

3.2 EXPERIMENTAL

The molecular weight reported in this chapter for cracked Athabasca bitumen was determined by the Micro Analytical Laboratory at the University of Alberta using vapour pressure osmometry, with p-dichlorobenzene as a solvent. Other data are from Chapter 2.

3.3 MODEL DEVELOPMENT

3.3.1 The Monolayer Concept

Based on the data described in Chapter 2, a model must incorporate three observations: coke deposition on catalyst that approaches a constant value with increasing feed oil to catalyst ratio, the decrease in coke deposition with increasing hydrogen pressure and the insensitivity of the carbon concentration to composition in the reactor and reaction time.

During the experiments described in Chapter 2, the total carbon content of the catalyst never exceeded 18%. In the data shown in Figure 2.3, a constant value of carbon content on the catalyst with respect to feed oil to catalyst ratio was observed for both batch and CSTR experiments. At the reduced hydrogen partial pressure in the batch reactor, carbon content reached approximately 18%, but did not exceed it. In the study of the effect of hydrogen pressure on carbon content of the catalyst, the maximum carbon content was observed at the lowest pressure at which experiments were performed, 6.9 MPa. At this pressure, it was not possible to maintain reactor operation for the desired period, because of bulk liquid phase coking. Despite this precipitation of coke from the fluid phase downstream of the reactor, the carbon content of the catalyst within the reactor again did not exceed 18%.

This consistent approach to a maximum carbon content prompted the question: Could the maximum amount of carbon correspond to monolayer coverage by residue molecules? Since the coke had a H/C atomic ratio well above petroleum coke materials (Chapter 2), use of residue properties to estimate monolayer coverage was a reasonable approximation. The residue fraction of hydroprocessed Athabasca bitumen had a measured molecular weight of 625 Da, by vapour pressure osmometry and a typical bulk liquid density of 1050 kg/m^3 (Gray, 1994). Given these values, the radius for a typical residue molecule would be given by:

$$r_r = \left(\frac{3MW}{NA\rho 4\pi}\right)^{1/3} \qquad 3.1)$$

where r_r is the radius of a residue molecule (m), MW is the molecular weight (Da), NA is Avogadro's number (6.02 x 10^{26} molecules / kmol) and ρ is the density of oil (kg/m^3). This calculation gave a molecular radius of 0.6 nm. Given that residue would contain a continuum of molecule sizes, and the molecules will be deformable, one can assume that there is 100% coverage of the surface. The carbon content at monolayer coverage is given by:

$$M_{max} = \frac{MWx_c}{Na\pi r_r^2} \qquad 3.2)$$

where M_{max} is the maximum carbon concentration (g carbon / m^2 of surface) and x_c is the mass fraction of carbon in the residue (0.82 was used as a typical value). Substituting the properties of Athabasca residue into equations 3.1 and 3.2 gives a predicted surface concentration of 7.1 x 10^{-4} g carbon / m^2. The maximum concentration observed in experiments was 18% carbon, corresponding to a surface concentration of 6.9 x 10^{-4} g carbon / m^2, consistent with the hypothesis of monolayer coverage of the catalyst surface by molecules similar to the residue. This value could be corrected for the surface area occluded by the metal crystallites since coke is not expected to deposit on the crystallites. The model which follows predicts that this correction would be between 10%, while the independent calculation of the "b" parameter from literature dispersion data (see Appendix 3.3) predicts a vlaue of 3%. Given the small magnitude of the correction, and the uncertainty of the value, this correction was not made. When this calculation was repeated for benzene and graphite (Appendix 3.1), the variation in predicted carbon content of the catalyst was less than a factor of two. The sensitivity of the predicted carbon content on the catalyst due to monolayer coverage of residue, was determined as a function of residue properties (Appendix 3.2). Changing the residue density by 10% resulted in a 10% change in the monolayer carbon content. Similarly, changing the assumed carbon content of the adsorbed molecules from the base case of 82% to values of 80% and 85% resulted in only a 3% change in the carbon content of the monolayer. Increasing the assumed molecular mass from 625 (measured) to 1000 Da caused an increase of 17% in the predicted carbon content of a monolayer. The detailed results are tabulated in Appendix 3.2. Despite these large changes in residue properties, outside the bounds of normal petroleum chemistry, changes in the predicted carbon content were relatively small. It should be noted that the asphaltenes present in the reactor liquids may flocculate. This situation was not explicitly taken into account since the asphaltene flocs would be too large to enter the pore structure of the catalyst. If flocculation occurred, asphaltene micelle structures in the liquid would equilibrate with dissociated molecules; these dissociated asphaltenes would be able to diffuse into the catalyst.

The hydrogen to carbon atomic ratio for the residue fraction of the liquid ranged from 1.0 to 1.3 (see Table 2.3). The corresponding spent catalysts had hydrogen to carbon ratios ranging from 1.0 to 1.2 (ignoring the extreme datum). Given the accuracy of the analysis, these values were consistent with the hypothesis that the deposited carbonaceous substance was similar to the residue fraction of the oil.

3.3.2 The Steady State Model

The data showed a weak but definite downward trend in carbon concentration with increasing hydrogen pressure (Figure 2.5). Diez et al. (1990) hypothesized that a zone near the metal sulfide crystallites would have a reduced carbon content due to the hydrogenating activity of the crystallites. Extending their model, we propose as a simplifying approximation that the active hydrogen species formed by metal crystallites will clear an annular zone on the alumina surface, as illustrated in Figure 3.1. Outside of

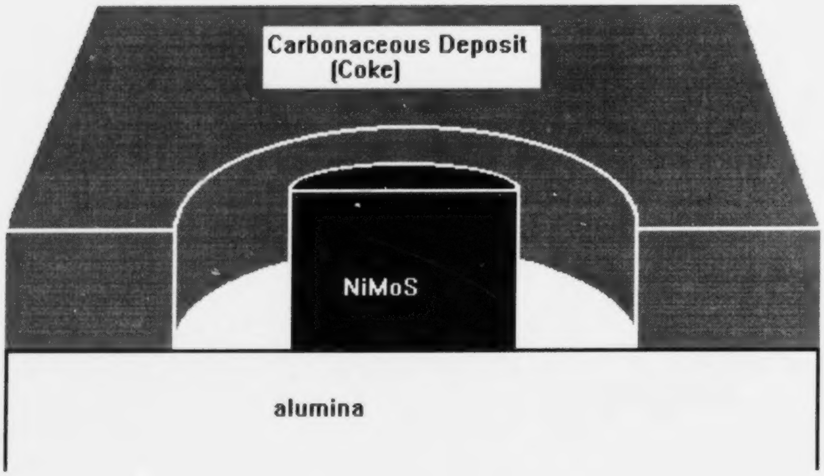

Figure 3.1: Schematic Representation of Catalyst Surface, Showing a Cross Section through the Metal Crystallite.

the cleared zone, the carbonaceous layer is of uniform thickness due to monolayer adsorption. Inside the cleared zone, any adsorbed material, i.e. coke, is immediately removed by the activated hydrogen species produced at the metal crystallite, so that no carbon remains on the surface. It is assumed that coke will not deposit on the top of the metal crystallite, therefore the maximum coverage should be corrected for this area. The distance to the boundary of the cleared zone is determined by the surface flux of hydrogen species from the metal crystallite, so that the alumina will remain clear if the surface flux is greater than a critical value.

From the geometry illustrated in Figure 3.1, the actual surface concentration on the surface as a function of the size of the cleared zone will be given by:

$$M = M_{\max}\left(1 - N\pi\left(r^2 - r_c{}^2\right)\right) \qquad 3.3)$$

where M is the actual surface concentration (g carbon / m^2), r_c is the radius of the metal crystallite (m), N is the number of crystallites (crystallites / m^2) and r is the radius of the cleared zone (m).

Generation of surface hydrogen at the crystallite is assumed to be proportional to hydrogen pressure. This assumption will be discussed following the development of the model. The rate of hydrogen leaving the cleared region by surface diffusion into the adsorbed monolayer will be the product of the critical flux of hydrogen and the circumference of the cleared zone. This assumption that hydrogen diffuses across the alumina surface is consistent with the literature on hydrogen spill-over from metal crystallites (Paal and Menon, 1988; Kapoor, et al., 1989). Diffusion of hydrogen away from the catalyst surface into the liquid in the pores would result in an additional sink term in the mass balance However, this diffusion into the bulk should be proportional to the production of activated hydrogen at the crystallite, which in turn is proportional to the hydrogen pressure. Therefore the net production of surface hydrogen is proportional to hydrogen pressure, even if hydrogen escapes the surface. Since hydrogen which has left the catalyst surface will not participate in coke removal, the magnitude of this effect is not important.

The rate of reaction of hydrogen within the annular zone will be equal to the rate of deposition of hydrocarbon times an unknown stoichiometric ratio for the reaction of hydrocarbon and hydrogen species, times the area of the zone. The mass balance on hydrogen for the annular zone, therefore, is given in equation 3.4.

$$kP_{H_2} - 2\pi r\ F_{crit} - \pi\left(r^2 - r_c^{\ 2}\right)\sigma k_d C_p = 0 \qquad 3.4)$$

where k is the rate constant for production of surface hydrogen, P_{H2} is the pressure of hydrogen (MPa), F_{crit} is the critical surface flux of hydrogen (mol/ms), σ is the stoichiometric coefficient for reaction of surface hydrocarbon with hydrogen, k_d is the deposition coefficient for hydrocarbon (m^{-1}) and C_p is the concentration of coke precursor (mol/m^2).

Solving equation 3.3 for r, then substituting into 3.4 and simplifying, gives a function of the form:

$$P_{H_2} = a\left(1 - \frac{M}{M_{max}} + b\right)^{1/2} + c\left(1 - \frac{M}{M_{max}}\right) \qquad 3.5)$$

where a, b and c are functions of the parameters from equations 3.3 and 3.4.

$$a = \frac{2\pi^{1/2}F_{crit}}{kN^{1/2}}$$

$$b = N\pi r_c^2$$

$$c = \frac{\sigma k_d C_p}{kN}$$

In this form, the first term of the equation includes the production of hydrogen at the crystallite and the hydrogen leaving by surface diffusion. The second term gives the consumption of hydrogen necessary to maintain the cleared surface, i.e. the pressure of hydrogen to remove carbon which deposits in the cleared region.

Equation 3.5 was fitted to the data from Runs C2 through C7 using the least squares method. The equation gave a good fit to the data. The regression results are shown as Model 1 in Table 3.1, and the resulting curve is shown in Figure 3.2. The regression, however, predicted a negative value for c, indicating a negative reaction rate. Since a negative value for c was physically meaningless, the parameter estimation was repeated using the form shown below in equation 3.6, in which the second term was deleted. The total residual for this fit had only increased slightly, despite the removal of one adjustable parameter. Consequently, if the hydrogen consumption within the annulus is negligible (c=0), the following model equation is consistent with the data:

$$P_{H_2} = a\left(1 - \frac{M}{M_{max}} + b\right)^{1/2} \qquad 3.6)$$

The results of this regression are shown as Model 2 in Table 3.1 and Figure 3.2.

The value of parameter b in equation 3.6 is given by:

$$b = \pi N r_c^2 \qquad 3.7)$$

Table 3.1: Estimated Parameters for Alternative Models for Coke Deposition. Models are defined below.

		Model Number and Regression Parameters			
		Model 1 a = 22.5 b = 0.089 c = -0.40 Sum of Errors Squared = 3.144	Model 2 a = 22.2 b = 0.09 Sum of Errors Squared = 3.148	Model 3 a = 6.93 b = 0.146 c = -2.90 Sum of Errors Squared = 3.36	Model 4 a = 4.68 b = 0.34 c= 2.0e-8 Sum of Errors Squared = 3.73
Carbon Surface Concentration ($g\ C / m^2$)	Experimental Pressure (MPa)	Predicted Pressure (MPa)			
0.00109	6.9	7.1	7.1	7.4	7.5
0.00100	8.37	9.5	9.4	9.6	9.3
0.00102	10.3	9.0	9.0	9.2	8.9
0.00090	11.7	11.6	11.6	11.8	11.2
0.00078	13.8	13.7	13.7	13.9	13.6
0.00069	15.2	15.1	15.2	15.3	15.4

Model Definitions:

Model 1: Assumes that the production of active hydrogen species on the catalyst surface is proportional to the hydrogen pressure:

$$P_{H_2} = a\left(1-\frac{M}{M_{max}}+b\right)^{1/2} + c\left(1-\frac{M}{M_{max}}\right)$$

Model 2: Assumes that the production of active hydrogen species on the catalyst surface is proportional to the hydrogen pressure and the surface reaction rate is negligible compared to the production and surface flux terms:

$$P_{H_2} = a\left(1-\frac{M}{M_{max}}+b\right)^{1/2}$$

Model 3: Assumes that production of active hydrogen species on the catalyst surface is proportional to ${P_{H_2}}^{1/2}$:

$${P_{H_2}}^{1/2} = a\left(1-\frac{M}{M_{max}}+b\right)^{1/2} + c\left(1-\frac{M}{M_{max}}\right)$$

Model 4: Assumes that production of active hydrogen species on the catalyst surface is proportional to ${P_{H_2}}^{1/2}$. Regression constrained to $c>0$ to reflect physically meanginful chemistry. Equation as in Model 3.

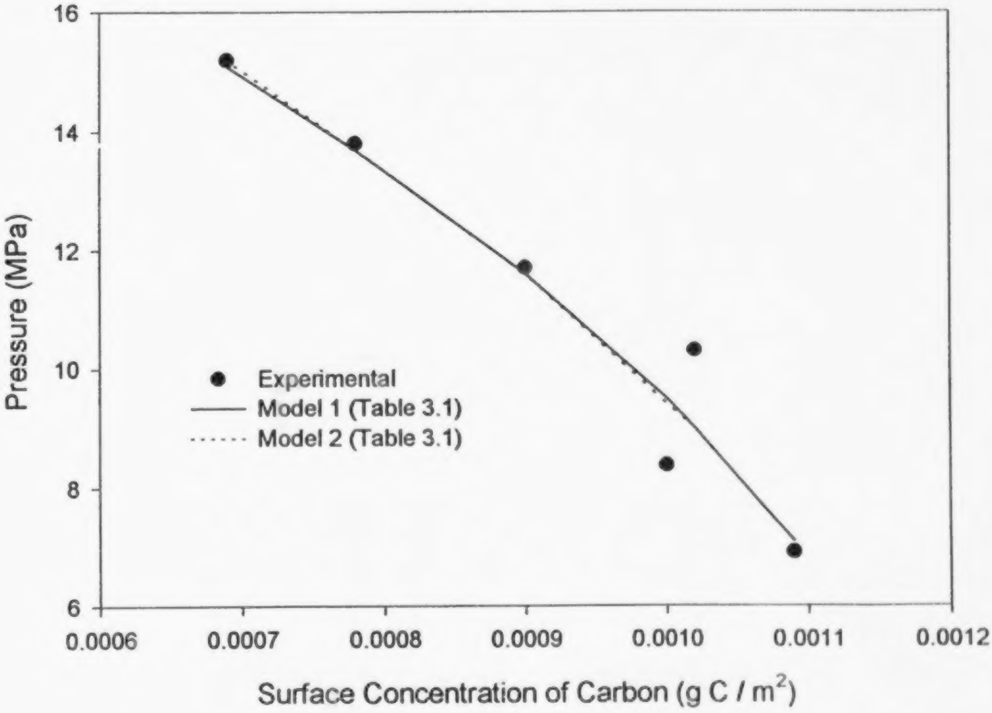

Figure 3.2: Surface Concentration of Carbon as a Function of Hydrogen Pressure (Models 1 and 2). Figure shows experimental data, and the curves fitted to Models 1 and 2, as defined in Table 3.1.

Data for the size of crystallites from the work of Madeley and Wanke (1986) for a similar sulfided Ni Mo catalyst predicted that the fractional coverage of the alumina surface with metal crystallites, b = 0.036 m^2 metal / m^2 surface for our catalyst (see Appendix 3.3), compared to 0.09 m^2 metal / m^2 surface from the regression of the model to the experimental data. The value for parameter b from the regression was, therefore, of the same order as one would expect from experimental data. As discussed previously, the total catalyst surface area could be corrected by the above values to determine the alumina surface area.

Alternate functional forms for the surface hydrogen production term were considered. These included production α $P_{H2}^{1/2}$ and production rate independent of hydrogen pressure (zero order). The latter situation would result if the hydrogen pressure were high enough to saturate the catalyst surface with hydrogen at the lowest pressure used in the experiments. The regression results for the former case are shown as Model 3 in Table 3.1 and in Figure 3.3. The fit is similar to that obtained by fitting equations 3.5 and 3.6. The regression results, however indicate that a relatively large (compared to a) negative value for c was required to fit the data. This negative value contradicts the physical meaning of the parameter. If the value of c is constrained to values greater than 0, the curve becomes slightly concave up, inconsistent with the experimental data which indicated a concave down trend (see Figure 3.3, Model 4). If one assumes that the catalyst is saturated, i.e. the production rate of the active hydrogen species is independent of the bulk hydrogen pressure, a vertical curve results, as shown as Model 5 in Figure 3.3. This result is clearly inconsistent with the data. These results indicated that equation 3.4, based on first order production of active hydrogen as a function of the hydrogen pressure, gave the best fit to the data.

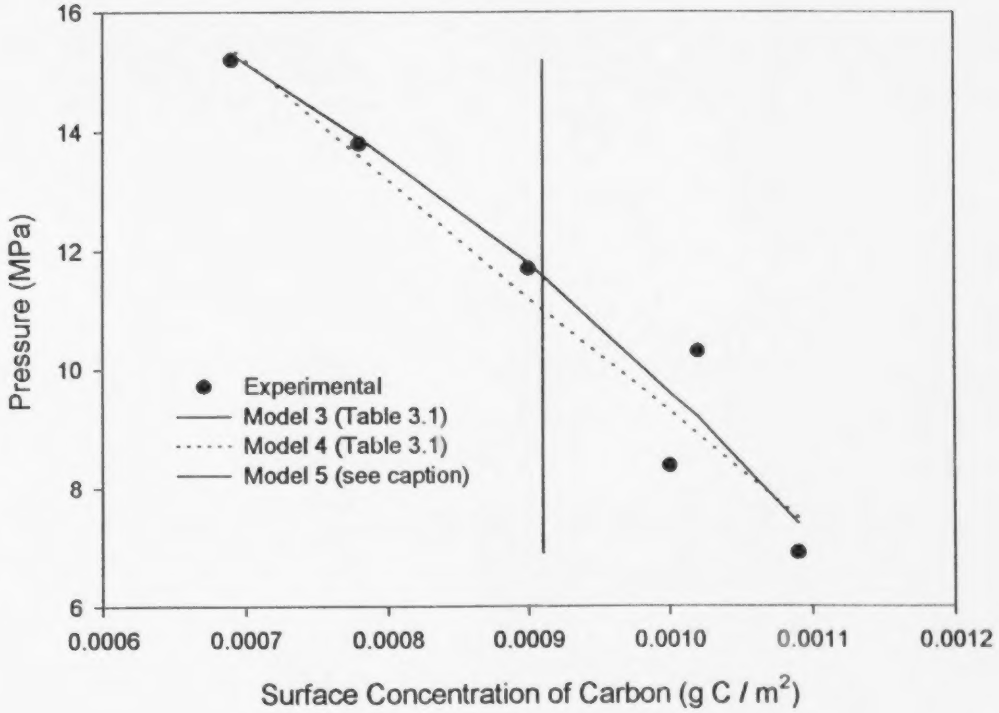

Figure 3.3: Surface Concentration of Carbon as a function of Hydrogen Pressure. Figure shows experimental data, and the curves fitted to Models 3 and 4, as defined in Table 3.1. Figure also shows the results of Model 5, as described in the text. It assumes that production of active hydrogen species is independent of hydrogen pressure.

3.3.3 Transient Deposition of Coke

The model developed above, which assumes that residue adsorbs to form a monolayer, predicts that the maximum carbon coverage on the catalyst surface is limited at a given hydrogen pressure and temperature. For the purposes of modelling, this maximum coverage can be represented by a number of "sites". The rate of adsorption will depend on surface vacancies as follows:

$$r_{dep} = -\frac{d\theta_v}{dR} = k\theta_v \qquad 3.8)$$

where r_{dep} is the rate of carbon deposition, θ_v is the fraction of possible adsorption "sites" currently vacant, R is the cumulative feed to catalyst ratio (g feed / g catalyst), a pseudo time coordinate and k is an adsorption rate constant (g catalyst / g feed).The concentration of carbon on the catalyst (expressed at weight percent carbon) (C) would be related to the maximum carbon concentration (C_{max}) and θ_v as:

$$\frac{C}{C_{max}} = 1 - \theta_v \qquad 3.9)$$

Substitution of equation 3.9 into equation 3.8 and solving gives equation 3.10, which indicates that the build-up of carbon will follow first-order kinetics:

$$C = C_{max}\left(1 - e^{-kR}\right) \qquad 3.10)$$

Figure 3.4 shows the results of a least squares non-linear regression through the batch data first shown in Figure 2.3 The resulting parameters are C_{max} = 18.6 % carbon and k = 0.15 (g cat / g feed). The units for k appear unusual, but stem from the use of R as the pseudo time co-ordinate, with units of g feed / g catalyst. If an effective feed rate was defined for the batch sequential experiments, then an alternate form of equation 3.11 could be written with time as the independent variable. Good agreement was obtained between the data and the model. Below approximately 15 g oil / g catalyst, the full monolayer was not developed and capacity remained for further adsorption. Beyond this value of feed oil to catalyst ratio, there would be reversible exchange of surface hydrocarbon with bulk hydrocarbon, but since the layer was filled, no net change in carbon content was observed.

3.3.4 The Model Predictions for Other Reaction Parameters

The regression results shown in Table 3.1 indicate that the data can be equally well represented by a model which includes a dependency on feed composition as one from which the dependency has been removed (i.e. equation 3.5 versus equation 3.6). The result indicated there was not a strong dependence of surface coverage on the concentration of coke precursors in the liquid. Experimentally, the carbon concentration was very insensitive to composition (see Figure 2.4). Only when the residue concentration fell to 1% of total liquid product did the carbon concentration on the catalyst decrease significantly. This observation may have been due to limitations on the amount of adsorbate available. In Run C12, the catalyst was only exposed to sufficient residue in the reactor liquids during the entire experiment to form a monolayer. Under these conditions, a monolayer would not have been achieved unless the capture of residue by adsorption was 100% efficient.

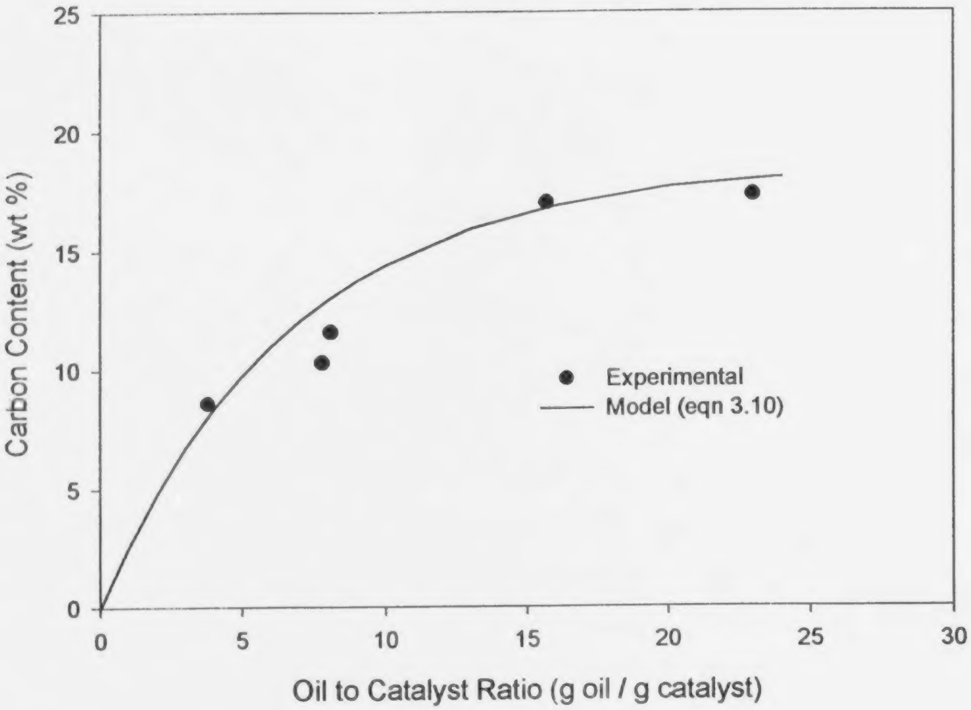

Figure 3.4: Carbon Concentration in Spent Catalyst as a Function of Cumulative Feed Oil to Catalyst Ratio in the Batch Reactor. All experiments at 13.8 MPa, 430°C. Model shown is per equation 3.10, where C_{max} = 18.56 (wt%) and k = 0.15 (g cat/ g bitumen) .

The insensitivity of the carbon content to reaction time, as presented in Chapter 2, suggests that the adsorption of the oil onto the catalyst surface occurs within 0.5 h at operating conditions.

3.4 COMPARISON OF MODEL TO LITERATURE DATA

The general literature on catalyst coking was described in Sections 2.1 and 3.1. Despite the possible significance of the effect of hydrogen on catalyst coking, very little systematic study has been dedicated to this issue. Zeuthen et al. (1995) studied a three stage pilot plant, in which they observed higher carbon concentrations on the third stage catalyst at the end of run. Because the series of reactors was operated without hydrogen makeup, the third stage would contain a lower hydrogen partial pressure, and should accumulate higher carbon contents based on the present model. The authors observed a phenomenon similar to breakthrough during the early portion of the run when the third bed accumulated coke more slowly than the first bed. During accumulation of the coke on the first bed, the supply of coke precursors to the third bed was reduced, causing a slower rate of accumulation. These observations are consistent with the model presented in this chapter.

3.5 CONCLUSIONS

A model for coke deposition in hydroprocessing catalysts was presented in this chapter. The model was based on an annulus structure around active metal crystallites, a schematic of which appears in Figure 3.1. This model suggested that a monolayer of residue molecules was adsorbed onto the alumina support, except in the immediate vicinty of the active metal crystallites, which maintained a clear alumina surface. The model predicted transient coke accumulation behaviour observed with respect to oil to catalyst ratio and was consistent with observed insensivity of the catalyst carbon concentration to reaction time and feed composition.

3.6 LITERATURE CITED

Absi-Halabi, M.; Stanislaus, A.; Trimm, D.L. Coke Formation on Catalysts During the Hydroprocessing of Heavy Oils. *Appl. Catal.* **1991**, 72, 193-215.

Ayasse, A. Hydrocracking of Athbasca Bitumen. MSc Thesis, University of Alberta, 1994.

Diez, F.; Gates, B. C.; Miller, J.T.; Sajkowski, D.J.; and Kukes, S. G. Deactivation of a Ni-Mo / γ-Al_2O_3 Catalyst: Influence of Coke on the Hydroprocessing Activity. *Ind. Eng. Chem. Res.* **1990**, 29, 1999-2004.

Egiebor, N.O.; Gray, M.R.; Cyr, N. ^{13}C-NMR Characterization of Organic Residues on Spent Hydroprocessing, Hydrocracking, and Demetallization Catalysts". *Appl. Catal.* **1989**, 55, 81-91.

Gray, M. R. Upgrading Petroleum Residues and Heavy Oils, Marcel Dekker, Inc., New York, **1994**.

Kapoor, A.; Yang, R.T.; Wong., C.; Surface Diffusion. *Catal Rev. Sci. Eng.* **1989**, 31, 129-214.

Madeley, R.; Wanke, S. E. "Characterization of (Ni-Mo)/Al_2O_3 Catalysts by X-ray Diffraction", *PREPRINTS Tenth Canadian Symposium on Catalysis, Kingston, Ontario, (June 15 - 18, 1986).* **1986**, 134-143.

Melo Faus, F.; Grange, P.; Delmon, B. Influence of Asphaltene Deposition on Catalytic Activity of Cobalt Molybdenum on Alumina Catalysts. *Applied Catal.* **1984**, 11, 281-293.

Muegge, B.D.; Massoth, F.E.; Basic Studies of Deactivation of Hydrotreating Catalysts with Anthracene. *Fuel Proc. Tech.* **1991**, 29, 19-30.

Nishijima, A.; Shirada, L.T.; Yoshimura, Y.; Sato, T.; Matsubayashi, N. Deactivation of Molybdenum Catalysts by Metal and Carbonaceous Deposits During the Hydrotreating of Coal-Derived Liquids and Heavy Petroleums. in Catalyst Deactivation Elsevier, Amsterdam. **1987**, 39-43.

Paal, Z.; Menon, P.G. Hydrogen Effects in Catalysis, Fundamentals and Practical Applications, Marcel Dekker, New York. **1988**.

Ternan, M.; Furimsky, E.; Parsons, B.I. Coke Formation of Hydrodesulfurization Catalysts. *Fuel Proc. Tech.* **1979**, 2, 45-55.

Thakur, D.S.; Thomas, M.G.; Catalyst Deactivation During Direct Coal Liquefaction: A Review. *Ind. Eng. Chem Prod. Res. Dev.* **1984** 23, 349-360.

Zeuthen, P.; Cooper, B.H.; Clark, F.T.; Arters, D. Characterization and Deactivation Studies of Spent Resid Catalysts from Ebullating Bed Service. *Ind. Eng. Chem. Res.* **1995**, 34, 755-762.

CHAPTER 4 - VALIDATION OF THE MODEL

4.1 INTRODUCTION

The model presented in Chapter 3 describes a catalyst surface which is covered with a carbonaceous substance, except in the vicinity of the metal sulfide crystallites. This model does not predict the nature of the carbonaceous deposit or the nature of the interaction between the deposit and the surface. As well, the possibility of alternate coke deposition geometries has not been ruled out. The experiments described in this chapter were designed to probe the nature of the coke deposit and its geometry.

4.1.1 The Chemistry of the Carbonaceous Deposit

The current literature does not fully address the chemistry of the coke deposit on hydroprocessing catalyst surfaces. Many authors (e.g. McKnight and Nowlan, 1993; deJong et al., 1994), describe the carbonaceous deposit as being highly condensed polynuclear aromatics, similar in nature to solid petroleum coke. Chu et al. (1994) compared the coke deposited from an anthracene solution to that deposited from a residue solution, and did observe differences between the coke in the two cases, but ascribed it to physical differences (porosity) instead of possible chemical variations. Only Ternan et al. (1979) suggested that the coke may be a mobile, less condensed phase. Definition of coke chemistry is further complicated by the comparison of coke deposits of radically different ages, ranging from several hours (Chu et al., 1994) to several weeks (McKnight and Nowlan, 1993, deJong et al., 1994, Zeuthen et al., 1995). The nature of the "coke" being reported also varies greatly depending on the preparation of the catalyst sample prior to analysis and the type of analysis performed. Obviously a catalyst sample washed with toluene, air dried and analyzed by loss on ignition would report a significantly different "coke" content than one which was Soxhlet extracted in dichloromethane, vacuum dried and analyzed for elemental carbon content. Knowing the nature of the deposited coke is important, because a highly condensed polynuclear aromatic deposit would be expected to be irreversibly adsorbed on the catalyst surface. This type of adsorption would lead to very different behaviour of the deposit, and would preclude many strategies for coke removal and coking prevention.

4.1.2 Nature of the Carbon - Surface - Interaction

One of the important features of the alumina support is its inherent acidity. This acidity results from the asymmetry of the atoms at the surface of the solid alumina, and imperfections in the alumina structure. Given the acidic nature of the alumina, and the basic components in the feed, an acid-base interaction is assumed to be the first step in coke deposition. Absi-Halabi et al. (1991) emphasized the importance of acid-base interactions in coking of hydrocracking catalysts, while Korre et al. (1995) determined that adsorption of polyaromatic hydrocarbons on a CoMo / γ- Al_2O_3 catalyst surface was correlated to the gas phase basicity of the component. Other possible effects of support acidity are discussed in detail in Chapter 6.

4.1.3 Distribution of Carbon on Catalyst Surface

The model proposes a structured arrangement of coke, or carbonaceous deposits, on the catalyst surface. Verification of this structure is desired, however "observation" of the catalyst surface at nanometer resolution was not possible. Surface spectroscopic techniques such as X-ray Photoelectron Spectroscopy (XPS) or Secondary Ion Mass Spectrometry (SIMS) could provide surface measurements of overall aluminum concentration from which it mght be possible to infer an annular structure. Tunneling Electron Microscopy might be able to resolve the surface structure. For both surface spectroscopy and microscopy, however, catalyst preparation involves two fundamental complications. Observation of the catalyst would be complicated by artifacts particular to the exterior of a pellet or granule, which would not be observed on internal surfaces. Fracturing the pellet to obtain a cross section would expose alumina which had not been part of the surface during reaction, thus obscuring the results. Also, since the pellets are made up of a compressed powder, the pellet would be expected to fracture between these powder partices, exposing very limited amounts of micropore structure, which is primarily found within the powder particles. Since surface polishing is required before some forms of analysis, fine detail would be lost. For these reasons, surface spectroscopic and microscopic techniques are of limited use in validating the proposed annular structure of carbonaceous deposits.

Since the alumina surface has a range of strengths of acid sites, analysis of this distribution will provide some information about the surface. Chapter 3 showed that the coke likely deposits in a monolayer at the maximum carbon concentration observed in this study. Given this assumption of maximal coverage, carbon concentrations less than the maximum value can only be achieved if the monolayer is incomplete. This partial coverage can be achieved in two basic ways: a structured pattern of openings as in Figure 3.1, or random gaps in the monolayer without any association with metal crystallites. Given the acid-base interactions one expects between the surface and the oil, a randomly deposited coke layer (with respect to crystallites) would be expected to deposit on the strongest acid sites first. If a moderately coked catalyst shows more very strong acid sites than a highly coked catalyst, then this observation would support a structured carbonaceous surface because random adsorption of bases would preferentially fill strong acid sites. It cannot be verified that the surface structure consists of annuli around the metal crystallites, but the hydrogenation activity of the metal crystallites is expected to repress condensation reactions in the neighbourhood of the crystallite, thus resuting in less coke deposited in the region nearest the crystallite.

4.1.4 Proposed Validation Experiments

A group of experiments was designed to evaluate some of the issues discussed above. The reversibility of coke deposition was examined by evaluating the effect of treatment with tetralin and coker gas oil on carbon concentration in the catalyst. The importance of acid-base interactions in the deposition of coke on the catalyst surface was studied through the use of model compounds of varying basicities in solution, as well as deasphalted oil. The possible annular structure of the deposited coke was investigated by analyzing the distribution of strengths of acid sites of fresh, moderately coked and highly coked catalysts.

4.2 EXPERIMENTAL

4.2.1 Materials

Athabasca bitumen was provided by Syncrude Canada Ltd., with the properties listed in Table 2.1. Coker gas oil (CGO) was supplied by Syncrude, with properties described in Yui and Sandford (1991). Tetralin (99%) was supplied by Fluka, carbon disulfide (99.9%) and acridine (99%) were supplied by Aldrich, anthracene (98%) was supplied by Sigma and dibenzofuran (95%) was supplied by Eastman Kodak. The dibenzofuran was purified by dissolving the chemical in dichloromethane, mixing with activated carbon, filtering the solution and recrystallizing the dibenzofuran.

The catalyst was a commercial NiMo /γ-Al_2O_3 catalyst with 12.5 wt % MoO_3 and 3.5 wt % NiO. The catalyst had a surface area of 317 m^2/g and a pore volume of 0.57 mL/g (see section 2.2.2 for analytical details). The catalysts were not presulfided prior to use. For the batch experiments the catalyst was crushed and sieved to +350µm -500µm size. In the CSTR experiments, the catalyst was used in the 1 mm cylindrical extrudate form in which it was delivered.

4.2.2 Model Feed Preparation

One sequence of experiments was performed with deasphalted oil. Athabasca bitumen was mixed with a volume of toluene (in mL) equal to the weight of bitumen (in g), then diluted with 50 volumes of pentane. The sample was shielded from light and stirred for 16 h. The precipitate was removed using a Millipore filter. The liquid portion was dried to constant weight, using a rotary evaporator and vacuum drying at 65°C and 0.01 MPa.

Three model compounds were chosen based on their basicity. Acridine was chosen as a highly basic compound, anthracene was chosen as a neutral analog and dibenzofuran was included as a slightly basic analog. The model compounds were prepared for reaction by mixing the desired amounts of the model compound with tetralin. The concentrations are given in Table 4.1. These concentrations were chosen based on expected coke deposition and the number of planned reaction steps. In the case of anthracene, a suspension of solid in tetralin resulted. A sample of this suspension was brought to the reaction temperature of 430°C, then cooled. Inspection of the liquid showed that the suspension remained, but had become extremely finely dispersed. The redispersion of the anthracene indicated that a solution had formed at operating conditions then reprecipitated upon cooling. One sequence was performed with acridine in 1-methylnaphthalene to explore possible solvent

Table 4.1: Model Compound Feed Experiments in Batch Reactor with 1 h Reaction Time Per Step at 430 °C and 13.8 MPa

Feed	Catalyst (Initial Carbon Content %)	Number of Reaction Steps	Final Carbon Content (%)
Tetralin (Blank)	Fresh (0)	5	2.6
Tetralin	Spent (17.5)	1	11.1
Tetralin	Spent (17.5)	6	6.6
Coker Gas Oil	Spent (17.5)	2	11
2.5 % Anthracene in Tetralin	Fresh (0)	6	1.3
3.2 % Dibenzofuran in Tetralin	Fresh (0)	6	1.8
3.3 % Acridine in Tetralin	Fresh (0)	6	1.1
6.5% Acridine in Methlynaphthalene	Fresh (0)	2	2.1
Athabasca maltenes	Fresh (0)	4	3.8

effects. CS_2 was added to maintain the catalyst in a sulfided form. Four percent CS_2 by weight was used in experiments using fresh oxide catalyst, while the concentration was reduced to 2% for subsequentexperiments using the same catalyst. Two experiments used previously coked catalyst with tetralin as a solvent to study the reversibility of coke deposition. Coker gas oil was also used with previously coked catalyst to explore this phenomenon.

4.2.3 Analysis Techniques

Prior to carbon determination, catalysts were Soxhlet extracted for 6 h (or until the extract ran clear, whichever was longer) in dichloromethane, then vacuum dried at 65°C and 0.01 MPa for 2 h. In order to ensure representative sampling, a 50 mg portion of the catalyst was crushed to a powder, and a 2 mg sample used for analysis. The concentration of carbon in the catalyst was measured at the Micro Analytical Laboratory, University of Alberta. This analysis, performed on a Carlo Erba Stumentazione Elemental Analyzer

1108, used combustion of the sample, followed by gas chromatographic separation of the combustion productions and analysis by thermal conductivity detection.

Measurement of the distribution of strengths of the acid sites on the surface of the catalyst was performed at Guelph Chemical Laboratories by stepwise thermal desorption. The catalyst was packed into a stainless steel column which was attached to a Hewlett Packard gas chromatograph (5830A) equipped with a flame ionization detector. The catalyst was saturated with pyridine, and the excess was desorbed in flowing nitrogen at 373 K. The pyridine which was irreversibly adsorbed at 373 K was subjected to a stepwise increasing temperature. The temperature was raised at 15 K min^{-1} until the desired temperature was reached (see following temperature ranges), then the temperature was maintained until the desorption of pyridine stopped. This process was repeated for each temperature step. Four acid site categories were reported based on the following desorption temperature steps:

(i)	Very Weak	$373 \text{ K} < T_d \leq 423 \text{ K}$
(ii)	Weak	$423 \text{ K} < T_d \leq 523 \text{ K}$
(iii)	Strong	$523 \text{ K} < T_d \leq 623 \text{ K}$
(iv)	Very Strong	$623 \text{ K} < T_d$

Category (iv) was the material irreversibly adsorbed at 623 K, as determined by subtracting the total amount of pyridine eluted below 623 K from the total amount of pyridine added to the catalyst.

Surface area and pore volume measurements were performed in the Department of Chemical Engineering, as described in Section 2.2.2.

4.2.4 Reaction Procedures

Experiments studying the carbon deposition behaviour of various model feeds were performed in the micro-batch reactor, in the same manner described in section 2.2.4, with the feeds described in section 4.2.2. Smaller volumes of liquid were used in these cases; approximately 1 g of liquid was used with approximately 0.25 g of catalyst.

The three tetralin experiments listed in Table 4.1 were performed in a similar manner as those described above. In two cases, however, coked catalyst obtained from experiment C3 (Table 2.2) was used instead of fresh catalyst to study the removal of coke from the surface.

Catalyst samples from experiments C3 and C7 (Table 2.2) and a sample of fresh catalyst were subjected to analysis of the distribution of strengths of the acid sites, as described in the previous section.

4.3 RESULTS AND DISCUSSION

4.3.1 The Chemistry of the Carbonaceous Deposit

The annulus model for coke deposition satisfactorily explains the behaviour observed in the experiments with bitumen as the feed. The model proposes that the adsorbed coke is in a form which resembles the source oil, rather than a more highly condensed aromatic material. In order to determine the reactivity of the carbonaceous deposit, heavily coked catalyst was exposed to tetralin at standard reaction conditions. A similar experiment was performed with coker gas oil as feed. In the reactions using tetralin, significant coke removal was observed (see Table 4.1), with approximately one-third of the initial concentration of carbon removed during the first 1 h reaction, and an additional one-third removed after a total of six 1 h reactions. Somewhat less coke removal was observed with coker gas oil, with approximately one-third of the initial carbon concentration removed after two 1 h reactions. A control experiment was not performed to determine the carbon content that a fresh catalyst would have reached after repeated reactions with coker gas oil, so no information was obtained about removal rate and total possible removal in gas oil. This experiment does, however, generalize the results observed with tetralin, to include much heavier, less aromatic solvents. The removal of coke from the catalyst surface during these experiments was probably due to a combination of simple reversible desorption (at reaction conditions), and reaction of irreversibly adsorbed coke with the carrier solvent and the supplied hydrogen. The degree of reversibility of adsorption under reactive conditions indicated that the surface deposit was not highly condensed and unreactive.

The presence of a reactive carbonaceous deposit was also consistent with the densities of coke deposits reported by Zeuthen et al. (1995), which averaged 750 kg/m^3. This experimentally observed density was lower than expected on the basis of highly aromatic model compounds, and supported the assumption that the initial deposit was similar to the residue. Zeuthen et al. (1995) demonstrated that the coke ages and becomes more aromatic with time in the reactor, which is beyond the scope of our study.

4.3.2 Nature of the Carbon - Surface - Interaction

Current literature suggests that acid-base interactions between the feed molecules and the catalyst surface are important in the formation of coke on catalysts. The feed contains compounds which are basic, due to both basic nitrogen groups and large aromatic clusters which exhibit basicity in the gas phase (Absi-Halabi, et al., 1991; Korre, et al., 1995).

This hypothesis was tested through two experiments. In the first, adsorption of compounds with varying basicity: acridine, dibenzofuran and anthracene, were compared. In these experiments, the model compound was dissolved or suspended in tetralin, then exposed to catalyst at standard reaction conditions (430°C, 13.9 MPa hydrogen, 1 h reaction). No significant difference in carbon deposition on the catalyst was observed between the anthracene solution, the acridine solution and the tetralin blank (see Table 4.1). Solvent effects due to the use of tetralin, which is a strong hydrogen donor, were ruled out when a similar carbon content was obtained using acridine in 1-methylnaphthalene. The lack of dependence of carbon deposition on basicity indicated that adsorption of low-molecular weight basic nitrogen compounds in the feed was not the primary chemical interaction at experimental conditions.

The apparent lack of interaction between acridine and catalyst sites which interacted strongly with pyridine, which is a weaker base in the gas phase (Meot-Ner, 1979), can be explained by several factors. The maximum temperature at which the pyridine desorption was measured was 350 °C, while the reaction was carried out at 430 °C. Acridine that was successfully hydrotreated would not have deposited on the catalyst when the reactor was cooled. Unconverted acridine which was deposited on the catalyst surface was likely removed during the Soxhelt extraction with dichloromethane.

In the second experiment, a sample of maltenes from Athabasca bitumen was used as feed for a multistep reaction series. Removal of the asphaltenes from this feed reduced the concentration of polar and high-molecular weight species from the residue. Coke deposition on the catalyst was only marginally higher than was observed for the solvent and model compounds, and only one-third of that observed for the whole bitumen based on carbon concentration (Table 4.1, Figure 2.3). These results suggested that the coke precursors were mainly in the asphaltene fraction of the bitumen.

Basicity alone did not give deposition on the catalyst, but acid-base interactions may be important in adsorption of high-molecular weight compounds, particularly since large polynuclear aromatics can exhibit gas phase basicity (Korre, et al., 1995). Given that the asphaltenes are thought to consist of polyaromatic structures like benzofuran and anthracene, linked with bridges and substituted with side chains (Frakman, et al.,1990), we must conclude that molecular weight is more important for coke deposition than functional groups.

4.3.3 Validation of the Annulus Model

If annular zones of alumina are cleared in the vicinity of nickel molybdenum sulfide crystallites on the catalyst surface, as illustrated in Figure 3.1, then greater numbers of acid sites of all strengths would be expected as the zone was enlarged, i.e. at higher hydrogen pressure. The distributions of the strengths of acid sites of fresh, moderately coked and highly coked catalysts are shown in Figure 4.1 (data tabulated in Appendix 4.1). These stepwise thermal desorption results indicated the concentration of acid sites of different strengths on the surface. Since the least strongly adsorbed pyridine molecules will desorb in the lowest temperature range, this range defines the very weak acid sites, while the highest temperature range defines very strong acid sites. The two intermediate ranges define weak and strong acid sites, respectively. As carbon concentration decreased with higher hydrogen pressure, more strong acid sites were exposed on the surface of the catalyst. Given the concentration of nitrogenous and high boiling components found in these feeds, exposure of strong acid sites can only be explained by systematic clearing of the surface near metal crystallites. If removal of the carbon from the surface was random and not associated with crystallites, the strongly acidic sites would be expected to preferentially adsorb the available residue molecules. The apparent

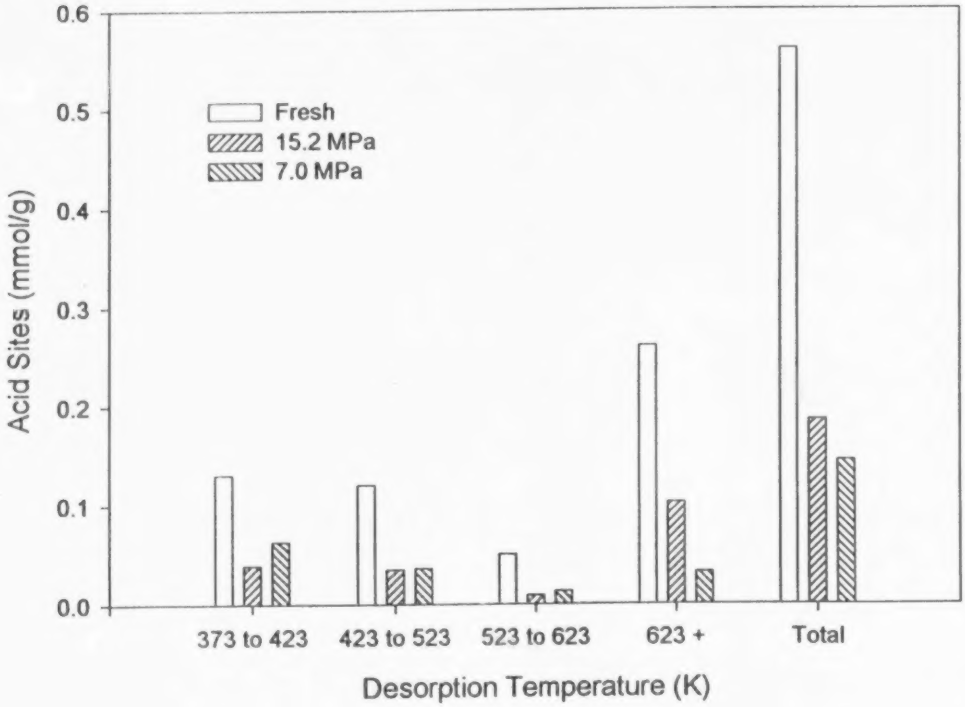

Figure 4.1: Distribution of Strengths of Acid Sites by Stepwise Thermal Desorption. The concentration of sites is shown on the ordinate while the abscissa values are the temperature ranges for desorption of pyridine.

increase in the number of very weak acid sites with increased carbon concentration was an artifact of the analytical method, caused by interactions between the coke and pyridine. In this procedure, weak acid sites are defined as those sites from which pyridine desorbed between 373 K and 423 K. A sample of solid coke derived from Athabasca bitumen under more severe reaction conditions, containing no alumina, retained approximately 1.1 mmol/g of pyridine at 373 K, which would correspond to 0.2 mmol/g catalyst. This coke-pyridine interaction would tend to give more pyridine release at 373-423 K with increasing carbon content, as observed in Figure 4.1.

4.3.4 Summary of Model Validations

The above experiments have provided support for several assumptions inherent in the model. The removal of the deposit with tetralin and gas oil showed that the deposit remains highly reactive, and possibly reversibly adsorbed on the catalyst surface. Measurements of the distribution of strengths of acid sites of coked catalysts indicated the coke layer which was deposited on the catalyst was structured. The model compound work showed that the interaction of the acid sites with low molecular weight bases was not an important factor in coke deposition. Asphaltenes were, however, shown to be important, suggesting that the combined influence of high molecular weight and basicity is responsible for the accumulation of carbonaceous deposits on the catalyst surface.

4.4 CONCLUSIONS

1. Coke deposited on a catalyst during the inital hours of use is highly reactive, and is removed from the surface at reaction conditions in residue-free feed.

2. High molecular weight components in the asphaltene fractions appear to be the most significant contributing factor for coke deposition.

3. The coke deposit on the surface is in a structured form, consistent with the annular structure proposed in Chapter 3.

4.5 LITERATURE CITED

Absi-Halabi, M.; Stanislaus, A.; Trimm, D.L. Coke Formation on Catalysts During the Hydroprocessing of Heavy Oils. *Appl. Catal.* **1991**, 72, 193-215.

Chu, K.-S.; Hanson, F.V.; and Massoth, F.E. Effect of Bitumen Derived Coke on Deactivation of an HDM Catalyst. *Fuel Proc. Tech.* **1994**, 40, 79-95.

deJong, K.P.; Reinalda, D.; and Emeis, C.A. Coke Deposition in Trickle-Bed Reactors During Heavy Oil Processing - Catalytic and Physical Effects. *Studies in Surface Science and Catalysis*. **1994**, 88, 155-166

Frakman, Z.; Ignasiak, T.M.; Lown, E.M.; Strausz, O.P. Oxygen Compounds in Athabasca Asphaltene. *Energy and Fuels* **1990**, 4, 263-270.

Korre, S.C.; Klein, M.T.; Quann, R.J. Polynuclear Aromatic Hydrocarbon Hydrogenation. 1. Experimental Reaction Pathways and Kinetics. *Ind. Eng. Chem. Res.* **1995**, 101-117.

Meot-Ner, M. Ion Thermochemistry of Low-Volatility Compounds in the Gas Phase. 2. Intrinisic Basicities and Hydrogen-Bonded Dimers of Nitrogen Heterocyclics and Nucleic Bases. *JACS.* **1979**, 101, 2396-2403.

McKnight, C.A. and Nowlan, V. Metals Accumulation and Particle Mixing in a Commercial Residue Hydroprocessor with Continuous Catalyst Addition. *ACS Div Pet Chem PREPRINTS.* **1993**, 37, 391-397.

Ternan, M.; Furimsky, E.; Parsons, B.I. Coke Formation on Hydrodesulfurization Catalysts. *Fuel Proc. Tech.* **1979**, 2, 45-55.

Yui, S.M.; and Sanford, E.C. Kinetics of Aromatics Hydrogenation of Bitumen-Derived Gas Oils. *Can. J. Chem. Eng.* **1991**, 69, 1087-1095.

Zeuthen, P.; Cooper, B.H.; Clark, F.T.; Arters, D. Characterization and Deactivation Studies of Spent Resid Catalysts from Ebullating Bed Service. *Ind. Eng. Chem. Res.* **1995**, 34, 755-762.

CHAPTER 5 - MASS TRANSFER EFFECTS IN COKED CATALYST

5.1 INTRODUCTION

A model for surface deposition of coke was presented in Chapter 3. Except in the extreme case, where a complete monolayer of coke forms and blocks metal crystallites, this model does not suggest catalyst deactivation, yet some short term deactivation is observed in nearly all residue hydroprocessing experiments and industrial examples (e.g. Oballa et al., 1994, deJong et al., 1994, Chu et al., 1994). Deposition of coke in catalyst pores would reduce the effective diameter, possibly reducing the diffusivity of large residue molecules. The reduction in diffusivity as a function of pore size was estimated through the use of hindered diffusion theory. The random pore model of Wakao and Smith (1964) was used with the data obtained from the experiments described in Chapter 2 to estimate the overall effective diffusivity for the catalyst pellets. These results are contrasted with an alternative mechanism for catalyst deactivation, based on plugging of pore mouths, in Section 5.3.3.

5.2 EXPERIMENTAL

Surface area and pore volume measurements were performed in the Department of Chemical Engineering, University of Alberta on an Omnisorb 360 (Coulter Scientific Instruments, Hialeah, Florida). Nitrogen desorption measurements were used with the Kelvin equation to determine the distribution of pore sizes. This distribution describes the total volume of the pores in the catalyst as a function of pore radius. Since catalytic activity is related to surface area, this distribution can be converted to a distribution of surface area with pore radius by assuming the pores are long, circular cylinders. The resulting pore size distribution is shown in Figure 5.1.

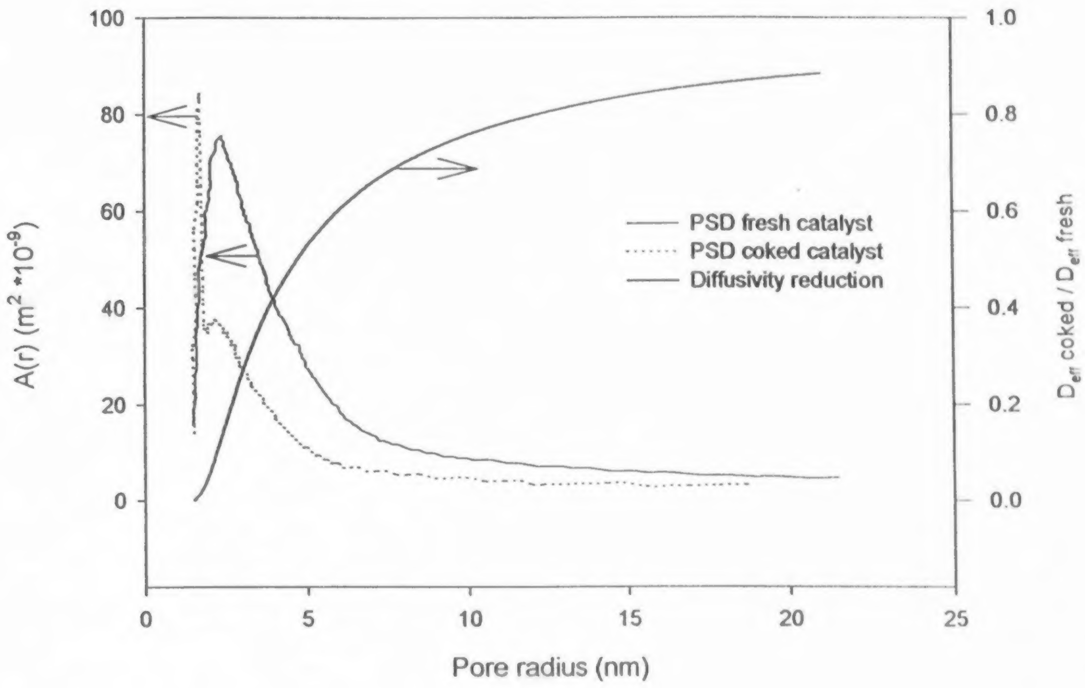

Figure 5.1: Pore Size Distribution (PSD) Based on Surface Area and the Reduction in Effective Diffusivity Caused by Coke Deposition. Total Surface Area $= \int_0^\infty A(r)dr$.

5.3 RESULTS AND DISCUSSION

5.3.1 Hindered Diffusion Theory

As the size of a diffusing species approaches the size of the pore into which it must diffuse, wall effects become important, and diffusion becomes dominated by what is called hindered diffusion. Lee et al. (1991a, 1991b) and Baltus and Anderson (1983) studied the hindered diffusion of asphaltene molecules in membranes and showed that the effective (hindered) diffusivity (D_e) was related to the bulk diffusivity (D_b) as follows:

$$\frac{D_e}{D_b} = \frac{\varepsilon_p}{\tau} e^{-B\lambda} \qquad 5.1)$$

where ε_p is the pellet porosity, τ is the tortuosity, B is an empirical coefficient, λ is the ratio of molecule size to pore size: $\lambda = r_r / r_p$, r_r is the radius of the diffusing residue molecule and r_p is the pore radius.

The pore size distribution of the fresh NiMo /γ-Al_2O_3 catalyst is illustrated in Figure 5.1. For any range of pore sizes, the contribution to total porosity for that size range can be calculated based on void volume. If one assumes that the coke is a monolayer of residue molecules with a radius defined by Equation 3.1, then the reduction in pore radius will be $2r_r$ (since it is assumed the the surface is covered with a monolayer of residue molecules), and the void volume can be determined. The porosity of the coked catalyst was related to the fresh catalyst porosity by:

$$\varepsilon_c = \varepsilon_f * \frac{(r_p - 2r_r)^2}{(r_p)^2} \qquad 5.2)$$

where ε_c is the porosity of the coked catalyst and ε_f is the porosity of the fresh catalyst.

Rewriting equation 5.1 as the ratio of diffusivities for coked and fresh catalyst gives:

$$\frac{D_{e,c}}{D_{e,f}} = \frac{\varepsilon_c}{\varepsilon_f} e^{-\left(\lambda_c - \lambda_f\right)} \tag{5.3)}$$

This ratio is shown in Figure 5.1 for $r_r = 0.6$ nm. From this figure, it is obvious that a significant reduction in diffusivity is observed for all pore sizes. Virtually all of the active catalyst surface is located in pores small enough that the deposition of a monolayer of coke would result in a diffusivity reduction of at least 40%.

5.3.2 Wakao and Smith's Random Pore Model

Wakao and Smith (1964) developed a model to describe the effect of micro and macro pores on overall diffusivity in a porous catalyst,based o catalyst geometry. In this model, the distinction between micro pores and macro pores can be somewhat arbitrary but the typical approach is to define pores smaller than 10 nm as micropores (Froment and Bischoff, 1990). This model will be used to estimate the overall reduction in effective diffusivity caused by the deposition of a monolayer of coke. Overall effective diffusivity, D_e, is defined by:

$$D_e = \varepsilon_m{}^2 D_m + \frac{\varepsilon_\mu{}^2\left(1 + 3\varepsilon_m\right)}{1 - \varepsilon_m} D\mu \tag{5.4)}$$

where ε is the porosity, D is the diffusivity and the subscript m represents macro pore and μ represents micro pore.

In Wakao and Smith's original work, the diffusivity in each range of pore sizes was determined using equations for molecular and Knudsen diffusion. Since the residue molecules were diffusing through a liquid medium within narrow pores, appropriate expressions for hindered diffusion must be used in equation 5.4. Rewriting the hindered diffusion relationship of equation 5.1 for a single pore gives:

$$D_{p,i} = D_b e^{-B\lambda_i} \qquad 5.5)$$

where the subscript i refers to micro or macro pores, and B is an empirical parameter. The reported value of the parameter ranges fro 3.9 to 4,6 for comparable hydrocarbons (Lee et al, 1995, Baltus and Anderson, 1983).

Values of λ for the micro and macro pores of the fresh catalyst were determined from the pore size distribution. The maximum of the pore size distibution, 3 nm, was chosen for r_μ, and 15 nm was chosen for r_m, based on the 10 nm cutoff for micropores and the maximum pore size detected. The radius of the diffusing molecules was $r_r = 0.6$ nm.

It should be reiterated at this point that the value of r_r used in these calculations was the result of an estimate based on bulk liquid properties of the residue fraction. This value represents a conformation in which the molecule is folded into a sphere. Hydrodynamic radii of asphaltenes, for example, can be several orders of magnitude larger than the estimate obtained in Chapter 3 from liquid density (Baltus and Anderson, 1983).

The porosities, ε_μ and ε_m, for the fresh catalyst were determined from the pore size distribution and the physical properties of the catalyst. Figure 5.1 shows the pore size distribution before and after coking. Before coking, the total surface area was 317 m^2/g and the pore volume was 0.57 mL/g. The maximum of the pore size distribution at a radius of 3 nm, was chosen for r_μ, and a value of 15 nm was chosen for r_m, based on the 10 nm cutoff for micropores and the maximum pore size detected.

Given the simplifications described above, we can estimate all parameters for the fresh catalyst. The estimation of the parameters for the coked catalyst, however, is somewhat more difficult. Figure 5.1 shows the pore size distribution for a catalyst with 17.5% carbon content. This catalyst had a surface area of 157 m^2/g and a pore volume of 0.25 mL/g. The data clearly show a reduction in total surface area, and an accompanying shift in the maximum of the distribution curve following deposition of coke on the catalyst. Since pore size distribution (PSD) data were available for a coked catalyst, radii and porosity values for the micro and macro pores could be determined directly from the PSD data, as was done for the fresh catalyst. Although the pore size distribution at reaction conditions may not entirely agree with that obtained at analysis conditions, this approach provides an estimate for the porosities required in equation 5.4 for the coked catalyst. Equations 5.4 and 5.5 predict: $\frac{D_{e_{coked}}}{D_{e_{fresh}}} = 0.105$. The pore size distributions were measured at low temperature, with the catalyst in a clean, dry state, therefore, the effect of the carbonaceous deposit on effective pore size at operating conditions of high temperature and liquid - wet catalyst surface, is unknown. The experimentally obtained pore size distribution likely represents the minimum effect of the deposition of the coke on the effective diffusivity.

The model from Chapter 3 predicts monolayer coverage of the surface with a layer 1.2 nm thick. This prediction can be used to reconstruct a pore size distribution for the coked catalyst, which would predict a maximum reduction in effective diffusivity of $\frac{D_{e_{coked}}}{D_{e_{fresh}}} = 0.070$ (equations 5.4 and 5.5). The actual reduction in effective diffusivity will likely fall between these two estimates:

$$0.070 \le \frac{D_{e_{coked}}}{D_{e_{fresh}}} \le 0.105 \qquad 5.6)$$

These two values place tight bounds on the expected effect of the deposition of a monolayer of residue on the diffusivity. The predicted effect of coke deposits is large; however, a 90% reduction in activity was not observed in experiments. Two possible explanations exist for this apparent discrepancy. The behaviour of the fresh catalyst with residue feed is unobservable. The adsorption of the residue on the catalyst surface occurs more rapidly than achievable reaction times, thus a true catalyst activity for residue hydrocracking, in the absence of catalyst coking may never be obtainable. Given the lack of an experimental value for fresh catalyst activity without coke, diffusivity reductions or activity reductions based on a comparison to the fresh catalyst must be used with some caution. The calculations above are for diffusivity only, they do not consider the kinetics of the reaction. If the fresh catalyst had a low Thiele modulus, then the effectiveness factor for the catalyst would be insensitive to effective diffusivity. This situation would result in much less than 90% loss of activity for a 90% reduction in diffusivity.

A number of studies have shown that a decrease in pore diameter, by altering the alumina, reduces effective diffusivity for hydroprocessing reactions, as one would expect from equation (5.1). Although a change in pore diameter is not the same as depositing a layer of coke, studies by Ammus and Androutsopoulos (1987), Li et al. (1995) and Seo and Massoth (1985) suggest that a reduction of D_e due to carbon deposition could range from 10% to 60%. The work of Lee et al. (1991b) on fresh and coked catalysts suggests that a reduction in D_e of as much as 65% could result from only 2-3% carbon deposition. Such a drastic change, however, indicated plugging of pore mouths which could not be extrapolated to the present study.

5.3.3 Uniform Deposition of Carbon Versus Pore - Mouth Plugging

Observations of drastic reductions in diffusivity due to small amounts of carbon, e.g. Lee et al. (1991b), indicate that in some cases the pore network in the catalyst can be blocked off at pore mouths. Such a mechanism cannot account for the observations from the present study. If one assumes the coke deposit has a carbon content and density similar to the residue fraction of the oil, then the maximum carbon concentration on the catalyst predicts that the volume of the deposited coke would account for approximately one half the total pore volume. This prediction was consistent with the measured pore volumes: 0.57 mL/g for the fresh catalyst and 0.25 mL/g for the coked catalyst. If micro pores were blocked at the pore mouth, this level of deposition would not be possible. Furthermore, macropore (10-20 nm) surface area would be almost unaffected by pore mouth deposition of coke, and virtually no surface area loss in the macro pore range would occur. In contrast, our results show a 48% reduction in macropore volume (Figure 5.1). The material deposited in pore mouths is assumed to be highly aromatic, unreactive material (Muegge and Massoth, 1991). The results presented in Chapter 4 clearly indicated that during the initial stages of the reaction, the material is reversibly adsorbed and/or reactive. While it is clear from the literature that pore mouth plugging may occur on hydrocracking and hydrotreating catalysts during operation under some conditions, our results with residue strongly support a model for deposition throughout the micropores. More study is required to determine the factors that determine the mode of coke deposition and to explain the conditions requisite for pore mouth plugging.

5.4 CONCLUSIONS

1. Hindered diffusion theory predicts that virtually the entire catalyst pore structure will be subject to at least 40% reduction in effective diffusivity.

2. Wakao and Smith's random pore model was combined with analytical results and estimates based on the model presented in Chapter 3 to predict that effective diffusivity of coked catalysts would be reduced by aproximately 90% relative to catalyst without coke.

3. Observations from this study are inconsistent with the existence of plugged pore mouths, suggested by some of the literature for hydroprocessing catalysts.

LITERATURE CITED

Ammus, J.M.; Androutsopoulos, G.P. HDS Kinetic Studies on a Greek Oil Residue in a Spinning Basket Reactor. *Ind. Eng. Chem. Res.* **1987**, 26, 494-501.

Baltus, R.E.; Anderson, J.L.; Hindered Diffusion of Asphaltenes Through Microporous Membranes. *Chem. Eng. Sci.* **1983**, 38, 1959-1969.

Chu, K.S.; Hanson, F.V.; Massoth, F.E. Effect of bitumen derived coke on deactivation of an HDM catalyst. *Fuel Proc. Tech.* **1994**, 40, 79-95.

deJong, K.P.; Reinalda, D.; Emeis, C.A. Coke deposition in trickle bed reactors during heavy oil processing - Catalytic and physical effects. *Studies in Surface Science and Catalysis.* **1994**, 88, 155-166.

Froment, G.F.; Bischoff, K.B. Chemical Reactor Analysis and Design, second ed., John Wiley and Sons, New York. **1990.**

Lee, S.Y.; Seader, J.D.; Tsai, C.H.; Massoth, F.E. Restrictive Liquid Phase Diffusion and Reaction in Bidispersed Catalysts. *Ind. Eng. Chem. Res.* **1991a**, 30, 1683-1693.

Lee, S.Y.; Seader, J.D.; Tsai. C.H.; Massoth, F.E. Restrictive Diffusion Under Catalytic Hydroprocessing Conditions. *Ind. Eng. Chem. Res.* **1991b**, 30, 29-38.

Li, C.; Chen, Y.W.; Tsai, M.C. Highly Restrictive Diffusion Under Hydrotreating Reactions of Heavy Residual Oils. *Ind. Eng. Chem. Res.* **1995**, 34, 898-905.

Muegge, B.D.; Massoth, F.E. Basic Studies of Deactivation of Hydrotreating Catalysts with Anthracene. *Fuel Proc. Tech.* 1991, 29, 19-30.

Oballa, M.C.; Wong, C.; Krzywicki, A. "Catalyst Deactivation in Residue Hydrocracking", in Catalytic Hydroprocessing of Petroleum and Distillates, eds Oballa, M.C. and Shih, S. S., Marcel Dekker, Inc., New York, **1994**, 33-54.

Seo, G.; Massoth, F.E.; Effect of Pressure and Temperature on Restrictive Diffusion of Solutes in Aluminas. *AIChE J.* **1985**, 31, 494-496.

Wakao, N.; and Smith, J.M. Diffusion and Reaction in Porous Catalysts. *Ind. Eng. Chem. Fund.* **1964**, 3, 123-127.

CHAPTER 6 - BASE DOPING OF HYDROPROCESSING CATALYSTS

6.1 INTRODUCTION

The utility of supports for metal catalysts depends on a variety of chemical, physical and mechanical properties. The attractiveness of γ-alumina is due to a combination of favorable surface area, mechanical strength and a surface chemistry which allows dispersion of metal phases varying from platinum group metals to mixed transition metal sulfides (Beaton and Bertolacini, 1991; Topsoe et al., 1986) . The acidity of the surface of γ-alumina has been linked to its catalytic activity, its tendence to accumulate coke and its ability to disperse metals (Absi-Halabi et al, 1991; Topsoe et al., 1986). The importance of the surface acidity of the alumina has led a number of researchers to investigate the addition of alkaline earth and alkali metal salts, in order to modify the acid/base characteristics of the surface.

6.1.1 Surface Acidity

Various authors have studied the effect of deposition of alkali metal and alkaline earth salts on alumina supported metal catalysts with two objectives in mind, the possibility of neutralization of surface acid sites to alter the interactions of reactants with the alumina surface, or altering interactions between the oxide phase and the active metal. Changes in the interactions between the aluminum oxide surface and the active metal, or metal sulfide, tend to alter the dispersion of the metal on the surface of the catalyst. A variety of alkali metal and alkaline earth metal salts have been used to dope catalysts, and these studies are summarized in Table 6.1. This section discusses the role of surface acidity, while the following section will deal with the other effects.

Table 6.1: Prior Studies on Doping of γ-Alumina Catalysts with Alkali and Alkaline Earth Metals.

Reference	Reaction / Active Metals	Dopant	Dopant Conc. g metal/ 100 g catalyst	Order of Addition of Components
Chen and Chen, 1990a	Catalytic cracking of n-hexane / Ni	$LiNO_3$ Na_2CO_3 KNO_3 $Mg(NO_3)_2$ $Ca(NO_3)_2$	0.1 0.4 0.4 0.162 0.243	coprecipitation
Papaioannou and Haynes, 1990	Hydrotreating of coal derived liquids / CoMo	$Mg(NO_3)_2$ $Ca(NO_3)_2$	2.3 3.8	Dopant follows transition metals
	Acidity measurement only / CoMo	KNO_3 $NaNO_2$ $LiNO_3$ $Be(NO)_3$ $BaNO_2$	0.3 - 2.0 0.2 - 1.2 0.06 - 0.4 0.08 - 0.5 1.1 - 6.9	Dopant follows transition metals
Masuyama et al., 1990	Hydroprocessing coal liquid bottoms / NiMo	Calcium salt, anion unknown	1.9	Calcium follows transition metals
Kelly and Ternan, 1979	Bitumen hydroprocessing / CoMo	Li_2CO_3 Na_2CO_3 K_2CO_3	0.09 - 0.9 0.27 - 2.9 0.41 - 2.1	Coprecipitation
Lycourghiotis et al., 1980	X-ray Powder Analysis, Diffuse Reflectance Spectroscopy, Differential Scanning Calorimetry / Co	KNO_3 $NaNO_3$ $LiNO_3$	3.8 - 6.0 2.7 - 4.2 1.0 - 1.6	Dopants before transition metals
Centeno et al., 1995	Hydrodeoxygenation of model biomass compounds / CoMo	KOH NH_4OH	1.0 (unknown, "blank preparation")	Dopants after transition metals
Baker et al., 1987	Hydrotreating coal derived distillate / NiMo	$NaNO_2$	3.11	Dopants after transition metals
O'Young, 1989	Thermogravimetric Analysis, NO chemisorption, FT - IR / Mo	K_2CO_3 Cs_2CO_3	1 - 10 1-20	Dopant after transition metals

Table 6.1 (continued) : Prior Studies on Doping of γ-Alumina Catalysts with Alkali and Alkaline Earth Metals.

Reference	Reaction / Active Metal	Dopant	Dopant Conc. g metal/ 100 g catalyst	Order of Addition of Components
Sulima and Echigoya, 1976	Reduction of NO / Co	$LiNO_3$ $NaNO_3$ $RbNO_3$ $CsNO_3$	0.004 - 0.36 0.012 - 1.2 0.044 - 4.2 0.069 - 6.4	not given
Haensel, 1960	Naphtha hydrotreating / Pt	$LiNO_3$	1.0	Dopant before Platinum
Baird and Shoukry, 1990	Naphtha hydrotreating / Pt	$MgNO_3$	0.0001 - 0.003	Dopant before Platinum
Mauldin and Baird, 1982	Naphtha reforming / Cr or Mo	Na_2CO_3 K_2CO_3 Cs_2CO_3 Li_2CO_3	1.0 0.37 1.66 0.004	Dopant following Chromium
Hayes and Pilotzer, 1973	Dehydrogenation of model paraffins / Pt, Rh and W	$LiNO_3$ KNO_3	0.5 - 0.6 2.8	Dopants after Platinum / Rhenium
Lowenthal, et al., 1995	Methanol dehydrogenation / Rh Mo	KNO_3	0.03 - 14	Dopants after Mo / Rh
O'Hara et al., 1980	Residue hydrocracking / Group VIB or VIII metals	$CaCl_2$ $MgNO_3$	1 0.5	Dopants before transition metals

The alumina support typically used for hydroprocessing catalysts has surface acid sites with a range of acidity. These acid sites contribute to coke formation on the alumina surface especially in the absence of hydrogenating transition metals (Gray et al., 1992). Since typical hydroprocessing feeds contain basic components such as pyridines and quinolines, neutralization of the strong acid sites found on alumina may reduce the coking propensity of the catalyst surface.

The literature summarized in Table 6.1 shows a wide variation in concentration and choice of dopants. The sequence of addition of components to the catalyst was also varied. This variation in technique is perhaps the major cause of inconsistencies in performance observed within the literature. In most cases, nitrates and carbonates are used to deposit the dopant metal. Nitrates were frequently chosen because the transition metals were deposited using the corresponding nitrates. These compounds were then calcined with the goal of achieving the alkali or alkaline earth metal oxide on the surface.

Chen and Chen (1990) added moderate concentrations of a variety of alkali and alkaline earth metal nitrates and carbonates. Addition of these compounds caused lower Ni dispersion, which would tend to reduce the catalyst activity. This reduction might be expected to increase coking due to the lower hydrogenation activity of the catalyst, but the catalyst doped with K had a lower coking tendency than the material with Ni alone. This trend was not consistent in that some alkali-metal doped samples had greater rates of coking than those observed for Ni alone (Chen and Chen, 1990). The variation may be due to inconsistent and incomplete calcining of the salts, but it may also represent a need to optimize the acidity of the support and the dispersion of the active metals.

Papaioannou and Haynes (1990) studied the effect of acidity on a Co-Mo/alumina catalyst for coal liquefaction by using a number of dopants over a wide range of concentration. The acidity of the doped catalysts was determined using temperature programmed desorption of tert-butylamine. Ca and Ba gave total elimination of the catalyst acidity, but at similar molar loadings neutralization could not be obtained with Mg or Be. Three catalysts were chosen for testing with a coal liquid feed: a high concentration Ca-doped catalyst which had been completely neutralized, a sample of a Mg-doped catalyst at a similar concentration which had not been entirely neutralized, and the reference commercial catalyst. Their study found no trend in hydrogenation activity, but found lower hydrodenitrognation activity and lower coke deposition for the Ca-doped catalyst compared to the base commercial catalyst. The Ca-doped catalyst had a slightly lower initial hydrogen consumption than the base commercial catalyst, but suffered less deactivation over the first 800 g oil/g catalyst, leading to higher activity following the initial deactivation. The Mg-doped catalyst gave an intermediate result, with activity for most reactions falling between the Ca-doped and undoped catalysts.

Masuyama et al. (1990) also studied Ca doped Ni-Mo alumina catalysts in coal liquefaction trials, using similar Ca concentrations to Papaioannou and Haynes (1990) work. As in the Papaioannou and Haynes (1990) study, less coke deposition was observed on the Ca-doped catalyst than on the undoped sample but there was no substantial change in catalyst activity for conversion of coal liquid bottoms that was attributable to the Ca doping.

Kelly and Ternan (1979) performed a study on the effect of alkali addition to Co-Mo-alumina catalyst in the hydrocracking of Athabasca bitumen. They used alkali metal carbonates at concentrations ranging from those used by Chen and Chen (1990) to those used by Papaioannou and Haynes (1990). They discovered that the various metals caused different changes in surface area. Na and K caused a linear decrease in surface area with metal concentration. Li caused an increase in surface area at low concentrations, followed by a decrease at higher concentrations. Similar trends were observed for activity, coke deposition and surface area. The authors normalized the activity change to a surface area basis. On a surface area basis, Li caused an increase in activity and a decrease in coke deposition at low concentrations. Improvements in performance were not observed with Na or K.

Baker et al. (1987) used a high concentration of $NaNO_2$ to totally neutralize the acidity of a hydrotreating catalyst. The catalyst was used in a continuous reactor to hydrotreat coal liquids at 13.9 MPa, 412°C for 900 g oil /g catalyst. The surface neutralization resulted in lower carbon content, but little effect was observed on initial catalyst activity, or deactivation during hydrotreating of coal liquids .

The patent literature includes five examples of alkali-doped hydrocarbon conversion catalysts (summarized in Table 6.1), all claiming lower carbon contents and higher activity (Baird and Shoukry, 1990; Haensel, 1960; Haynes and Pollitzer, 1973; Mauldin and Baird, 1982; and O'Hara, et al., 1980)). Mauldin and Baird (1982) found that doping with KCO_3 was more effective than doping with KNO_3, and that doping with K following the metals deposition was much more effective than doping before. Since the solutions used to deposit the transition metals were acidic, the role of the K in modifying surface acidity was not clear.

McCormick et al. (1989a) studied the effect of surface acidity on coking of the catalyst surface through the use of alumina, silica, titania, magnesia and combinations of these compounds as supports for coal liquefaction catalysts. The catalysts were chosen from commercially available catalysts, and therefore contained a range of concentrations of Ni or Co and Mo. Coke deposition, expressed as a surface concentration, decreased with an increase in support acidity following reaction of a mildly hydrogenated creosote oil. The authors explained this result by proposing that higher acid-site density led to higher cracking rates. Cracking rates were not measured, however, and neither hydrogen consumption nor hydrodenitrogenation rates correlated well with acidity. They did not discuss the possible variations in metal/support interactions, or metal dispersion. In experiments with the same feed and catalysts, increased hydogen donor contents (fraction of hydrogen associated with naphthenic rings and paraffinic branches) of the products were observed with the lower acidity catalysts (McCormick et al., 1989b). The authors attribute this apparent contradiction to lower rates for retrograde condensation reactions on the lower acidity catalysts.

6.1.2 Other Effects of Alkali Treament

Alkali doping can change other catalyst characteristics, such as metal dispersion and the strength with which the active metals interact with the alumina support (metal-support interaction). Lowenthal et al. (1995) observed decreased catalyst acidity after neutralization of a Mo/Rh catalyst with approximately 10 wt% KNO_3. No evidence of changes in dispersion was observed. Lewis et al. (1992), however, found dispersion of Ni and Ni-Mo to increase with increasing acidity when P was added to the alumina prior to deposition of the transition metals. Huang and Schwartz (1987) also found that decreasing the pH of the solution during deposition of the transition metals resulted in higher dispersion.

Sulima and Echigoya (1976) studied catalytic reduction of NO on Co/alumina catalysts doped with alkali metals. They observed an increase in conversion with increasing concentration of alkali metal to an optimum concentration of approximately 0.1 g metal / 100 g catalyst, followed by a decrease in conversion at higher alkali metal concentrations. They hypothesized that increased alkali concentration reduced adsorption of both reactant and product molecules on the catalyst surface. They reasoned that at low concentrations, this would be beneficial as it would accelerate product desorption and allow higher catalyst turnover and activity. At higher concentrations, however, this would hinder reactant adsorption, leading to lower apparent catalyst activity.

Topsoe et al. (1986), using Mössbauer emission spectroscopy, observed active metal species which were less strongly bonded to the support surface when the transition metals are supported on activated carbon (not acidic) instead of (acidic) alumina. They proposed that this would increase the effectiveness of the transition metals. Lycourghiotis et al. (1980) concluded that X-ray spectra for the supported catalysts indicated higher metal/support interaction when Co/alumina catalysts were doped with Na and K following the deposition of transition metals. Lower levels of interaction were observed when they were doped with Li in the same manner. O'Young and co-workers (O'Young, 1989; O'Young et al., 1988) found that low levels of K doping, following deposition of Mo on γ-Al_2O_3· showed virtually no effect on the reducibility of Mo in hydrogen at 500 ° C. At higher levels of K, reducibility was decreased, indicating the Mo would sulfide less readily, and be less active.

These prior studies of addition of bases to catalyst are highly contradictory, and give no indication that treatment with alkali metals would consistently increase the effectiveness of transition metals for hydroprocessing reactions. Dispersion studies do not indicate that increased dispersion will be achieved if the catalyst is doped with base following the deposition of the active transition metals. Similarly, work on metal-support interaction was contradictory about the effect of decreased acidity on metal-support interactions. These results indicate that any beneficial effect may be attributable to changes in the alumina support, such as neutralization of the acid sites, rather than any improvement in the active metals on the alumina surface.

The effect of doping of a commercial NiMo / alumina catalyst is described in this chapter. The effect of anion, cation and concentration was studied through deposition of KNO_3, KOH, NaOH and LiOH on a commercial catalyst. Screening of the various catalyst formulations was performed using the microbatch reactor described in Chapter 2. Carbon content of the spent catalyst and activity for hydrodesulfurization were used as performance criteria. Based on the initial screening experiments, a base-doped catalyst was selected for a more comprehensive test of performance. Activity for hydroprocessing reactions such as hydrodenitrogenation, microcarbon residue conversion, pitch conversion and asphaltene conversion were measured using the 1 L CSTR reactor described previously.

6.2 EXPERIMENTAL

6.2.1 Materials

Athabasca bitumen was provided by Syncrude Canada Ltd, with the properties listed in Table 2.1. CS_2 (99.9%) was supplied by Aldrich. KOH solution (45.4 wt%), NaOH solution (50 wt%), KNO_3 (Certified) and LiOH•1 H_2O (Purified) were supplied by Fisher Scientific.

6.2.2 Catalyst Properties and Base Doping

The catalyst was a commercial NiMo /γ-Al_2O_3 catalyst with 12.5 wt % MoO_3 and 3.5 wt % NiO. The catalyst had a surface area of 317m^2/g (by nitrogen BET measurement) a pore volume of 0.57 mL/g and distribution of strengths of an acid sites as shown in Figure 4.1. In three experiments the catalyst was presulfided using CS_2 (see section 6.2.4 for details). In all other experiments, the catalyst was not presulfided, so that the sulfur was provided by the bitumen. For the batch experiments the catalyst was crushed and sieved to +350μm -500μm size. For CSTR experiments, the catalyst was used in the 1 mm cylindrical extrudate form in which it was received. The commercial catalysts were doped using KNO_3, KOH, NaOH and LiOH. The total concentrations of the compounds of interest are shown in Table 6.2 The concentrations were chosen as multiples of the amount of base required to neutralize the strong acid sites of the commercial catalyst. At the highest KNO_3 concentrations, the solution was heated to allow dissolution of the salt. The alkali metal salts were added to the catalyst using the incipient wetness technique, in which the desired amount of the dopant was dissolved in enough water to dampen the catalyst, leaving no free liquid. The catalysts were allowed to equilibrate over night. The catalysts were calcined in air at 450°C for 4 h.

Table 6.2: Alkali Metal Content for Base Doped Catalysts

Dopant	Dopant Concentration (g metal/ g fresh catalyst)	Dopant Concentration meq/g
KNO_3	0.01	0.26
KNO_3	0.385	9.8
KOH	0.011	0.28
KOH	0.023	0.59
KOH	0.204	5.22
NaOH	0.0059	0.26
LiOH	0.0018	0.26

6.2.3 Analytical Techniques

The carbon content of spent catalysts was determined using the procedure described in Section 2.2.2.

Measurement of the distribution of strengths of acid sites on the surface of the catalyst was performed at Guelph Chemical Laboratories by stepwise thermal desorption by pyridine. A detailed description of the techniques can be found in section 4.2.3.

Sulfur content of the oil was determined using the Leco sulfur analyzer (SC132). This instrument combusts the oil in pure oxygen at 1600°C, and analyzes the sulfur dioxide content of the combustion gases using infrared spectrophotometry.

Asphaltene content of the feed and products from the CSTR experiments was determined using pentane precipitation. In this technique, the oil sample was mixed with toluene in a ratio of 1 mL / g sample. Pentane was added at a ratio of fifty times the volume of toluene. The sample was shielded from light and stirred for 16 h. The asphaltene precipitate was removed by filtration on a 0.22μm Millipore filter, then washed in pentane and vacuum dried at 65°C and 0.01 MPa for 2 h.

The metals content of the oil was measured using direct aspiration of diluted oil into a inductively coupled argon plasma at Syncrude Canada Ltd.

6.2.4 Reactors and Reaction Procedures

The batch reactor and CSTR reactor described in Chapter 2 were used for these experiments.

Three catalyst samples were presulfided prior to use in the batch reactor. These catalysts were loaded into the batch reactor with 140 μL CS_2/g catalyst. The reactor was then sealed and purged with low pressure nitrogen. The reactor was then pressurized with sufficient hydrogen to reach 13.8 MPa at operating temperature. The reactor was heated in a sand bath at 350°C for 2 h with agitation.

Multistep batch experiments were performed as described in Chapter 2. CSTR experiments were performed in the manner described in Chapter 2 for single stage experiments. The reactor pressure was 13.8 MPa, temperature was 430°C, liquid feed rate was 410 mL/h and hydrogen was supplied at 4.75 std L/min. Liquid samples were taken during the last 2 h of the 6 h CSTR experiments. This allowed time for the reactor to reach steady state with regard to temperature, pressure and gas and liquid flow rates (approximately 1 h), and composition by thorough purging of the non-steady state product (3 h, approximately three times the liquid residence time) before sampling. A different shutdown procedure was used for these samples than those described in Chapter 2. In the previous experiments, the feed and product lines were both closed at the end of the reaction, shutting in the reactor at reaction pressure. The heater was turned off and the reactor was allowed to cool. Concerns regarding the safety of blocking in the reactor at high temperature led to the development of an alternate shutdown procedure. In the experiments described in this chapter, the liquid feed line was closed at shutdown, but the product lines remained open, and the gas supply was switched to nitrogen. The nitrogen pressure and flowrate were slowly reduced over a period of approximately 0.5 h during which time the reactor cooled to approximately 400°C.

6.3 RESULTS AND DISCUSSION

6.3.1 Catalyst Deactivation and the Effect of Presulfidation.

Figure 6.1 shows the sulfur conversion as a measure of HDS activity achieved with the commercial catalyst during two series of stepwise reactions. The data were obtained from two catalyst samples, which underwent a total of four and six reaction steps respectively. The HDS activity for the first reaction in each series is not shown on the graphs, but can be found in Appendix 6.1, Table A6.1. The activity for sulfur removal during this first reaction step, approximately 70% sulfur removal during 30 min of reaction, was much higher than in the second and subsequent steps (typically 65% sulfur removal during a 1 h reaction). This high reactivity may be attributed to the fact that the catalyst was initially in the oxide state and was undergoing active sulfidation. The data do show some scatter, but no deactivation trend with successive steps is observable. Also shown in Figure 6.1 is the HDS activity of three presulfided samples. The data for these samples suggest a slight deactivating trend, however, it was not significant within the scatter of the data, because the sulfur removal values for the different catalyst samples ranged over approximately 10%. It appears from the data that presulfidation does not give a significant difference in HDS activity relative to presulfidation by the bitumen feed. Any deactivation trend was within the range of the scatter of the experimental data from the untreated catalyst. The higher activity observed for the commercial catalysts during the first reaction step can be directly attributed to the presence of the Ni and Mo oxides, since presulfided catalyst with no previous exposure to the bitumen behaved approximately the same way as catalyst which had had at least one previous exposure to bitumen.

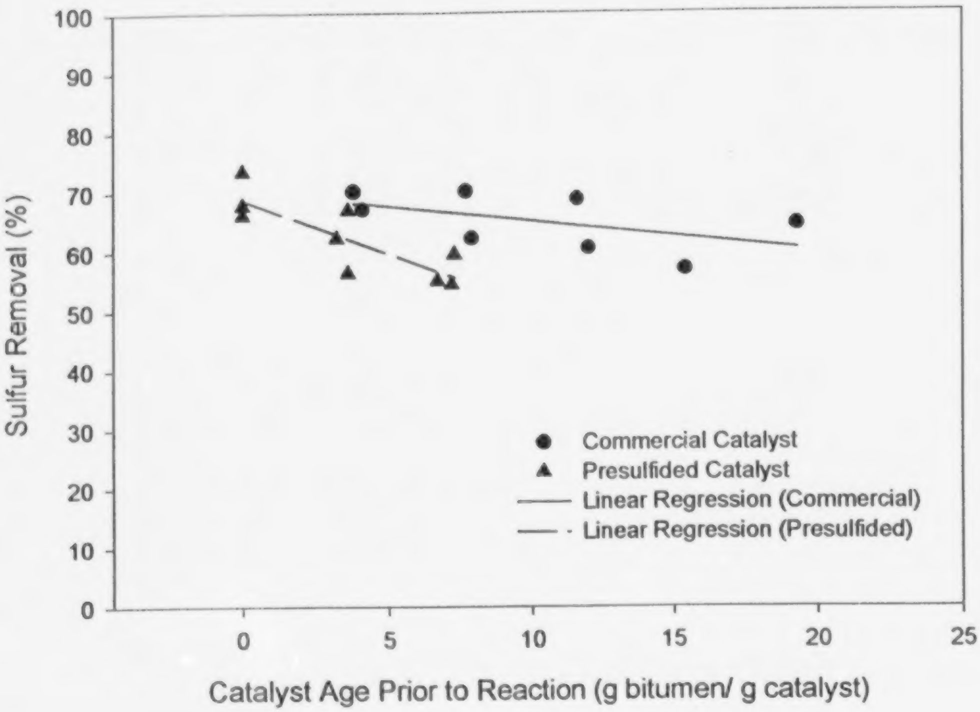

Figure 6.1: Hydrodesulfurization Activity for Commercial Catalyst and Presulfided Commercial Catalyst. (See Appendix 6.1.) All experiments were 1 h long at 430°C, 13.8 MPa.

The scatter in the data for sulfur removal can be attributed to several causes. Feed to catalyst ratios were nominally held constant, but difficulties in transfering the bitumen from the storage container to the reactor prevented exact reproduction of feed to catalyst ratios. Mixing in the reactor was assumed to be good, based on post-reaction observations that the catalyst was well dispersed in the liquid, and the liquid wetted the entire reactor interior. In some cases, catalyst may have agglomerated, reducing access to the catalyst surface. Analysis of the sample may also have contributed to the scatter. Since crushed catalyst was used, particles of catalyst may have been carried into the liquid sample that was analyzed for sulfur content. Coke particles may also have been included. This contamination would have affected the measured values. Repeat analysis of sulfur content was performed when possible, but not enough liquid sample was decanted from the batch reactor in all cases to allow repeats. Samples subjected to repeat analysis typically showed variations in sulfur content of ±0.1% (absolute).

6.3.2 Addition of KNO_3

Two catalyst samples were prepared with KNO_3 using an incipient wetness technique (see Table 6.2). The first sample showed no change in surface acidity (see Figure 6.2). This result, combined with literature evidence (McVicker et al., 1978) that temperatures of at least 600°C are necessary to calcine nitrates, led to the conclusion that the nitrates were not being converted to oxides. A high concentration of KNO_3 in the catalyst gave severe poisoning for sulfur removal (see Figure 6.3).

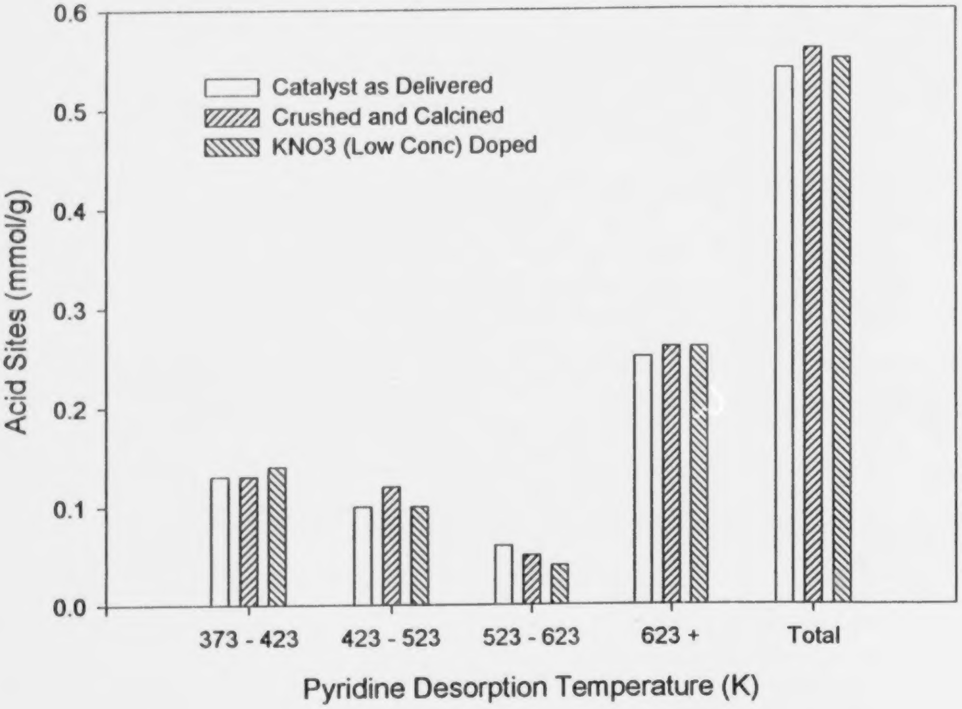

Figure 6.2: Distribution of Strengths of Acid Sites for Commercial Catalyst as Delivered, Crushed and Calcined Commercial Catalyst and Low Concentration (0.26 meq/ g catalyst) KNO_3 Doped Catalyst. (See Appendix 6.2)

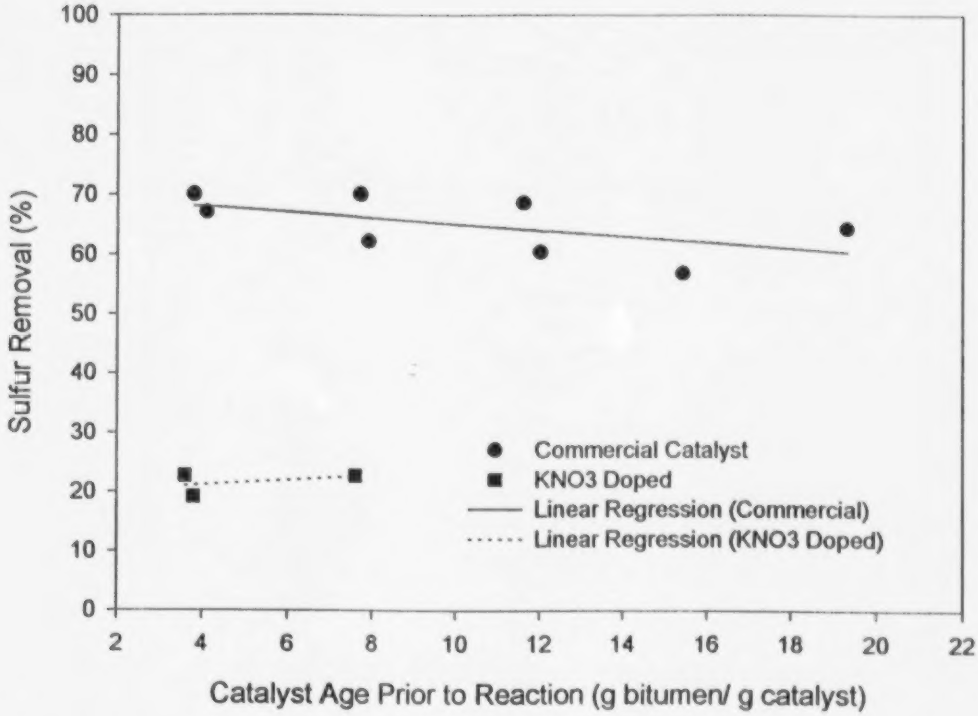

Figure 6.3: Hydrodesulfurization Activity for Commercial Catalyst and Catalyst Doped with 9.8 meq KNO_3/g catalyst. (See Appendix 6.1) All experiments were 1 h long at 430°C, 13.8 MPa.

6.3.3 Addition of Alkali Metal Hydroxide - Catalyst Screening Experiments

The effect of dopant concentration and dopant cation were investigated by preparing five catalysts with the appropriate hydroxides (see Table 6.2). K was chosen for initial screening, and three catalysts of varying dopant concentration were prepared. The activities of these catalysts for sulfur removal are shown in Figure 6.4, compared to the control (untreated commercial catalyst). A slight improvement was observed for HDS activity, along with a reduction in coke deposition (see Figure 6.4 and Table 6.3) at the two lower concentrations of KOH. The mean sulfur conversion for the commercial catalyst was 63.8% and for catalyst doped with 0.28 meq KOH / g catalyst, conversion of sulfur was 71.9%. These mean values were statistically different at the 98% confidence level (Appendix 6.3). No deactivation was observed for these KOH doped catalysts (see Appendix 6.3). Use of very high levels of KOH caused poisoning of the catalyst of the same order of magnitude as observed with the high concentration KNO_3.

Table 6.3: Carbon Content of Base Doped Catalyst

Description	Dopant Concentration (meq/g)	C (%)
Commercial	n/a	17.3
KOH Low Concentration	0.28	15.7
KOH Mid Concentration	0.59	15.5
KOH High Concentration	5.22	n/a
NaOH	0.26	14.4
LiOH	0.26	14.4

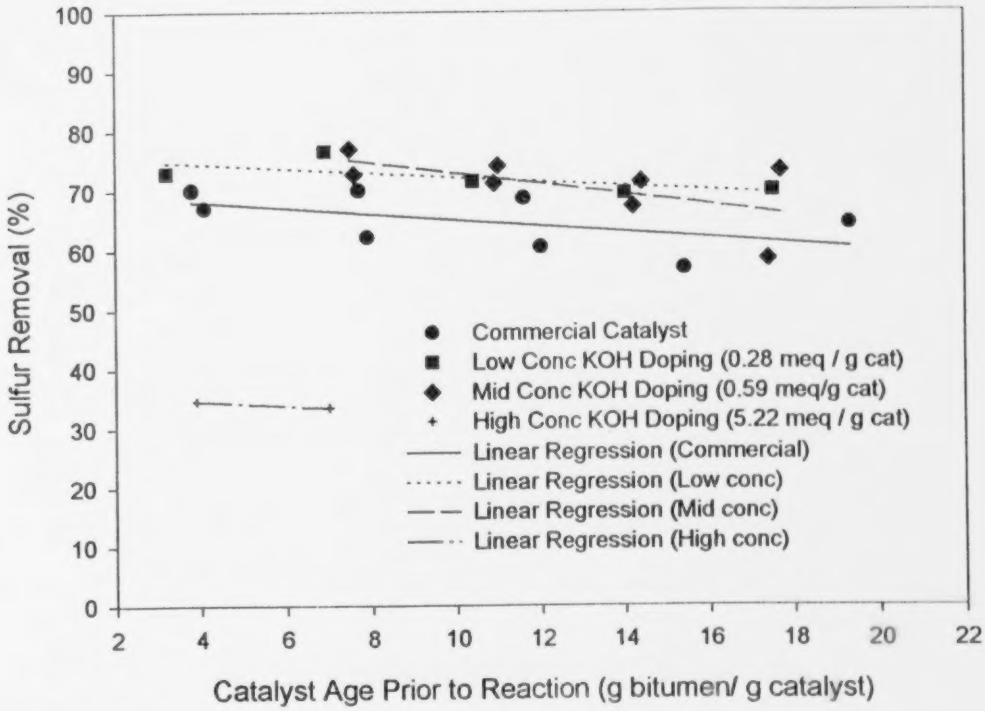

Figure 6.4: Hydrodesulfurization Activity for Commercial Catalyst and Catalyst Doped with 0.28 meq KOH / g catalyst, 0.59 meq KOH / g catalyst and 5.22 meq KOH / g catalyst. (See Appendix 6.1.) All experiments are 1 h long at 430°C, 13.8 MPa.

The data in Figure 6.5 show the HDS activity of three hydroxide-doped catalysts, compared to the commercial catalyst. In this figure the LiOH and NaOH doped catalysts clearly show higher HDS activity than the commercial and KOH doped catalysts. The mean HDS conversion for the NaOH and LiOH doped catalysts, taken as a group, of 80.1%, was significantly greater than the 71.9% HDS activity of the KOH catalyst (99% confidence level; see Appendix 6.3 for statistical analysis). No deactivation was observed for the NaOH or LiOH treated catalysts taken as a group (see Appendix 6.3). Figure 6.6 gives the average HDS activity for the last four reactions in the series plotted versus the carbon content of the catalyst. These data clearly show a relationship between carbon content on the catalyst and the HDS activity. This relationship is consistent with the model presented in Chapter 3, and the mass transfer implications presented in Chapter 4. If the base treatment has been successful in neutralizing the strong acid sites, a discontinuous layer of carbonaceous deposits would result, giving less mass transfer resistance, and higher activity for catalytic reactions.

Figure 6.7 shows the data for the distribution of strengths of acid sites for the KOH and NaOH treated catalysts. These catalysts were treated with sufficient base (0.26 to 0.28 meq/g catalyst) to neutralize the strong acid sites which occur on the commercial catalyst. The data of Figure 6.7 show significant differences between replicate samples. In contrast, the data of Figure 6.2 show three samples which were expected to be of similar acidity. This figure shows the reproducibility from the analytical technique on independent samples. Acid site concentrations were reproducible to within 0.03 mmol/g. In the case of the NaOH sample (Figure 6.7), the discrepancy between samples is somewhat greater than that observed in Figure 6.2, with variations up to 0.08 mmol/g. The incipient wetness technique used to dope the catalyst may result in uneven

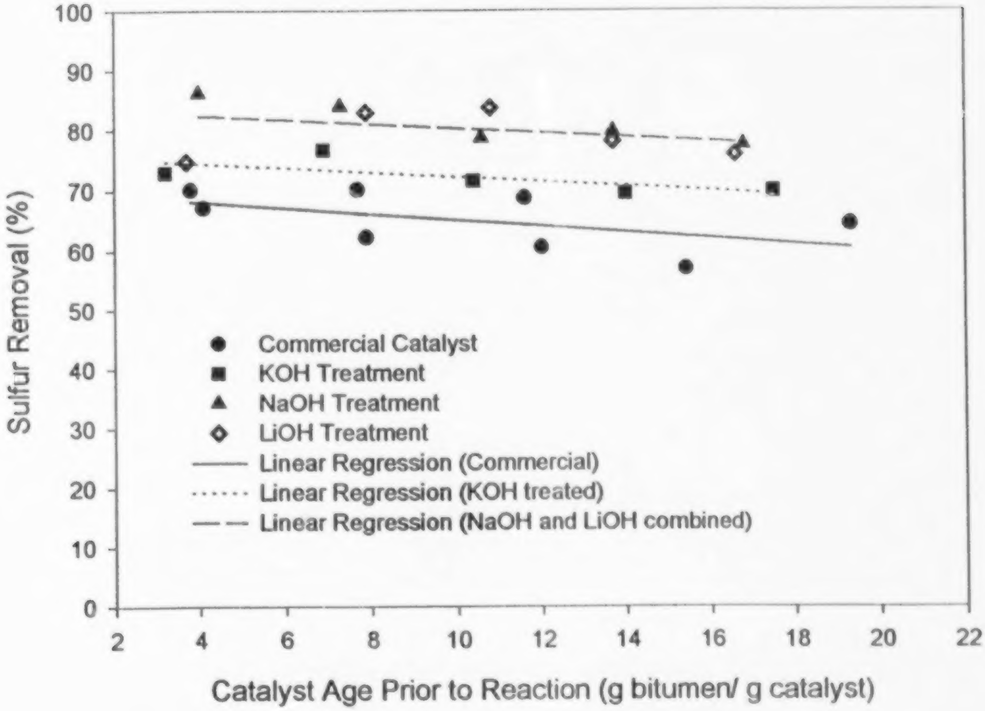

Figure 6.5: Hydrodesulfurization Activity for Commercial Catalyst and Catalysts Doped with 0.28 meq KOH / g catalyst, 0.26 meq NaOH / g catalyst and 0.26 meq LiOH / g catalyst. (See Appendix 6.1) All experiments were 1 h long at 430°C, 13.8 MPa.

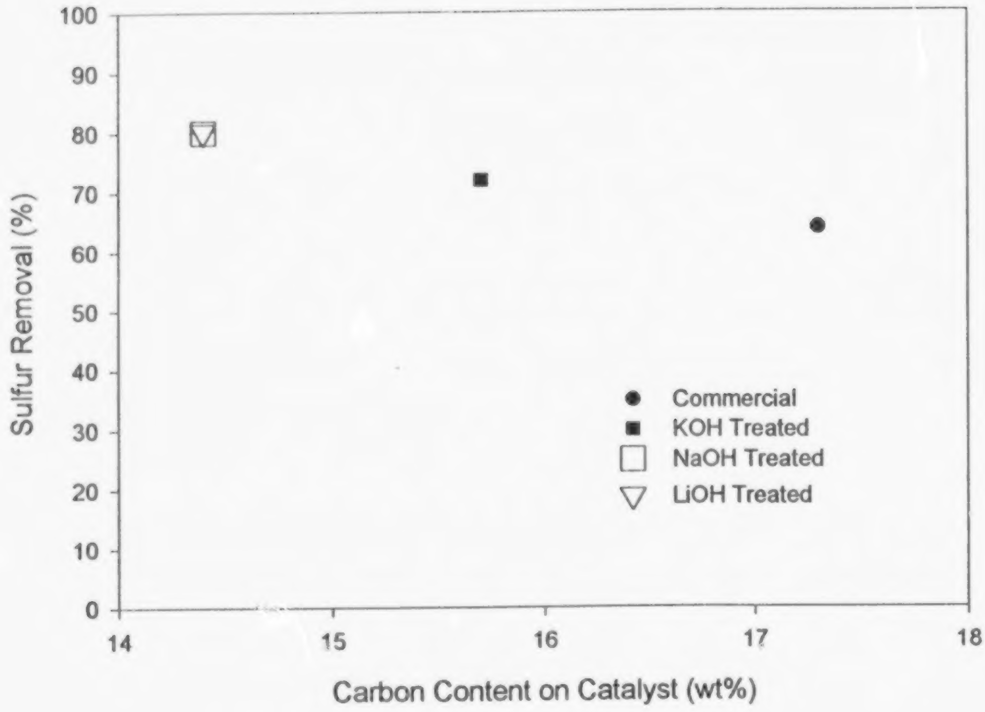

Figure 6.6: Average Hydrodesulfurization Activity for Commercial Catalyst and Catalysts Doped with 0.28 meq KOH / g catalyst, 0.26 meq NaOH / g catalyst and 0.26 meq LiOH / g catalyst versus Carbon Content of the Catalyst. All experiments were 1 h long at 430°C, 13.8 MPa.

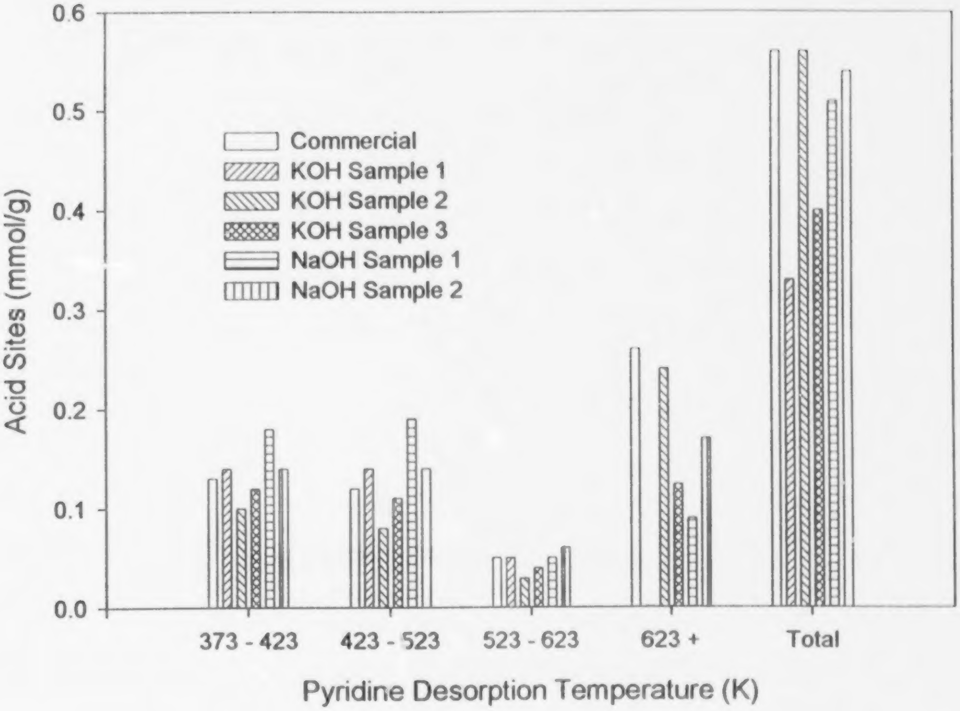

Figure 6.7: Distribution of Strengths of Acid Sites for Commercial, KOH Doped Catalyst (0.28 meq / g catalyst) and NaOH Doped Catalyst (0.26 meq / g catalyst). (See Appendix 6.2.)

distribution of the dopant. This heterogeneity may cause subsampling errors leading to somewhat larger variations between analysis of separate samples. The NaOH data do suggest that partial neutralization has occured. Total acidity was not reduced significantly, but very strong acid sites were partially neutralized, resulting in a shift of the acid site distribution towards weaker acidity sites. The discrepancy between KOH samples is so large it cannot be entirely attributed to sample heterogeneity. Although the variation is very large, the data suggest that partial neutralization of the very strong acid sites has been achieved. The data do not support the hypothesis that KOH and NaOH have different efficiencies for neutralizing the very strong acid sites.

When the catalysts are soaked in aqueous solutions, it is expected that Lewis acid sites may convert to Bronsted acid sites (Benesi and Winquist, 1978). The Bronsted acid sites are then expected to revert to Lewis acid sites under the high temperature reducing conditions employed in hydroprocessing. If Bronsted acid sites can be neutralized by ion exchange with the alkali metal dopants under hydrated conditions, they will be prevented from converting to Lewis acid sites under reaction conditions.

Although the acidity of the catalyst was not reduced as much as expected, the data in Figure 6.6 clearly show a positive effect on catalytic activity. Given the literature on the possible effects of alkali treatment on the transition metals, this effect can be tentatively attributed to neutralization of the alumina surface. While alterations in dispersion of the metal sulfide crystallites cannot be ruled out, neutralization of some of the strong acid sites would give results consistent with the experimental observations.

The data of Figure 6.5 show a clear difference in HDS activity between KOH doped catalysts and those doped with LiOH or NaOH, but the reason for differences between the cations is unclear. Possible hypotheses include the effect of cation size, neutralization efficiency and morphological changes in the support. Cation size was probably unimportant, since the cations co-existed on the surface with hydrocarbon molecules which were at least one order of magnitude larger than the largest cation used. As well, no systematic variation was observed between cation size and HDS activity. No chemical basis exists to support the idea that neutralization efficiency may be a function of cation choice, since the hydroxide salts were used in all cases. Analysis of the distibution of strengths of acid sites of the doped samples was subject to error, but the data suggest both KOH and NaOH gave only partial neutralization of strong acid sites. Possible changes in the surface area after base doping were not investigated, but were not expected at the calcination temperatures used in this investigation (450 °C). The variation of catalyst activity with cation cannot be explained based on the data obtained in this study.

The inconsistent results with different cations are consistent with the literature, in which no universal trend was observed with cation. Kelly and Ternan (1979) obtained the highest activities with Li doped catalysts, but less improvement with Na and K. The concentration ranges used by Kelly and Ternan fell well above those used in the current study, making comparisons between the two studies difficult. Chen and Chen (1990a) did not observe a systematic variation in HDS activity with a series of alkali metals, nor did Papaioannou and Hayes (1990) find a systematic trend with a series of alkaline earth cations. The inconsistent results observed in this study and in others with series of alkali and alkaline earth metal cations suggest that the role of these dopants in altering catalyst activity goes beyond simple relationships of Lewis acidity or cation size. The mechanism is, as yet, unknown.

6.3.4 Catalyst Stability and Multi-Function Activity

Several concerns arise whenever a modification to an existing catalyst formula is proposed. Increased initial activity is of limited benefit if the catalyst deactivates more rapidly than available formulations. As well, when screening studies are performed which do not allow thorough testing of activity for all reactions of interest, then misleading conclusions may be reached. Given these two concerns, CSTR experiments were performed to compare the activity of the commercial catalyst to the Na doped catalyst (0.26 meq/g catalyst). This experiment gave slightly higher catalyst to oil ratios than the micro batch reactor and provided product samples which were large enough to allow analysis of the product for pitch conversion, MCR conversion, asphaltene conversion, heavy metals removal, overall sulfur and nitrogen removal and sulfur and nitrogen removal in each of four distilled fractions. The results of the product analysis are given in Table 6.4 and Table 6.5.

Total liquid product yield and pitch conversion did not change as a result of doping the catalyst. This result was consistent with high levels of thermal cracking expected under these reaction conditions (Ayasse, 1994). The high levels of carbonaceous residue typically found on these catalysts is expected to result in significant deactivation of the acid cracking function of the alumina, regardless of the presence of the Na dopant.

The batch experiments showed a 20% relative increase in HDS activity for the Na doped catalyst for feed to catalyst ratios up to 24 g oil / g catalyst. The final oil to catalyst ratios for the CSTR experiments were approximately 32 g/g. At this catalyst age, the HDS

Table 6.4: Characterization of the Feed and CSTR Products from Experiments Using the Commercial Catalyst and a Na Doped Catalyst.

	Bitumen Feed	Commercial Catalyst Product	Na Doped Catalyst Product
C (%)	82.67	83.31	84.92
H (%)	10.21	11.36	11.54
S (%)	4.89	1.63	1.27
N (%)	0.45	0.44	0.41
Total Liquid Product Yield (wt %)	N/A	94	93
Naptha (IBP-177 C) (% TLP)	0	12.2	14.3
Mid Distill (177-343 C) (% TLP)	7.0	30.5	30.0
Gas Oil (343-524 C) (% TLP)	38.0	34.2	33.8
Residue (524 C+) (% TLP)	55.0	20.4	19.1
MCR (% of TLP)	13.73	6.0	5.7
MCR (% of Residue)	N/A	37.0	39.0
Asphaltenes (wt %)	16.0	4.7	3.5
Ni (ppm in TLP)	73.4	28.7	24.6
Ni (ppm in Residue)	N/A	157.0	163.5
V (ppm in TLP)	191.31	43.9	37.4
V (ppm in Residue)	N/A	231.2	242.7
Carbon Content of Catalyst (%)	N/A	17.0	17.4

Table 6.5: Sulfur and Nitrogen Content of Product Fractions

Sample - Fraction	Yield (wt % TLP)	S (%)	N (%)
Commercial IBP -177	12.2	0.17	0.03
Commercial 177 - 343	30.5	0.51	0.16
Commercial 343 - 524	34.2	1.58	0.38
Commercial 524 +	20.4	3.61	0.97
Na Doped IBP - 177	14.3	0.11	0.03
Na Doped 177 - 343	30.1	0.34	0.15
Na Doped 343 - 524	33.8	1.24	0.40
Na Doped 524 +	19.1	3.22	0.98

conversion (calculated based on a 2 h mixing cup sample) was 11% higher for the Na doped catalyst than for the commercial catalyst. Calculation of the apparent first-order rate constant for the removal of sulfur gives a more accurate comparison of these values. If one assumes that the removal of sulfur is first order in sulfur concentration, the values of the apparent rate constant (k^*) times the reaction time or mean residence time are shown below.

Table 6.6: Comparison of the Apparent First Order Rate Constants for Sulfur Removal for the Na-Doped and Commercial Catalysts.

Reactor	$k^{*}_{commercial} \times t$ (or $k^{*}_{commercial} \times \tau$)	$k^{*}_{Na} \times t$ (or $k^{*}_{Na} \times \tau$)	$\frac{k^{*}_{Na}}{k^{*}_{commercial}}$
Batch	1.0	1.5	1.5
CSTR	2.0	2.9	1.4

The two sets of reactor data, therefore, showed a consistent improvement in catalyst activity due to addition of NaOH. The elemental analysis of the product fractions from the CSTR experiments with the commercial and doped catalysts show reduced sulfur in all product fractions, with the greatest effect observed in the residue fraction.

The overall nitrogen concentrations for the two products (Table 6.4) suggest an improvement in HDN activity for the soldium treated catalyst. Closer inspection of the nitrogen analysis of the distilled fractions (Table 6.5), however, does not support this observation. Given the very low nitrogen removal obtained with the commercial catalyst, significant improvement of the nitrogen removal was not expected. Similarly, the product MCR concentration was not affected by the Na addition.

Asphaltenes are the highest molecular weight, most polar components found naturally in bitumen. Conversion of these components requires a combination of thermal cracking and catalytic heteroatom removal. The lower product asphaltene concentration observed for the Na-doped catalyst may reflect lower mass transfer restrictions

Data from the analysis of the whole oil for Ni and V content suggested doping with Na gave approximately a 10% increase in metals conversion, similar to the improvement shown by HDS. Unfortunately, the analysis of Ni and V in the residue fraction was inconsistent with this observation. The residue fraction of the product from the Na doped catalyst, which was expected to contain all the metals, and comprise 20% of the total product weight, gave appproximately six times the metals concentrations found in the product oils. If one predicts the whole oil concentration based on the residue concentration and yield then the whole oil concentration is approximately 30% higher than was obtained by direct analysis. The analysis of the residue was repeated, and the results were consistent within approximately 2% relative variation between repeats (See Appendix 6.4). A discrepancy of a similar nature was observed for the commercial catalyst product, although the magnitude was less. Given this analytical inconsistency, it was not possible to draw conclusions about changes in the metals conversion.

The two catalysts used in these experiments showed unexpectedly high carbon contents - 17.0% for the commercial catalyst and 17.4% for the Na doped catalyst. These values were well above those observed in any previous CSTR experiment, despite similar conditions employed for the commercial catalyst trial in this section and CSTR experiments discussed in Chapter 2. The new shutdown procedure described in the experimental section left a very viscous, oil/coke paste in the bottom of the reactor, unlike the light product oil which was retrieved from the reactor in previous experiments. The use of nitrogen during shutdown probably induced a pyrolysis-like environment in the reactor between shutdown and the final cooling of the reactor. This environment likely caused coking of the catalyst following shutdown.

The results described above show a trend towards higher activity for reactions involving catalytic hydrogenation / hydrogenolysis such as hydrodesulfurization, asphaltene conversion and possibly metals conversion. These observations were consistent with the hypothesis that partial neutralization of the catalyst support will result in lower carbon content on the catalyst and reduced mass transfer restrictions within the catalyst pore network. These data were obtained from short term experiments. Although these experiments show a significant improvement in catalyst activity following alkali doping, longer term testing of the stability of the catalyst must be performed before the industrial implications of catalyst doping can be determined.

6.4 CONCLUSIONS

1. Doping of Ni-Mo / alumina catalyst using KNO_3 was not effective for neutralizing the surface at low concentrations, and resulted in catalyst poisoning at high concentrations.

2. Doping of the catalyst using KOH gave a marginal change in coke deposition and activity at low concentrations. Doping at very high concentrations resulted in poisoning of the catalyst.

3. Doping of the catalyst using NaOH and LiOH resulted in decreased coke deposition and significantly increased the HDS activity in micro-batch reactions.

4. Increased HDS activity following doping of the catalyst with NaOH was confirmed by larger scale CSTR experiments.

5. Asphaltene conversion increased marginally following doping of the catalyst with NaOH. Pitch conversion, MCR conversion and nitrogen removal were unaffected by doping of the catalyst with NaOH. The effect on metals conversion could not be determined.

6.5 LITERATURE CITED

Absi-Halabi, M.; Stanislaus, A.; Trimm, D.L. Coke Formation on Catalysts During the Hydroprocessing of Heavy Oils. *Appl. Catal.* **1991**, 72, 193-215.

Ayasse, A. Hydrocracking of Athbasca Bitumen. MSc Thesis, University of Alberta, 1994.

Baird Jr., W. C.; Shoukry, E. I. Reforming with Modified Alumina Catalysts. *US Patent 4,966,682.* October 30, **1990.**

Baker, J. R.; McCormick, R. L.; Haynes Jr., H. W. Effect of Sodium Impregnation on Catalyst Performance When Hydrotreating a Coal Derived Liquid. *Ind. Eng. Chem. Res.* **1987,**.26, 1895-1901

Beaton, W.I.; Bertolacini, R.J. Resid Hydroprocessing at Amoco. *Catal. Rev. Sci. Eng.* **1991**, 33, 281-317.

Benesi, H.A.; Winquist, B.H.C. *Advances in Catalysis,* **1978**, 27, 97-182.

Centeno, A.; Laurent, E.; Delmon, B. Influence of the Support of CoMo Sulfide Catalysts and of the Addition of Potassium and Platinum on the Catalytic Performances for the Hydroxygenation of Carbonyl, Carboxyl and Guaiacol-Type Molecules. *J Catal.* **1995**, 154, 288-289.

Chen, I; Chen, F. L. Effect of Alkali and Alkaline Earth Metals on the Resistivity to Coke Formation and Sintering of Nickel -Alumina Catalysts. *Ind. Eng. Chem. Res.* **1990,** 29, 539-543.

Gray, M. R.; Khorasheh, F.; Wanke, S. E.; Achia, U.; Krzywicki, A.; Sanford, E. C.; Sy, O. K. Y.; Ternan, M. Role of Catalyst in Hydrocracking of Residues from Alberta Bitumens. *Energy and Fuels.* **1992,** 6, 478-485.

Haensel, V. Hydrocarbon Conversion Catalyst *US Patent 2,930,763*. March 29, **1960**.

Hayes, J.C; Pilotzer, E. L. Dehydrogenation with a Catalytic Composite Containing Platinum, Rhenium, a Group VI Transition Metal and an Alkali or Alkaline Earth Metal. *US Patent 3,714,281*. Jan 30, **1973**.

Huang, Y.-J.; Schwartz, J.A. The Effect of Catalyst Preparation on Catalytic Activity: IV. The Design of Ni/Al_2O_3 Catalysts Prepared by Incipient Wetness. *Appl. Catal.* **1987,** 32, 59-70.

Kelly, J. F.; Ternan, M. Hydrocracking of Athabasca Bitumen with Alkali Metal Promoted CoO-MoO_3-Al_2O_3 Catalysts. *Can. J. Chem. Eng.* **1979** 57, 726-733.

Lewis, J.M.; Kydd, R.A; Boorman, P.M; Van Rhyn, P.H. Phosphorous Promotion in Nickel-Molybdenum/ Alumina Catalysts: Model Compound Reactions and Gas-Oil Hydroprocessing. *Appl. Catal. A.* **1992**, 84, 103-121.

Lowenthal, E. E; Schwarz, S.; Foley, H.C. Surface Chemistry of Rh-Mo/γ-Al_2O_3: An Analysis of Surface Acidity. *J. Catal.* **1995** 156, 96-105.

Lycourghiotis, A.; Vattis, D.; Aroni, P. Investigation of the Cobalt Species Formed on γ-Al_2O_3 Doped with Alkali Metals. *Z. Phys Chem Neue Folge, Bd.* **1980,** 121, 257-265.

Masuyama, T.; Kageyama, Y.; Kawai, S. A Ca-Modified Ni-Mo Catalyst for Hydroprocessing of Coal Liquid Bottoms in Two Stage Coal Liquefaction. *Fuel.* **1990,** 69, 245-250.

Mauldin, C. H.; Baird, Jr., W. C. Reforming with Multimetallic Catalysts. *US Patent 4,347,123* Aug 31, **1982.**

McCormick, R.L.; King, J.A.; King, T.R.; and Haynes, H.W. Influence of Support on the Performance of Coal Liquid Hydrotreating Catalysts. *Ind. Eng. Chem. Res.* **1989,** 28, 940-947.

McCormick, R.L.; Haynes, H.W.; Netzel, D.A. Effect of Catalyst Acidity on the Hydrogen- Donor Content of a Hydrotreated Coal Liquid. *Ind. Eng. Chem. Res.* **1989,** 28, 1156-1161.

McVicker, G.B.; Garten, R.L.; Baker, R.T.K. Surface Area Stabilization of Ir/Al_2O_3 Catalysts by CaO, SrO and BaO Under Oxygen Atmospheres: Implications on the Mechanism of Catalyst Sintering and Redispersion. *J. Catal.* **1978**, 54, 129-142.

O'Hara, M.J.; Johnson, R.W.; Hilfman, L. Hydroprocessing of Hydrocarbons. *U.S. Patent 4,202.758*, May 13, **1980.**

O'Young, C.L. Effects of Alkali-Metal Promoters (Potassium and Cesium) on a Mo/γ-Al_2O_3 Catalyst. *J Phys. Chem.* **1989,** 93, 2016-2018.

O'Young, C.L.; Yang, C.H.; DeCanio, S.J.; Patel, S.; Storm, D.A. CO_2 and NO Chemisorption on Mo/γ-Al_2O_3. *J Catal.* **1988**, 113, 307-316.

Papaioannou, A.; Haynes, H.W. Alkali-Metal- and Alkaline-Earth-Promoted Catalysts for Coal Liquefaction Applications. *Energy and Fuels* **1990,** 4, 38-42.

Sulima, R.; Echigoya, E. Catalytic Reduction of NO with Hydrogen over a Cobalt - Alumina Catalyst. Effect of Alkali Metal Additives. *Reac. Kin. and Catal. Lett.* **1976,** 4, 295-299.

Topsoe, H.; Clausen, B. S.; Topsoe, N.-Y.; Pedersen, E. Recent Basic Research in Hydrodesulfurization Catalysis. *Ind Eng. Chem. Fundam.* **1986,** 25, 25-36.

7 CONCLUSIONS

This thesis describes progress toward two basic goals, the understanding of the coking behaviour of bitumen hydroprocessing catalyst, especially as it relates to hydrogen pressure, and the modification of this behaviour to allow higher activity catalysts. The following is a summary of the new understanding which has evolved regarding the initial catalyst activity, and the success achieved in modifying the catalyst.

Coke deposition on the catalyst was generally less dependent upon reaction conditions than initially assumed. It was found to be independent of reaction time, feed composition and feed to catalyst ratio over wide ranges, when all other reaction parameters were held constant. At low feed to catalyst ratios, total carbon content of the catalyst showed an exponential approach followed by a constant value when correlated to feed oil to catalyst ratio, consistent with first order dynamics. Differences in catalyst carbon content observed between CSTR experiments and batch experiments were attributable to the differences in hydrogen partial pressure. Carbon content decreased from 17.5% at 6.9 MPa hydrogen to 11.3% at 15.2 MPa in CSTR experiments. Coke deposition on the catalyst was not coupled to liquid phase coking reactions.

A model for coke deposition in hydroprocessing catalysts was developed. The model was based on an annular geometry. The basic features of this model were monolayer adsorption of residue molecules onto the alumina support, except in the immediate vicinity of the active metal crystallites, which maintained a clear alumina surface. The transient coke deposition behaviour observed with increasing oil to catalyst ratio was consistent with a surface adsorption model. The assumption that a monolayer was adsorbed was consistent with observed insensivity of the catalyst carbon content to reaction time and feed composition.

Further investigation showed the carbon deposited on a catalyst during the inital hours of use was highly reactive, and was removed from the surface at reaction conditions in residue-free feed. High molecular weight components from the asphaltene fraction appear to be the most significant contributing factor for coke deposition. Analysis of the distribution of strengths of the acid sites on the catalyst surface confirmed that the coke deposit on the surface was in a structured form, consistent with the annular structure proposed in Chapter 3.

Deactivation observed with these catalysts appears to be related to mass transfer limitations in the catalyst pores. Hindered diffusion theory predicts that virtually all of the catalyst surface area will be subject to at least 40% reduction in effective diffusivity. Wakao and Smith's random pore model was combined with analytical results and estimates based on the model presented in Chapter 3 to predict that effective diffusivity would be reduced by approximately 90% relative to catalyst without coke. Observations from this study are inconsistent with the existence of plugged pore mouths suggested by some of the literature for hydroprocessing catalysts.

Given the acidic nature of the catalyst surface and the basic nature of the feed, it was proposed that lower catalyst coking, and therefore less mass transfer restriction could be achieved if the catalyst surface was selectively neutralized to reduce the concentration of strong acid sites. KNO_3, KOH, NaOH and LiOH were used to modify the surface. KNO_3 did not neutralize the surface at low concentration, and poisoned the catalyst at very high concentration. KOH gave a slight decrease in catalyst coking, and an increase in HDS activity in the microbatch reactor at low concentration. At high concentrations, KOH also posioned the catalyst. NaOH and LiOH showed a greater decrease in catalyst carbon concentration and a significant increase in HDS activity in the microbatch reactor.

Increased HDS activity was confirmed in a larger scale CSTR experiment. In this experiment, pitch conversion was maintained and asphaltene conversion increased. Nitrogen and MCR conversion remained the same. A meaningful conclusion regarding the removal of nickel and vanadium was not possible due to analytic uncertainties.

This study has allowed the construction of a model for the coke deposition observed early in the life of a bitumen hydroprocessing catalyst. This information has been combined with knowledge of the chemistry of the catalyst surface to allow successful modification of the surface leading to higher catalytic activity.

APPENDIX 2.1: CARBON CONCENTRATIONS ON CATALYSTS FROM BATCH REACTOR EXPERIMENTS

Table A2.1: Carbon Concentrations on Catalysts from Batch Reactor Experiments.

Experiments B1 through B5 indicate the carbon content as a function of reaction time at constant feed to catalyst ratio (samples B1 through B5) and as a function of feed to catalyst ratio (B1, B2, B, B7, B8)

Sample	Total Reaction Time (h)	Cumulative Feed to Catalyst Ratio (g oil/g cat)	Carbon Content (wt%)
B1	1.5	8.1	11.6
B2	2	7.8	10.3
B3	3	8.3	12.2
B4	5	7.5	13.2
B5	5	8.1	11.1
B6	3.5	15.7	17.0
B7	5.5	23.0	17.3
B8	1	3.8	8.6

APPENDIX 2.2: CATALYST CARBON CONTENT RELATED TO PRODUCT RESIDUE CONTENT AND MCR CONTENT.

Table A2.2: Catalyst Carbon Content Related to Product Residue Content and MCR Content. All data are from CSTR experiments. Samples correspond to those shown in Table 2.2: Summary of Reaction Conditions and Carbon Content for CSTR Experiments. Samples C8 and C9 each represent a group of identical CSTR experiments. Samples C10 and C 11 are two representatives from a third group of experiments. Several experiments were required at each of the first three stages in this multistage hydrocracking experimental progam in order to provide enough feedstock for the fourth stage (single) experiment represented by C12..

Sample	Residue Content of the Product (wt%)	MCR Content of the Product (wt%)	Carbon Content on the Catalyst (wt%)
C8	32.2	9.9	12.9
C9	21.3	7.6	14.8
C10	8.5	2.3	11.2
C11	8.5	2.3	14.1
C12	0.74	0.1	6.9

APPENDIX 3.1: DETERMINATION OF SURFACE CARBON CONCENTRATION RESULTING FROM A MONOLAYER OF VARIOUS SUBSTANCES.

The physical/chemical properties of benzene, graphite and residue are used to determine the surface concentration of carbon in a monolayer of each of these substances. The BET measured surface area will be used for all calculations. Coke is not expected to deposit on the transition metal crystallites. Appendix 3.3 indicates that the surface area covered by metal crystallites is between 3 and 10% of the total area. The loadings below could be corrected by this figure, but since the error is low, and the surface coverage is only an estimate, this correction will not be made.

Benzene - lying flat on the catalyst surface.

Molecular diameter of benzene = 0.498 nm
Molecular weight of benzene = 78.06 g / gmol
Carbon content of benzene = 72/78.06 = 92.2%

$$\frac{\text{surface area}}{\text{molecule}} = \frac{\pi}{4} * d^2$$

$$\frac{\text{surface area}}{\text{molecule}} = \frac{\pi}{4} * \left(.498 * 10^{-9}\text{m}\right)^2$$

$$\frac{\text{surface area}}{\text{molecule}} = 1.297 * 10^{-19}\text{m}^2 / \text{molecule}$$

$$\text{Monolayer Surface Concentration of Carbon} = \frac{\text{weight / molecule * carbon content}}{\text{area / molecule}}$$

$$\text{Monolayer Surface Concentration of Carbon} = \frac{78.06\text{g / gmol}*0.922\text{g C / g benzene}}{6.023*10^{23}\text{molecules / gmol}*1.95*10^{-19}\text{m}^2\text{ / molecule}}$$

$$\text{Monolayer Surface Concentration of Carbon} = 6.14*10^{-4}\text{gC / m}^2$$

Graphite

Graphite density = $2.25*10^6$ g / m^3
Monolayer thickness = 0.34 nm

$$\text{Monolayer volume} = \text{surface area} * \text{thickness}$$

$$\text{Monolayer volume} = 1\text{m}^2 * 0.34 * 10^{-9}\text{m}$$

$$\text{Monolayer volume} = 3.4 * 10^{-10}\text{m}^3 / \text{m}^2$$

$$\text{Surface Concentration of Carbon} = \rho * V$$

$$\text{Surface Concentration of Carbon} = 2.25 * 10^6 \text{g} / \text{m}^3 * 3.4 * 10^{-10}\text{m}^3 / \text{m}^2$$

$$\text{Surface Concentration of Carbon} = 7.65 * 10^{-4} \text{ g C} / \text{m}^2$$

Residue

Density = $1.05 * 10^6$ g / m^3
Molecular weight = 625 g / gmol
Carbon content = 82.6 %

$$\frac{\text{mass}}{\text{molecule}} = \frac{625 \text{ g} / \text{gmol}}{6.02 * 10^{23} \text{ molecules} / \text{gmol}}$$

$$\frac{\text{mass}}{\text{molecule}} = 1.038 * 10^{-21} \text{ g} / \text{molecule}$$

$$\frac{\text{volume}}{\text{molecule}} = \frac{\frac{\text{mass}}{\text{molecule}}}{\text{density}}$$

$$\frac{\text{volume}}{\text{molecule}} = \frac{1.04 * 10^{-21} \text{ g} / \text{molecule}}{1.05 * 10^6 \text{ g} / \text{m}^3}$$

$$\frac{\text{volume}}{\text{molecule}} = 9.89 * 10^{-28} \text{ m}^3 / \text{molecule}$$

$$\text{radius} = \left(\frac{\text{volume} * 3}{4 * \pi}\right)^{1/3}$$

$$\text{radius} = \left(\frac{9.89 * 10^{-28} * 3}{4 * \pi}\right)^{1/3}$$

radius = 0.61 nm.

projected area = $\pi * r_r^2$

projected area = $1.16*10^{-18}$ m^2/molecule

$$\text{Surface concentration} = \frac{\text{mass / molecule} * \text{carbon content}}{\text{area}}$$

$$\text{Surface concentration} = \frac{1.038*10^{-21}\ \text{g / molecule}*0.826\text{gC / gresid}}{1.16*10^{-18}}$$

Surface concentration $= 7.1*10^{-4}$ g C / m^2

Experimental Surface Carbon Concentration

Maximum Concentration = 18% (based on spent catalyst weight)
Catalyst Surface Area = 317 m^2/g

Normalize carbon content to fresh catalyst weight - assume spent catalyst weight represents only fresh catalyst + carbon.

$$\text{Catalyst Carbon Content (fresh)} = \frac{\text{weight carbon}}{\text{weight catalyst} - \text{weight carbon}}$$

Catalyst Carbon Content (fresh)

$$\text{Catalyst Carbon Content (fresh)} \frac{18\text{g}}{100\text{g} - 18\text{g}}$$

Catalyst Carbon Content (fresh) =0.22g C / g fresh catalyst

$$\text{Surface Concentration} = \frac{\text{Catalyst Carbon Content (fresh)}}{\text{surface area}}$$

$$\text{Surface Concentration} = \frac{0.22\ \text{g C / g catalyst}}{317\text{m}^2\ \text{/ g catalyst}}$$

Surface Concentration = $6.92*10^{-4}$ g C / m^2

APPENDIX 3.2: SENSITIVITY ANALYSIS OF MONOLAYER CARBON CONTENT

Table A3.2 Effect of Density, Carbon Content and Molecular Weight on the Prediction of Carbon Content Arising from Monolayer Coverage.

ρ (kg/m^3)	MW (Da)	Carbon Content (g C / g oil)	Monolayer Coverage ($x10^4$ g C/ m^2)	Change (%)
1050	625	0.826	7.10	Base Case
950	625	0.826	7.85	+10
1150	625	0.826	6.50	-8.5
1050	450	0.826	6.34	-11
1050	1000	0.826	8.30	+17
1050	625	0.800	6.87	-3
1050	625	0.85	7.30	+3

APPENDIX 3.3: COMPARISON OF MODEL PARAMETER b TO LITERATURE VALUES

Work by Madeley and Wanke (1986) showed typical dimensions of MoS_2 crystallites to be 5 nm across the hexagonal plane and 2.5 nm thick. These crystallite sizes resulted following presulfiding at 400 °C. Although most catalysts in this thesis were not presulfided, this temperature was similar to operating temperatures used during hydroprocessing experiments.

If one approximates the hexagonal crystallites by circular cylinders of the same diameter:

$V = \pi r^2 h$
$V = \pi * (2.5x10^{-9} m)^3$
$V = 4.91x10^{-26}\ m^3$/crystallite

The catalyst used in this thesis contained 12.5 % MoO_3.

This converts to 12.5 g MoO_3/ 100 g catalyst, or 13.7 g MoS_2 / 100 g of catalyst.

Since the surface area of the catalyst is 317 m^2/g, this corresponds to 0.00433 g MoS_2 / m^2.

The density of MoS_2 is $4.80x10^6$ g/m^3. This results in $9.00x10^{-11}$ m^3 of MoS_2 / m^2 of catalyst surface.

Dividing the total volume by the volume per crystallite results in $N = 1.83x10^{15}$ crystallites / m^2 catalyst.

Multiplying the number of crystallites, N, by πr_c^2, gives
$b = 0.036$ m^2 crystallite/ m^2 catalyst.

It should be noted that this is not the active surface area of the metal crystallites, but rather the total area of the top surfaces of the metal crystallites.

APPENDIX 4.1: DISTRIBUTION OF THE STRENGTHS OF ACID SITES OF SELECTED CATALYSTS

Table A4.1: Distribution of the Strengths of Acid Sites of Fresh Catalyst and Spent Catalysts. Pressures in brackets refer to hydrogen pressure of the CSTR reactor. Acid strength is defined through pyridine desorption temperature, as described below.

Catalyst	Number of Acid Sites (mmol/g catalyst)				
	Very Weak	Weak	Strong	Very Strong	Total
Fresh	0.13	0.12	0.05	0.26	0.56
Spent (15.3 MPa)	0.04	0.04	0.01	0.1	0.19
Spent (6.9 MPa)	0.06	0.04	0.01	0.03	0.14

Acid strength is defined by pyridine desorption temperature. Very weak acid sites are sites from which pyridine desorbed at temperatures ranging from 373 K to 423 K. Similarly weak acid sites correspond to desorption temperatures 423 K to 523 K; strong acid sites correspond to 523 K to 623 K and very strong acid sites correspond to sites on which pyridine is irreversibly adsorbed at 623K.

APPENDIX 5.1: CALCULATIONS FOR THE RANDOM PORE MODEL OF WAKAO AND SMITH

These calculations will be broken into sections: determination of the fresh catalyst diffusivity (will include an unknown related to feed properties), the coked catalyst diffusivity based on the coked catalyst pore size distribution and the coked catalyst based on the assumption of the deposition of a monolayer of thickness 1.2nm. For all calculations, the division between micro and macro pores will be defined as 10 nm. For the both calculations, the "micropore radius" will be taken as the maximum in the pore size distribution, the "macropore radius" will be the midpoint between the cutoff (10nm) and the maximum pore size detected, 200 nm. For the estimation of the coked catalyst diffusivity based on the assumption of monolayer coverage, the pore sizes used will be the fresh catalyst values, minus the thickness of the monolayer, 1.2 nm.

Fresh catalyst

V_m, the macro pore volume = 0.0368 mL/g catalyst (from pore size distribution results)
V_μ, the micro pore volume = 0.5328 mL/g catalyst
$r_{mf} = 15$ nm
$r_{\mu f} = 3$ nm

$$\rho_{pellet} = \frac{1g}{1/\rho(\text{fused alumina}) + \text{volume voids}}$$

$$\rho_{pellet} = \frac{1g}{0.286\text{mL alumina} + (0.0368 + 0.5328\text{mL voids})}$$

$$\rho_{pellet} = 1.169 \text{ g / mL catalyst}$$

$$\varepsilon_{mf} = \text{macropore porosity} = \frac{\text{voids}}{\text{pellet density}}$$

$$\varepsilon_{mf} = \text{macropore porosity} = \frac{0.0368\text{mL}}{1.169\text{g / mL}}$$

$$\varepsilon_{mf} = 0.0315 \text{ mL void/mL pellet}$$

$$\varepsilon_{\mu f} = \text{micropore porosity} = \frac{\text{voids}}{\text{pellet density}}$$

$$\varepsilon_{\mu f} = \text{micropore porosity} = \frac{0.5328\text{mL}}{1.169\text{g / mL}}$$

$\varepsilon_{\mu f}$ = 0.456 mL void / mL pellet

Given the fact that the ratio of the maximum of the pore size distribution to the residue molecule radius is 2.5, diffusion will be dominated by hindered diffusion.

Hindered diffusion in a single pore, i, is defined by:

$$D_{p,i} = D_b e^{-B\lambda_i}$$

$$\lambda_i = \frac{r_r}{r_{p,i}}, \ B = 4.6$$

$$D_{mf} = D_b e^{\frac{-4.6*0.6}{15}}$$

$$D_{mf} = 0.83D_b$$

$$D_{\mu f} = D_b e^{\frac{-4.6*0.6}{3}}$$

$$D_{\mu f} = 0.40D_b$$

The random pore model defines the effective diffusivity as:

$$D_{ef} = \varepsilon_{mf}^2 D_{mf} + \frac{\varepsilon_{\mu f}^2 (1 + 3\varepsilon_{mf})}{1 - \varepsilon_{mf}} D\mu f$$

$$D_{ef} = (0.0315)^2 * 0.83D_b + \frac{(0.456)^2 (1 + 3(0.0315))}{1 - 0.0315} * 0.40D_b$$

$$D_{ef} = 0.0946D_b$$

Coked catalyst - based on pore size distribution results

V_m, the macropore volume = 0.01798 mL/g catalyst (from pore size distribution results)
V_μ, the micro pore volume = 0.2349 mL/g catalyst
r_{mc} = 15 nm
$r_{\mu c}$ = 2.5 nm

$$\rho_{pellet} = \frac{1\text{g alumina} + 0.18\text{g carbon}}{1/\rho(\text{fused alumina} + \text{volume voids})}$$

$$\rho_{\text{pellet}} = \frac{1\text{g} + 0.18\text{g}}{0.286\text{mL alumina} + (0.0368 + 0.5328\text{mL voids})}$$

ρ_{pellet} = 1.38 g / mL catalyst

$$\varepsilon_{mc} = \text{macropore porosity} = \frac{\text{voids}}{\text{pellet density}}$$

$$\varepsilon_{mc} = \text{macropore porosity} = \frac{0.01798\text{mL}}{1.38\text{g / mL}}$$

ε_{mc} = 0.0129 mL void/mL pellet

$$\varepsilon_{\mu c} = \text{micropore porosity} = \frac{\text{voids}}{\text{pellet density}}$$

$$\varepsilon_{\mu c} = \text{micropore porosity} = \frac{0.2349\text{mL}}{1.38\text{g / mL}}$$

$\varepsilon_{\mu c}$ = 0.168 mL void / mL pellet

Hindered diffusion in a single pore, i, is defined by:

$$D_{p,i} = D_b e^{-B\lambda_i}$$

$$\lambda_i = \frac{r_r}{r_{p,i}}, \; B = 4.6$$

$$D_{mc} = D_b e^{\frac{-4.6 * 0.6}{15}}$$

$D_{mc} = 0.83 D_b$

$$D_{\mu c} = D_b e^{\frac{-4.6 * 0.6}{2.5}}$$

$D_{\mu c} = 0.33 D_b$

The random pore model defines the effective diffusivity as:

$$D_{ec} = \varepsilon_{mc}{}^2 D_{mc} + \frac{\varepsilon_{\mu c}{}^2 (1 + 3\varepsilon_{mc})}{1 - \varepsilon_{mc}} D_{\mu c}$$

$$D_{ec} = (0.0129)^2 * 0.83D_b + \frac{(0.168)^2 (1 + 3(0.0129))}{1 - 0.0129} * 0.33D_b$$

$$D_{ec} = 0.00985D_b$$

The minimum reduction in diffusivity upon depositing the reported coke is:

$$\frac{D_{e,coked,min}}{D_{e,fresh}} = 0.104$$

Coked catalyst - based on the assumption of the deposition of a uniform 1.2 nm layer of coke

$r_{mc} = 13.78$ nm
$r_{\mu c} = 1.78$ nm

Assume that the porosity for each pore type is reduced in the following way by the coke deposition

$$\varepsilon_c = \varepsilon_f * \frac{(r_c)^2}{(r_f)^2}$$

then:

$$\varepsilon_{mc} = \varepsilon_{mf} * \frac{(r_{mc})^2}{(r_{mf})^2}$$

$$\varepsilon_{mc} = 0.0315 * \frac{(13.78)^2}{(15.0)^2}$$

$\varepsilon_{mc} = 0.0266$ mL void/mL pellet

$$\varepsilon_{\mu c} = \varepsilon_{\mu f} * \frac{(r_{\mu c})^2}{(r_{\mu f})^2}$$

$$\varepsilon_{\mu c} = 0.456 * \frac{(17.8)^2}{(30)^2}$$

$\varepsilon_{\mu c}$ = 0.160 mL void / mL pellet

Hindered diffusion in a single pore, i, is defined by:

$$D_{p,i} = D_b e^{-B\lambda_i}$$

$$\lambda_i = \frac{r_r}{r_{p,i}}, \quad B = 4.6$$

$$D_{mc} = D_b e^{\frac{-4.6*0.6}{13.78}}$$

$D_{mc} = 0.82D_b$

$$D_{\mu c} = D_b e^{\frac{-4.6*0.6}{1.78}}$$

$D_{\mu c} = 0.21D_b$

The random pore model defines the effective diffusivity as:

$$D_{ec} = \varepsilon_{mc}{}^2 D_{mc} + \frac{\varepsilon_{\mu c}{}^2(1+3\varepsilon_{mc})}{1-\varepsilon_{mc}} D_{\mu c}$$

$$D_{ec} = (0.0266)^2 * 0.82D_b + \frac{(0.160)^2(1+3(0.0266))}{1-0.0266} * 0.21D_b$$

$D_{ec} = 0.006602D_b$

The maximum reduction in diffusivity upon depositing the experimental carbon content is:

$$\frac{D_{e,coked,max}}{D_{e,fresh}} = 0.070$$

The previous two estimates place bounds on the reduction in diffusivity:

$$0.070 \geq \frac{D_{e,\text{coked}}}{D_{e,\text{fresh}}} \geq 0.104$$

The sensitivity of the above estimate n the value of B was investigated. Using B values from 3.9 to 5.1 gives the range:

$$0.068 \geq \frac{D_{e,\text{coked}}}{D_{e,\text{fresh}}} \geq 0.105$$

APPENDIX 6.1: SULFUR REMOVAL ACTIVITY OF VARIOUS CATALYSTS

Table A6.1: Sulfur Removal Activity of Various Catalysts. Experiments performed in the batch reactor, at 13.8 MPa, 430 °C.

Catalyst	Reaction # in series	Reaction time (h)	Catalyst Age (g bitumen/ g catalyst)	S (%)	Sulfur removal (%)
B6 Commercial Catalyst	1	0.5	0.0	1.35	72.4
	2	1	4.1	1.61	67.1
	3	1	7.9	1.85	62.2
	4	1	12.0	1.93	60.5
B7 Commercial Catalyst	1	0.5	0.0	1.45	70.3
	2	1	3.8	1.46	70.1
	3	1	7.7	1.46	70.1
	4	1	11.6	1.53	68.7
	5	1	15.4	2.11	56.9
	6	1	19.3	1.74	64.4
B8 Commercial Catalyst Presulfided	1	1	0.0	1.66	66.1
	2	1	3.6	2.13	56.4
	3	1	7.2	2.23	54.4
B9 Commercial Catalyst Presulfided	1	1	0.0	1.58	67.7
	2	1	3.6	1.62	66.9
	3	1	7.3	1.98	59.5
B10 Commercial Catalyst Presulfded	1	1	0.0	1.30	73.4
	2	1	3.2	1.85	62.2
	3	1	6.7	2.20	55.0
B11 KNO3 Treated	1	0.5	0.0	NA	NA
	2	1	3.8	3.95	19.2
	3	1	7.6	3.78	22.7
B 12 KNO3 Treated	1	1	0.0	3.78	22.7
	2	1	3.6	3.77	22.9
B13 KOH Low Treatment	1	1	0.0	0.99	79.8
	2	1	3.2	1.32	73.0
	3	1	6.9	1.14	76.7
	4	1	10.4	1.39	71.6
	5	1	14.0	1.49	69.5
	6	1	17.5	1.47	69.9

Table A6.1 (continued): Sulfur Removal Activity of Various Catalysts

Catalyst	Reaction # in series	Reaction time (h)	Catalyst Age * (g bitumen/ g catalyst)	S (%)	Sulfur removal (%)
B14 KOH Mid Treatment	1	1	0.0	0.77	84.3
	2	1	3.9	NA	NA
	3	1	7.6	1.33	72.8
	4	1	10.9	1.41	71.2
	5	1	14.2	1.60	67.3
	6	1	17.4	2.03	58.5
B 15 KOH Mid Treatment Repeat	1	1	0.0	0.77	84.3
	2	1	4.0	NA	NA
	3	1	7.5	1.12	77.1
	4	1	11.0	1.26	74.2
	5	1	14.4	1.40	71.4
	6	1	17.7	1.31	73.2
B15 KOH High Treatment	1	1	0.0	0.94	80.7
	2	1	3.9	3.20	34.6
	3	1	7.0	3.25	33.5
B16 NaOH Treatment	1	1	0.0	0.48	90.2
	2	1	4.0	0.67	86.3
	3	1	7.3	0.78	84.0
	4	1	10.6	1.04	78.7
	5	1	13.7	0.99	79.8
	6	1	16.8	1.10	77.5
B17 LiOH Treatment	1	1	0.0	0.55	88.8
	2	1	3.7	1.23	74.8
	3	1	7.9	0.83	83.0
	4	1	10.8	0.79	83.8
	5	1	13.7	1.07	78.1
	6	1	16.6	1.18	75.9

APPENDIX 6.2: DISTRIBUTION OF THE STRENGTHS OF ACID SITES OF SELECTED CATALYSTS

Table A6.2: Distribution of the Strengths of Acid Sites of Selected Fresh Catalysts. Acid strength is defined through pyridine desorption temperature, as described below.

Catalyst Description	Number of Acid Sites (mmol/g catalyst)				
	Very Weak	Weak	Strong	Very Strong	Total
Pellets, as delivered	0.13	0.1	0.06	0.25	0.54
Crushed, calcined catalyst	0.13	0.12	0.05	0.26	0.56
KNO_3	0.14	0.1	0.04	0.26	0.55
KOH sample1	0.14	0.14	0.05	0.001	0.33
KOH sample 2	0.1	0.08	0.03	0.24	0.56
NaOH sample 1	0.18	0.19	0.05	0.09	0.51
NaOH sample 2	0.14	0.14	0.06	0.17	0.54

Acid strength is defined by pyridine desorption temperature. Very weak acid sites are sites from which pyridine desorbed at temperatures ranging from 373 K to 423 K. Similarly weak acid sites correspond to desorption temperatures 423 K to 523 K; strong acid sites correspond to 523 K to 623 K and very strong acid sites correspond to sites on which pyridine is irreversibly adsorbed at 623K.

APPENDIX 6.3: STATISTICAL ANALYSIS OF HDS CONVERSIONS FOR ALKALI DOPED CATALYST

Raw Data: Data shown include reactions #2 - #6 in the six step reaction series. Regression Analysis was performed on reactions #2 to #6 to determine possible deactivation. Reactions #3 - #6 were used to determine average values for the HDS activities

Commercial Catalyst		KOH Catalyst (0.28 meq/g cat)		NaOH and LiOH Catalysts (0.28 meq / g cat)	
feed / cat (g/g)	HDS conv (%)	feed / cat (g/g)	HDS conv (%)	feed / cat (g/g)	HDS conv (%)
4.1	67.1	3.2	73	4	86.3
7.9	62.2	6.9	76.7	7.3	84
12	60.5	10.4	71.6	10.6	78.7
3.8	70.1	14	69.5	13.7	79.8
7.7	70.1	17.5	69.9	16.8	77.5
11.6	68.7			3.7	74.8
15.4	56.9			7.9	83
19.3	64.4			10.8	83.8
				13.7	78.1
				16.6	75.9

Analysis of the Means:

Sample	Mean HDS conversion	Variance
Commercial	63.8	5.00
KOH	71.9	3.31
NaOH/LiOH	80.1	3.11

Define:

$$t_{data} = \frac{\bar{x} - \bar{y}}{\sqrt{\left(\frac{s_x^2}{n_x}\right) + \left(\frac{s_y^2}{n_y}\right)}}$$

$$\nu = \frac{\left(\left(s_x^2 / n_x\right) + \left(s_y^2 / n_y\right)\right)^2}{\frac{\left(s_x^2 / n_x\right)^2}{n_x + 1} + \frac{\left(s_y^2 / n_y\right)^2}{n_y + 1}} - 2$$

Then, comparing KOH doped sample (x), to commerical catalyst samples (y): $t_{data} = 3.08$, $\nu = 9.98$ and $t_{0.01,9} = 2.821$. This shows that the mean activity of the KOH catalyst is higher than the commercial catalyst at the 98% confidence level.

Comparing the NaOH/LiOH doped catalysts (x) to the KOH doped catalyst (y), then $t_{data} = 4.13$, $\nu = 7.37$ and $t_{0.005,7} = 3.499$. This shows that the mean activity of the NaOH and LiOH catalysts is higher than that of the KOH doped catalyst at the 99% confidence level.

Analysis of the slopes of the "deactivation" curves.

The standard error $s_{y|x}^2$, of the regression line with x coefficient a_1 is given by:

$$s_{y|x}^2 = \frac{1}{n-2}\left(\sum y_i^2 - a_1 \sum y_i x_i\right)$$

The variance of the slope is then given by:

$$s_{a1}^2 = \frac{s_{x|y}^2}{\sum\left(x_1 - \overline{x}\right)^2}$$

To test the hypothesis that the slope is equal to 0,

$$t_{data} = \frac{a_1}{s_{a1}}$$

Sample	a_1 (slope)	Σy_1^2	$\Sigma y_i x_1$	$\Sigma(x_1 - \overline{x})$	t_{data}
Commercial	-0.499	33964	5215	205	0.0915
KOH	-0.373	26054	3704	127	0.044
NaOH/LiOH	-0.358	64438	8355	203	0.056

These t_{data} values are all well below the t values at any confidence interval. The slopes of these lines are not statistically different from 0 and there is no statistical evidence that the catalysts are deactivating.

APPENDIX 6.4: METALS ANALYSIS OF PRODUCT RESIDUE FRACTIONS

Table A6.4: Metals Analysis of Product Residue Fractions. Products were produced in the CSTR usng the commerical NiMo alumina catalyst and a Na doped catalyst.

	Ni (ppm)	Ni repeat (ppm)	V (ppm)	V repeat (ppm)
Commercial (TLP)	28.43	29.02	43.41	44.30
Commercial (Residue)	153.04	160.93	226.32	236.10
NaOH (TLP)	22.74	26.54	34.21	40.64
NaOH (Residue)	159.57	167.45	236.35	249.06